

On the Gait Robustness of Passive Dynamic Robots, and a Novel Variable Stiffness
Series Elastic Actuator

受動歩行ロボットのロバスト性と新しい可変剛性アクチュエータ

Ivar Thorson

Nagoya University, February 2008

Abstract

This thesis is perhaps most succinctly summarized as being a qualitative design manual which addresses the question “How do we design efficient, stable legged robots?” The contents of this manual can be divided into responses to four particular subquestions:

1. *How do we quantify a passive-dynamic robot’s robustness to gait disturbances?* This thesis proposes that the robustness of passive-dynamic robots is well characterized by the magnitude of the smallest, deterministic change of the system momenta that move the system from its limit cycle to an unstable region. The length of this impulse disturbance is called r_{IDR} or r_{EDR} .

2. *Which mechanical structures are important to the energetics and gait robustness of legged robots?* This thesis presents data, acquired via a custom numerical simulation, on the effect on robustness and nondimensionalized forward velocity of several mechanical structures present in many commonly-studied passive-dynamic robot models. These structures include mass distribution, arc feet, a constrained torso, ankle-joint springs, and hip-joint springs.

3. *How do we add control to passive-dynamic robots?* Conventional control techniques are not suitable for selecting control torques for a passive-dynamic robot. This thesis presents some conjectures on the mechanical/control design of passive and natural dynamic systems.

4. *What actuators are appropriate for passive dynamic robots?* Conventional actuation systems are stiff and would overwhelm the passive dynamics of a mechanical system. This thesis presents the design of a variable stiffness series elastic actuator well-suited for actuating a passive-dynamic system.

本論文は、「どのように効率のよい、安定な脚式ロボットを設計すればよいのか」という疑問に対する定性的な設計マニュアルである。本論文の内容は以下の4つの疑問に対する答えで構成される。

1. 【どのように受動歩行・走行ロボットのロバスト性を測るか。】本論文では、リミットサイクルから引き込み領域の外まで移動させる最小運動外乱の大きさにより、受動歩行ロボットのロバスト性を計測する手法を提案する。この最小運動外乱の大きさを r_{IDR} または r_{EDR} と呼ぶ。

2. 【どのような機械構造がエネルギー効率と歩容ロバスト性に大きな影響を与えるか。】本論文では、いくつかの受動歩行ロボットに対して、数値シミュレーションにより得られたロバスト性と無次元化した歩行速度を示す。ここでは、質量分布、円弧状の足部、胴体、足首・股関節バネが与える影響について検討する。

3. 【どのように受動歩行ロボットに制御を付加するか。】通常の制御方法は受動歩行ロボットには適切ではない。本論文では、機械・制御設計に対する一手法を提案する。

4. 【どのようなアクチュエータが受動歩行ロボットに適しているか。】通常のアクチュエータはインピーダンスが高く、受動システムに用いた場合、アクチュエータが機械の自然ダイナミクスを打ち消す。本論文では、動的システムに適している可変剛性アクチュエータを導入する。

THESIS SUMMARY

Research Background and Objective: Legged robots are hard to build. Although stiffly-actuated, position-trajectory-controlled biped robots such as Asimo have been built, the energy efficiency of these robots is very low. Recently, robots which locomote based on the phenomenon of passive dynamic walking have been shown to have superior efficiency to such robots. Yet analyzing the gait robustness of passive dynamic robots remains difficult. The popular method for measuring gait robustness is use the spectral radius of the Jacobian of the Poincare map; in other words, the largest eigenvalue of the system linearized about a point. Unfortunately, in a recent paper, “A Disturbance Rejection Measure for Limit Cycle Walkers: The Gait Sensitivity Norm” by D. Hobbelen and M. Wisse, it was shown that real gait robustness does not correlate well with eigenvalues for a passive dynamic model with arc feet. Therefore, one objective of this research is to develop a new gait robustness metric which may correlate better with real-world robustness. This thesis also considers several practical problems of passive-dynamic robots. Conventional control and actuation techniques are not suitable for passive-dynamic robots because high actuator impedance can overwhelm a robot’s natural mechanical dynamics. The second objective of this thesis is to develop a new, variable-stiffness actuator suitable for passive-dynamic walking robots.

Research Description: This thesis proposes that the robustness of passive-dynamic robots is well characterized by the magnitude of the smallest, deterministic change of the momentum that moves a system from its limit cycle to an unstable region. Data is presented regarding the effect on the gait robustness and nondimensionalized forward velocity of several mechanical structures present in commonly-studied passive-dynamic robot models. Studied structures include mass distribution, arc feet, a constrained torso, and ankle and hip torques. Additionally, details on the design of the variable stiffness actuator are presented. Briefly, it uses two antagonistic quadratic springs to produce the effect of a linear spring with variable stiffness.

Research Results: A gait robustness metric was successfully developed and studied via simulation. We cannot say in general that simulation data is applicable to all models. However, for the simple models studied in this research we can make a few conclusions. Regardless of whether the change arises from torques, springs, or mass distribution changes, any change in leg swing frequency greatly affects gait robustness. Relatively heavy legs are more stable than light legs but move less efficiently. As arc feet get larger they increase walking velocity and robustness. A torso decreases walking velocity, and may either increase or decrease robustness. Feet which protrude more forward than backward decreased walking velocity but can improve robustness. Finally, simulation results show that using variable stiffness actuators can improve the gait robustness of a biped robot that is desired to walk at different speeds. It is shown that the actuator presented in this thesis may be more suitable for use in passive-dynamic systems than stiff actuators.

THESIS SUMMARY

【研究背景と目的】脚式ロボットを作ることは難しい。ASIMOのような、運動インピーダンスの高いアクチュエータと軌道追従制御を用いる2足ロボットは実現出来ているが、エネルギー効率が低い。近年、受動歩行の現象に基づいたロボットはより効率良く歩けるのではないかと考えられている。しかし、リミットサイクルを持つ受動歩行のロバスト性を測るのは困難である。よく用いられている安定性解析方法は、ボアンアレ写像のヤコビ行列のスペクトル半径で判断することである。つまり、最大固有値の大きさにより安定性を判断する。しかしながら、D.HobbelenとM. Wisseの論文“*A Disturbance Rejection Measure for Limit Cycle Walkers: The Gait Sensitivity Norm*”では、円弧状足の受動歩行ロボットのロバスト性は最大固有値とあまり相関しないことが示されている。従って、本論文の一つの目的は固有値よりも実際のロバスト性とより高く相関するロバスト性計測方法を開発することである。一方、通常の制御方法やアクチュエータは受動歩行ロボットには適切ではない。通常のアクチュエータはインピーダンスが高く、受動システムに用いた場合、アクチュエータが機械固有のダイナミクスを打ち消すことがある。そこで、本論文のもう一つの目的は受動歩行ロボットに適している新しい可変剛性アクチュエータを開発することである。

【研究内容】本論文では、リミットサイクルから引き込み領域の外まで移動させる最小運動外乱の大きさにより、受動歩行ロボットのロバスト性を計測する手法を提案する。いくつかの受動歩行ロボットに対して、数値シミュレーションにより得られた歩行ロバスト性と無次元化した歩行速度を示す。ここでは、質量分布や円弧状の足部、胴体、足首・股関節バネが与える影響について検討する。つぎに、可変剛性アクチュエータの設計、機械構造、仕様について説明する。アクチュエータの実機実験では、二つの相対する二乗関係バネを用いることで、一つの線形可変バネと等しい効果が得られるこことを示す。

【結果と課題】歩行ロバスト性の新しい測り方を開発し、シミュレーションで検討した。一般的にシミュレーションのデータは全てのロボットモデルの特徴を表すとは言えない。しかし、簡単なモデルのシミュレーション結果より、以下のようないくつかの結論が得られた。遊脚の固有振動数は、バネや質量分布により変化する。しかし生じた理由と無関係に、固有振動数の変化はロバスト性に大きな影響を与える。比較的重い足は軽いのより安定だが、運動効率は下がる。円弧状の足は大きくなればなるほど歩行速度がはやくなりロバスト性も高まる。拘束された胴体は歩行速度を遅くし、ロバスト性には有利にも不利にもなる。円弧状足の中心を前にすると歩行速度が減り、ある範囲までならばロバスト性を向上させる。最後に、可変剛性アクチュエータの適用は歩行速度の変わる受動歩行ロボットのエネルギー効率とロバスト性を改善することがシミュレーションにより示された。つまり、本研究のアクチュエータはインピーダンスの高い通常アクチュエータよりも受動歩行ロボットに適していることが示された。

TABLE OF CONTENTS

	Page
List of Figures	iv
List of Tables	vi
Preface	vii
Acknowledgments	viii
Chapter 1: Introduction	1
1.1 Research Question and Thesis Overview	1
1.2 Motivation: Why study bipedal walking robots?	2
1.3 Prior Research	3
1.4 Contributions of this Thesis	11
Chapter 2: Metrics of Gait Robustness	17
2.1 Stability vs. Robustness	17
2.2 r_{IDR} and r_{EDR} : Name and Definition	17
2.3 Applicability, Properties, and Limitations of r_{IDR}	20
2.4 Does r_{IDR} correlate well with multiple-disturbance robustness?	21
2.5 On the Difficulty of Finding r_{IDR} Analytically	23
2.6 Common Questions and Answers	24
Chapter 3: Optimizing the Gait Robustness of Passive-Dynamic Bipeds	27
3.1 Froude Number and Cost of Transport	28
3.2 Energetic Efficiency of Passive Dynamic Systems	28
3.3 On the Choice of Mechanical Structures Studied	29
3.4 The Reference Biped	31
3.5 Notes on Numeric Methods, Graphs	32
3.6 Effect of Slope	35
3.7 Effect of Mass Distribution	40
3.8 Effect of Hip Spring	45

3.9 Effect of Ankle Springs	50
3.10 Effect of Arc Foot Radius	53
3.11 Effect of Forward-Pointing Feet	57
3.12 Effect of a Mechanically Constrained Torso	58
3.13 Comparison of Effects of Mechanical Additions to Reference Biped	65
3.14 Future Engineering Goal	66
3.15 Evolution of a Robust Passive-Dynamic Biped	67
 Chapter 4: Variable Stiffness Series Elastic Actuator	70
4.1 Motivation for a New Actuator	70
4.2 Overview of the Variable Stiffness Series Elastic Actuator (VSSEA)	71
4.3 Advantages of the VSSEA	74
4.4 Disadvantages of the VSSEA	75
4.5 Mechanical Description	76
4.6 Electrical System and Control System Details	79
 Chapter 5: Conclusions and Future Research	80
5.1 Conclusions	80
5.2 Future Research	80
5.3 Mechanical/Control System Design in a Natural Dynamics Biped	81
 Bibliography	87
 Appendix A: Mathematical Conventions, Abbreviations, List of Symbols	92
 Appendix B: Equations of Motion, Impact Equations	95
B.1 Derivation of Equations of Motion	95
B.2 Derivation of Impact Model	98
B.3 Form of Equations of Motion for Easy Integration	101
B.4 Controllers Can Mimic Springs	101
B.5 Heelstrike Conditions	102
B.6 Equations for Compass Biped	102
B.7 Equations for Biped with Semicircular Feet	103
B.8 Equations for Biped with Interleg Spring	104
B.9 Equations for Biped with Forward-Pointing Feet	105
B.10 Equations for Biped with a Mechanically Constrained Torso	106

Appendix C: VSSEA Mechanical Design	109
Appendix D: Details on the Custom Simulator	114
D.1 Data Parameter Details	114
D.2 Numerical Integration and Root Finding	114
D.3 r_{IDR} Search Algorithm	116
D.4 Simulation Verification	118
Vita	119

LIST OF FIGURES

Figure Number	Page
1.1 Examples of stiffly-actuated, position-controlled humanoid robots	5
1.2 The compass biped	9
1.3 Examples of robots based on passive-dynamic walking	10
1.4 Disturbance rejection predicted by the Gait Sensitivity Norm	12
1.5 Mean First Passage Time of a compass biped	13
2.1 Graphical interpretation of r_{IDR}	19
2.2 Correlation between r_{IDR}^2 and the Gait Sensitivity Norm	22
2.3 Total system energy of reference biped when disturbed by Δp_{IDR} vs time . .	26
3.1 Sketch of proposed robot built from four VSSEA actuators	30
3.2 Functional models of proposed biped	31
3.3 Reference biped model	32
3.4 Reference biped data graphs	34
3.5 Cotangent spaces of the reference biped during a step at the limit cycle . . .	36
3.6 Effect of changing the slope ϕ	37
3.7 Data from robots at selected values of ϕ	38
3.8 Effect of varying lower leg length a	41
3.9 Effect of varying hip mass m_H	42
3.10 Data for selected values of a	43
3.11 Data for selected values of m_H	44
3.12 Effect of varying interleg spring k_{hip} on a slope of $\phi = 3.0$ degrees	47
3.13 Effect of varying interleg spring k_{hip} on a slope of $\phi = 1.0$ degrees	48
3.14 Data for selected values of k_{hip} on a $\phi = 3.0$ degree slope	49
3.15 Effect of varying ankle spring k_{ankle} at $\phi = 3.0$	51
3.16 Data for selected values of k_{ankle}	52
3.17 Picture of a robot with arc-shaped feet, showing dimensions	53
3.18 Effect of arc foot radius r	55
3.19 Data for selected feet radii r	56
3.20 A biped with forward-pointing feet	57
3.21 Effect of tilting $r = 0.2$ radius arc feet forward by ψ	59

3.22	Data for selected values of ψ	60
3.23	A biped with a torso constrained by the rule $\theta_t = \xi + \frac{1}{2}(q_f + q_s)$	61
3.24	Effect of increasing torso length d	63
3.25	Data for selected values of d	64
3.26	Combined data for experiments	65
3.27	Three generations of evolved compass bipeds	68
4.1	Functional schematics for the VSSEA	72
4.2	A comparison of variable stiffness actuator topologies	73
4.3	A computer rendered image of the VSSEA	77
4.4	Photos of the VSSEA	78
D.1	Screenshot of the simulation developed in for this thesis.	115

LIST OF TABLES

Table Number	Page
3.1 Energetic Efficiency of Various Robots	29
4.1 Parameters of Prototype Actuator	76
D.1 Simulation Parameters	115

PREFACE

My goal in this thesis is to compile the highlights of my research this past year and a half, and to explain what I have been thinking about in more detail than is appropriate for a published paper.

When I began my masters research, I originally planned to build a planar bipedal robot. Instead, I had so much fun programming and reading theoretical papers that I had to abandon such an ambitious practical goal when realistic time constraints became painfully obvious. I remain interested in constructing such a robot, as well as pursuing more ambitious theoretical goals in a Ph.D.

Having the luxury of copious amounts of time to pursue whatever research topics interest me has been exhilarating. The most difficult decision has not been *what* to research, but *what not* to research. I must therefore admit that the topics in this thesis are a bit scattered – merely looking at the title of this thesis should reveal my interest in classical dynamics, control theory, applied mathematics, and practical robots. Seen in this light, this thesis is my little qualitative design manual for bipedal robots.

As a result, I must beg the reader’s forgiveness for a such scattered thesis, and hope that I have drawn the connections between the different areas of research in a manner that is understandable. Each area presents just a tiny puzzle piece of an answer to the question “How do we design efficient legged robots?”

I begin many of the sections in this thesis with questions and subquestions. It is my belief that curiosity drives research, and starting from a question may often reduce the amount of introduction or explanatory text required.

They say that a thesis is never really completed, it is merely abandoned. It certainly feels that way. Besides cleaning up some of the warts that remain in the presentation of this thesis, there are a great deal more simple experiments that I wished to pursue. I have an unfortunate habit of finding the right way of doing something only after exhausting all possible ways of doing something wrong – a time-consuming heuristic, to say the least.

Finally, it is my hope that this thesis is as enjoyable to read as it was for me to think about!

ACKNOWLEDGMENTS

In the whirlwind that has been the last 4 years, I finished my undergraduate degree at the University of Washington, fell in love with Japan, learned its language, was awarded a generous scholarship¹, enrolled in Nagoya University, and was free to pursue my own research for a whole year. Such an amazing experience was only possible thanks to the good advice of friends, a dash of wanderlust, and the assistance of a great many people.

In chronological order, I would like to thank my friend Matt Boyce for first introducing me to things Japanese; Edward Miller for his enthusiasm and suggestion that I apply for the MEXT scholarship; Dr. Mikhail Svinin for his connections, corrections, good research advice, and sometimes overwhelmingly long suggested readings; Prof. Kouichi Taji for his kindness and patient work as my advisor at Nagoya University; Prof. Hosoe for his friendly smile, insightful questions, and generous research funding; Prof. Asano for his enthusiasm about passive-dynamic walking, which certainly spread to my lab at Nagoya University and influenced my own research direction; Prof. Uno for his advice and help in getting me to an international conference on his limited budget.

In alphabetical order, another round of thanks go to Masa, Masashi, Ozeki, Takuro, Yuuta and the other Japanese graduate students for patiently including me in their circle of friends and teaching me how walk and talk like a Japanese guy; may their Halo skills never weaken.

Thanks also to the Japanese population as a group, not just for their friendliness and generosity, but also for their combination of childlike nature and wise sophistication that has made me reflect upon my own culture's habits. Also, I would like to playfully thank them, tongue-in-cheek, for tolerating the foreign pirates like myself who plunder scholarship money, gorge ourselves on delicious Japanese food, and date lovely Japanese women in exchange for a bit of research.

Last but certainly not least, I would like to thank my good friends Babak, Branko, Devendra, Donato, Jo Anne, Kenbo, Monica, Nadia, Pierre, Phillip, Ricardo, Wael, Vera, and my many other international friends – all from different countries – who have made my stay in Japan a worldly, exciting, and unforgettable experience.

¹This thesis was made possible by the MEXT (Japanese Ministry of Education, Culture, Sports, Science and Technology) scholarship, which provides scholarship and a living stipend for foreign researchers, Masters students, and Ph.D students.

Chapter 1

INTRODUCTION

1.1 Research Question and Thesis Overview

If research begins with a question, then the most general question that this thesis addresses is

“How do we design efficient, stable legged robots?”

We can divide this general question into smaller, more manageable pieces with hopefully more specific answers. In this thesis, the field of inquiry is restricted to bipedal robots, and the particular subquestions addressed are:

1. *How do we quantify a passive-dynamic robot’s robustness to gait disturbances?* Legged robots are a subclass of nonlinear, dynamic, hybrid systems which are difficult to analyze mathematically unless significant simplifications are made. It is difficult to compare the robustness of legged robots with different degrees of freedom, mechanical structures and controllers.

In this thesis, the study of legged robots is restricted to bipedal robots that are constrained to the sagittal plane, exhibit the limit cycle walking effect, and possess no stabilizing control system. In Chapter 2, we propose a mathematical definition for limit-cycle robustness that is especially relevant to this class of legged robots. Using this definition, it is possible to rationally compare the gait robustness of bipedal robots with different mechanical structures and degrees of freedom.

2. *Which mechanical structures are important to the energetics and gait robustness of legged robots?* While the fields of biomechanics and passive-dynamic walking have yielded some exciting developments regarding the energetic benefit of certain types of structures in legged robots, the effect of a legged robot’s mechanical structure on its gait robustness is still relatively unstudied. Are big feet good for walking efficiency but bad for robustness? Does increasing leg swing frequency improve efficiency at the expense of gait robustness? These types of questions are studied in Chapter 3, and gait robustness results obtained via a custom rigid body simulator are presented.
3. *How do we add control to passive-dynamic robots?* There are a myriad of possible ways to control a legged robot. Commonly used control methodologies, such as trajectory generation, position control, and linearization are not well suited for controlling robots

which locomote based upon the delicate phenomenon of limit-cycle walking. Section 5.3 outlines how one might design a controller for the bipedal robots studied in this thesis, such that the controller complements the robot's passive mechanical dynamics.

4. *How do we actuate passive-dynamic walking robots?* In this thesis, it is argued that the traditional control/actuation systems used in many robots – that is, time-indexed, trajectory-based control using stiff actuators – is not suitable for controlling legged robots. Legged robots must withstand significant repeated shocks, interact softly with their environment, and like other mobile robots have significant practical restrictions on power consumption. As an alternative to using stiff actuators, Chapter 4 introduces a variable stiffness actuator well-suited for legged robots or soft actuation tasks.

Finally, Chapter 5 outlines some possible directions of future research.

1.2 Motivation: Why study bipedal walking robots?

If a robot's operating environment is restricted to motions on a well-defined and very flat surface, there is little reason to build a legged robot. Wheeled robots obviously have superior efficiency on flat surfaces; wheels can roll without dissipating energy, but a legged robot with a finite number of legs cannot help but dissipate energy via impacts between the foot and ground.¹

However, legged robots hold great promise for traversing very rough terrain that is currently impassable by wheeled vehicles. Wheeled robots cannot in general climb over obstacles larger than the radius of the wheel, and even small obstacles can greatly reduce locomotion velocity and efficiency. In contrast, legged robots can step over obstacles without significant energy loss, and traverse terrain with disconnected contact patches, such as when walking on stepping stones over a pond.

We should also not ignore how human-friendly legged robots are. In the experience of the author, legged robots have more personality than wheeled robots, and popularizations of robots by Hollywood generally depict bipedal robots. Indeed, most research in legged robots, particularly biped robots, seems to stem from a very human interest in making robots like ourselves. It seems likely that it will prove easier for most of us to interact with robots of similar shape to ourselves, robots that are able to navigate our living spaces as we do.

Theoretically, it can be very difficult to rigorously analyze the motions of bipedal robots. This is a good thing; many interesting developments in research come out of hard problems. This thesis focuses particularly on using simulation as a first step toward solving the theoretical problems of quantifying gait robustness, and on the engineering problem of improving biped mechanical design.

¹If a robot could be built to walk with infinitely soft footfalls, however, its efficiency might approach that of a wheel. Indeed, [McGeer, 1988] emphasized several parallels between walking and the rolling of a wheel.

1.3 Prior Research

In order to motivate the developments proposed in this thesis, it is necessary to stop and look at the current state-of-the-art in robot design and control.

1.3.1 Linear Feedback Control and Stiff Mechanical Systems

At present, it is reasonable to say that the dominant approach to control of industrial robots is that of linearized feedback control of position. This is all well and good; the strengths of linear feedback control systems include their simplicity, use of well-developed linear systems theory, and generality.

At risk of oversimplification, we will now summarize the general approach of linearized feedback control of a rigid body system – henceforth called the “plant”. A set of desired trajectories for the plant to follow are computed in some way, and the plant is forced to follow that trajectory via the feedback control. The art of feedback control system design thus becomes modeling the plant as accurately as possible so that its dynamics can be altered as accurately as possible. With luck, the model of the plant and the plant itself will be sufficiently close that the controller will not spend significant time or energy fighting the dynamics of the plant itself.

To rephrase: control is accomplished via precise specification of trajectories. High-gain feedback control then slaves the motion of the robot to the modeled trajectory.

A significant side-effect of the position-based approach to machine control is that it encourages the mechanical engineers to design very stiff, rigid robots; rigidity allows the position of a robot to be controlled more accurately. This naturally results in very poor shock tolerance, as rigid things tend to break under shock. This also makes them fairly dangerous systems; when a heavy, stiff robot collides with a soft human, the human is usually the one who undergoes a dangerous deformation.

Although linearized feedback control is a general method and need not be restricted to only controlling position, the majority of robot systems in the world use position control. For industrial robots, this is acceptable and appropriate. However, for walking robots, this approach has significant disadvantages.

1.3.2 Why are stiff, position-controlled bipeds fundamentally flawed?

The most significant disadvantage of using a naive position control system with stiff actuation is that it cannot handle *any* type of contact disturbance or uncertainty well.

Let us consider what happens when an disturbance or obstacle contacts a stiffly actuated position control system. For example, suppose a very rigid robot arm attempts to move from point A to point B along some trajectory, but obstacle C lies in the path and blocks the way. After the robot collides with the obstacle, the feedback will work increasingly hard to move the robot arm through the obstacle as the planned trajectory and actual trajectory diverge more and more. Very high forces may develop between the arm and the obstacle. These forces will likely either damage the robot arm or the obstacle, or both.

Contact uncertainty is similarly poorly handled by naive position control systems. Assume the task of the robot arm is now to move from point A to the point where it just

barely touches obstacle C, but let there be some uncertainty about the exact location of C. Without a system to monitor the force on the robot arm, a purely position-controlled robot will almost certainly move the actuator either not far enough or move it too far. In the first case, the robot is not contacting object C at all and the task has not been accomplished. In the second case, it will likely be pushing against the object very hard, depending on the gain of the feedback control system.

It should be clear that this is exactly the same problem that a legged robot experiences for *every single step that it takes!* In the real world, even on flat surfaces there is some inevitable uncertainty as to the floor height, angle, softness, and so on, relative to the robot's internal map of the world that was acquired via sensors.

That stiffly actuated position control would be a poor choice for systems which must routinely deal with contact uncertainty seems by now to be an obvious point, but it remains one than many engineers and researchers ignore. Often, attempts to rectify the situation with some sort of force or torque sensor are used. These approaches may also be similarly misguided if compliance is not used; the forces that develop when a stiff, position-controlled robot encounters a disturbance will occur so quickly that stiff actuators cannot react to the disturbance safely. Two quotes from other researchers support this line of thought:

“...making a rigid, heavy robot behave gently and safely is an almost hopeless task, if realistic conditions are taken into account.” – [Bicchi, Tonietti 2004]

“The trajectory-control approach to robotics has been called a ‘kinematic obsession’ (R.Q van der Linde, personal communication, 1999), and it often has a kind of rigor mortis as its negative consequence.” – [Collins, et al 2001]

Finally, for many systems another question arises: Does following a position trajectory really matter, or are there merely a few instants when the position need be controlled accurately? For example, the most important event during walking is the impact between the foot and ground at the end of each step. Arguably, it may not really matter how a robot moves its legs around during a step, as long as the foot lands in the proper place to act as the support foot for the next step. There may be many trajectories which satisfy this constraint. Selecting only one of these trajectories is clearly too strict for a system which will encounter disturbances.

1.3.3 Examples of Stiff, Position-Controlled Bipedal Robots

Despite the many weaknesses of linearized feedback control of position, it remains popular even in legged robots. Many widely-known humanoid bipedal robots such as Honda's Asimo [Kajita et al 2002] [Sakagami et al 2002], the HRP-2 [Kaneko et al 2004], and Sony's QRIO [Fujita et al 2003] use linearized feedback control to very precisely follow trajectories which result in stable motion that satisfy the ZMP criteria. Photos of these robots are shown in figure 1.1.

That these robots work as well as they do is a tribute to the precision engineering and talent of the Japanese researchers, and the author has great respect for their impressive accomplishments.



Figure 1.1: Examples of stiffly-actuated, position-controlled humanoid robots. *Left:* The humanoid robot “Asimo”, developed by the Honda Motor Corp. *Middle:* HRP-2, developed by Kawada Industries, Inc. together with Humanoid Research Group of National Institute of Advanced Industrial Science and Technology (AIST), Japan. *Right:* QRIO, developed by Sony Corp.

Yet in many ways, these robots remain nothing more than industrial robot arms that have been put into a different package. When scaled to human size, they are heavy, stiff, and probably dangerous machines. This is not a criticism of ZMP control; the concept of a ZMP constraint is arguably a useful one. Rather, this is a criticism of the unfortunate habit of control engineers of trying to restrict motion to a single time-indexed position trajectory. Allowing only one possible motion trajectory in response to most disturbances is too strict a constraint for robust legged robots to use, even if this trajectory is designed with the robots natural dynamics in mind. To rephrase: assume that the robot encounters a minor disturbance or obstacle. In this situation, using high-gain feedback to *force* the robot to continue moving along the idealized trajectory will be less efficient than just *letting* the robot’s natural dynamics unfold. Also, if the obstacle is heavy, then continuing to try to follow the idealized trajectory may be one of the *worst* things the robot could do.²

As a result, the robots shown in figure 1.1 are not particularly robust to shock, cannot interact softly with their environment, have poor energetic efficiency (see Section 3.2), and are only demonstrated to work reliably on flat, well-defined surfaces. The robots remain a long way from being practical, robust devices that can interact with humans, and in the long run, the rigid, position-controlled approach may be restricted only to well-defined

²It appears Asimo continually recomputes many such ZMP-satisfying trajectories to solve this problem by dynamically selecting a trajectory in real time. [Sakagami et al 2002] This improves gait robustness, but does not change the fact that the mechanical natural dynamics are largely ignored and that motion is still tightly constrained by the feedback controller and stiff actuation.

environments such as manufacturing facilities. This thesis adopts a different perspective on machine design. Rather than approach the two tasks of mechanical design and control design separately, as the position-control approach encourages us to do, this thesis proposes that we consciously balance design of the control and mechanical systems, considering their coupled interaction during the entire design process. This philosophical approach will be called “Natural Dynamics” throughout this thesis.

1.3.4 Natural Dynamics

The term “natural dynamics” as yet lacks a very concrete, objective, or even mathematical definition that is widely agreed upon. Nonetheless, it seems to be being used in a philosophical way by many researchers in the past 10-20 years, especially with respect to systems having the following properties:

- The dynamic behavior of the system is a result of the interaction between the control system, mechanical system, and the environment. The motion is not slaved to a trajectory by control system. Rather, the desired behavior emerges out of the interactions between these three systems.
- The intrinsic/unforced behavior of the mechanical system is “exploited” in some way so that only small control efforts are required. That is, the natural behavior of the uncontrolled mechanical system is carefully considered during design so that it closely matches the task the robot will perform.
- Compared to feedback control, which uses high-gain controllers, a relatively low-gain controller is used. The idea is to augment the mechanical system’s unforced dynamics with control, not forcefully redefine the whole system’s dynamics to match a control rule.

A collection of quotes from the literature may be the simplest way to show the philosophical approach of the natural dynamics community. These quotes are by no means a definitive list; indeed, it is even possible that several of these authors would be violently opposed to having their quotes included here.

“One could conceive of two extremes of actuator design...high-bandwidth actuators with all dynamics described by software control policies, or carefully designed mechanical systems with tuned natural dynamics that require no software control.” – [Hurst 2004]

“We believe that the inverse dynamics approach should only be used when high-performance requirements and other extreme situations dictate. This is because plant inversion adds computational complexity, and fighting the natural dynamics of the robot can be inefficient.” – [Pratt et al 2001]

“...we believe that robots cannot be *commanded* to perform a task; they can only be given *hints* and *suggestions*.” – [Pratt et al 2001]

“As observed by Marc Raibert, the central nervous system does not control the body, it can only make suggestions.” – [Buchli et al 2006]

“Reliable default behavior makes things easier to control.” – [Ringrose 1997]

“...a passive gait is of special appeal because it is *natural* and it does not require any external energy source.” – [Goswami et al 1996]

“Actuation is mainly present to sustain the [natural, mechanical] oscillation.” – [van der Linde 1998]

“...A common conjecture in the bipedal locomotion community is that controllers which exploit the ‘natural dynamics’ of the biped will prove to be more energy efficient and will produce more anthropomorphic motion.” – [Spong 1999].

“We stress here that we *augmented* the natural dynamics of the robot with simple virtual components rather than attempt to cancel the natural dynamics. In no case did we assume linear dynamics.” – [Pratt et al 2001]

“Emphasis in traditional robot design is often placed on mimicking animal movements rather than on mimicking the underlying mechanics animals use to produce movement.” – [Migliore 2005]

Some examples what the author considers to be related natural dynamics research include:

- [Buchli et al 2006], who used adaptive frequency Hopf oscillators to automatically adapt a robot’s motion to its surroundings, improving the performance of the robot.
- [Ahmadi, Buehler 1999], who constructed a running robot with very carefully designed mechanical passive dynamics, and an actuation system that works together with these dynamics.
- [Collins et al 2005], who presented four robots which walk based on passive dynamic principles.
- [Pratt et al 2001], who used a technique called Virtual Model Control to augment the passive dynamics of a bipedal robot using virtual components and build a stable robot.
- [Ringrose 1997], who designed running robots which self-stabilize through their interaction with the environment.

- [Vanderborght et al 2006], who advocated compliant actuation systems, designed a compliant actuator, and used these actuators in a humanoid robot.
- [Umedachi, Ishiguro 2006], who advocated a well-balanced coupling between control and mechanical systems.
- [Williamson 1998], who studied using central pattern generators to create emergent behavior resulting from interactions between a robot and the environment.

To summarize, the natural dynamics approach toward machine design is to analyze the interaction between environment, machine, and control system, and design the mechanical and control systems to complement each other. Control and mechanical systems are no longer separated, but studied as a tightly-coupled system. Finally, the interaction with the environment is closely studied.

There are many difficulties that this philosophical approach faces when theory is put into practice. Mechanical design is no longer completely fixed during the design of the control system, nor vice versa. There is no well understood engineering method to design a mechanical system so that its passive dynamics perform an arbitrary task. There is also no general method to design a controller for such a system, either. The behavior of natural dynamic systems is frequently highly nonlinear, making mathematical analysis very difficult.

1.3.5 Passive-Dynamic Walking

We might say that the field of passive-dynamics is an intellectual child of natural dynamics. Like natural dynamics, the word ‘passivity’ means many different things to many different researchers. In this thesis, the word passivity refers to the uncontrolled motions of a mechanical rigid body system. Passive-dynamic walking, as treated in this thesis, is thus an interaction between the mechanical walker and its environment. Once a control system is added, the system is no longer purely passive-dynamic and might be called pseudo-passive-dynamic, controlled passive-dynamic, or perhaps “natural-dynamic.”

The study of simple, passive-dynamic walking and running machines appears to have been largely popularized by [McGeer, 1988], but we should note that the concept of ballistic walking was studied a decade earlier still by [Formalski 1978]. [Arimoto 1980] also studied robots which moved along passive motions between two robot postures, although gravitational effects were not considered.

[McGeer, 1988]’s observation was that certain simple mechanical systems – even as simple as a two-link model such as the one shown in figure 1.2 – can walk stably down an inclined slope without any control system. In lieu of control, stability is achieved via the physical, mechanical impacts between foot and ground. For certain systems in certain environments, foot impacts self-stabilize the robot and the gravitational energy gained by descending the slope powers the motion. Such mechanical systems are said to have a stable limit cycle, and this limit cycle originates only from the machine-environment interaction. In Chapter 3, this thesis studies several such robot-environment systems in detail, and compares their robustness to disturbances.

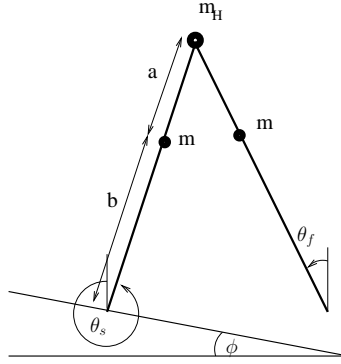


Figure 1.2: **The compass biped.** A well-studied passive dynamic biped model, it has two degrees of freedom, (θ_f, θ_s) , which specify the angles of the non-support and support legs respectively. It has three masses; one on each leg and one at the hip joint. It has no knees, and so its feet scuff the ground as it walks, but this problem is assumed to be solved by shortening the non-support leg infinitesimally.

In future years, we may perhaps realize that the concept of limit-cycle walking phenomena is not actually the most important achievement of [McGeer, 1988]; limit-cycle walking may prove too difficult or unstable to harness for practical use in robots of great complexity. [McGeer, 1988]’s greater contribution may be towards spreading the memes of natural dynamics to a wider audience.

Certainly, biomechanicists are now considering the importance of purely mechanical effects on animal locomotion. For examples, see[Geyer 2006][Collins, Ruina 2005].

We now turn to the benefits of natural dynamic system design. These include

- Greatly superior energy efficiency when compared to traditional approaches. See Section 3.2 for details.
- Purely mechanical stabilizing effects may allow designers to reduce the complexity of the control system.
- Motions of passive-dynamic systems generally look more “natural” to the human eye.
- Stiff actuation becomes less important, and actuators which are more compliant may be used, improving shock resistance and safety.

On the other hand, the present weaknesses of passive-dynamic walking approaches include

- A limited understanding of how stable or robust the interaction is between the mechanical system, control system, and environment.

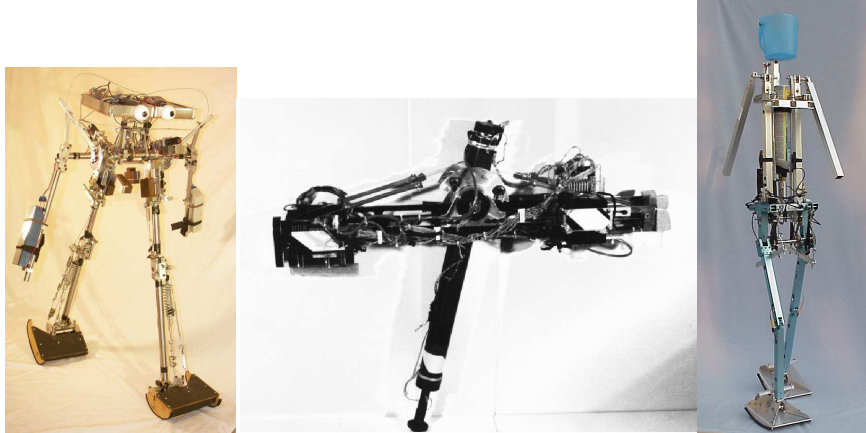


Figure 1.3: Examples of robots based on passive-dynamic walking. *Left:* The Cornell Biped, developed at Cornell University by [Collins et al 2005] *Middle:* The Monopod-II, developed at McGill University and described in [Ahmadi 1998]. *Right:* Denise, developed at Delft University by [Wisse 2004]

- Difficulty in actuating such systems without destroying their passive-dynamic behavior
- Difficulty in controlling and actuating motions that are substantially different from or oppose the passive-dynamic behavior of the machine. However, to be fair, this is an objection for *every* robot ever constructed; there will be some modes of motion that a robot's structure will naturally be optimized for, and other modes for which the structure is not optimal.
- A lack of common features already present in fully-actuated, stiff, position-controlled robots: an upper body, starting and stopping, turning, standing up after a fall, climbing stairs, stepping over obstacles, and so on. [Srinivasan, Ruina 2005]

In summary, it is hard to get passive-dynamic robots to behave properly in the real world; the passive-dynamic walking phenomena is extremely sensitive to disturbances and often disintegrates quickly without an active control system. Even with a controller, robust behavior is far from assured. For example, the Cornell Biped [Collins, Ruina 2005] had such sensitivity to actuation timing that the energetically advantageous ‘push-off’ control timing could not be used because it resulted in instability. The Cornell Biped and other robots based on passive dynamic robots are shown in figure 1.3.

Finally, people in the passive-dynamic walking community should humbly observe that in some ways, building a 2D bipedal robot is a solved problem; if energy efficiency is not a concern, a goose-stepping walk which kicks the leg forward sharply will walk stably with an embarrassingly simple control rule. Passive dynamic walking in 2D can be summarized with

a very simple, high level rule from [Wisse 2004]: take steps big enough to stop the forward falling motion, but not so big forward momentum is lost and you fall backward. 2D and 3D running can be similarly characterized by [Raibert 1986]’s now classic work, which appears to be used today in robustly moving robots such as Big Dog[Boston Dynamics 2008].

Thus, the great struggle is not to make robot walk or run, but to make it move with both great efficiency and robustness, and to develop design and analysis methods that will work for not just 2D but also 3D natural dynamic systems.

1.4 Contributions of this Thesis

This thesis makes three contributions to the fields of passive dynamics and natural dynamics:

1. A mathematical definition of gait robustness that is applicable to passive-dynamic legged robots with limit cycles.
2. A custom rigid body simulator for passive-dynamic robots calculates this robustness approximately using numeric methods. Data acquired via this simulator is also presented.
3. A design of an actuator suitable for use in passive-dynamic robots. The actuator not only actuates the robot, but it also adjusts the passive-dynamics of the robot via a variable stiffness spring mechanism.

In the following sections, we justify the merits of these three contributions.

1.4.1 Why do we need a new way to quantify gait robustness?

Why not use linearizations to characterize robustness?

The response to small disturbances of a robot walking at a stable limit cycle can be found in several ways. One common way to quantify robustness is to linearize the system, create a step-to-step linear equation, and find the eigenvalues of this matrix. This was first done by [McGeer, 1988]. A related technique is to use the theory of Floquet Multipliers, which linearizes about various points on an orbit[Su, Dingwell 2006]. These are differential quantities that measure asymptotic stability. Mathematically, they are quantifying robustness in terms of the spectral radius of the Jacobian of the Poincare map.

Although very accurate for small disturbances, one limitation of this type of analysis is that it may mislead us about how the system responds to larger disturbances. This is to be expected; linearized models will differ more and more from the nonlinear model as one ventures further from the linearization point. [McGeer, 1988] made an analogy to the basin of attraction of a limit cycle as being a well, and noted that the step-to-step eigenvalues of a system “tell us the depth of the well, but not how wide”.

As there is no general method for finding the large-disturbance robustness of a nonlinear system, most researchers are left with no recourse but to assume that there is a correlation

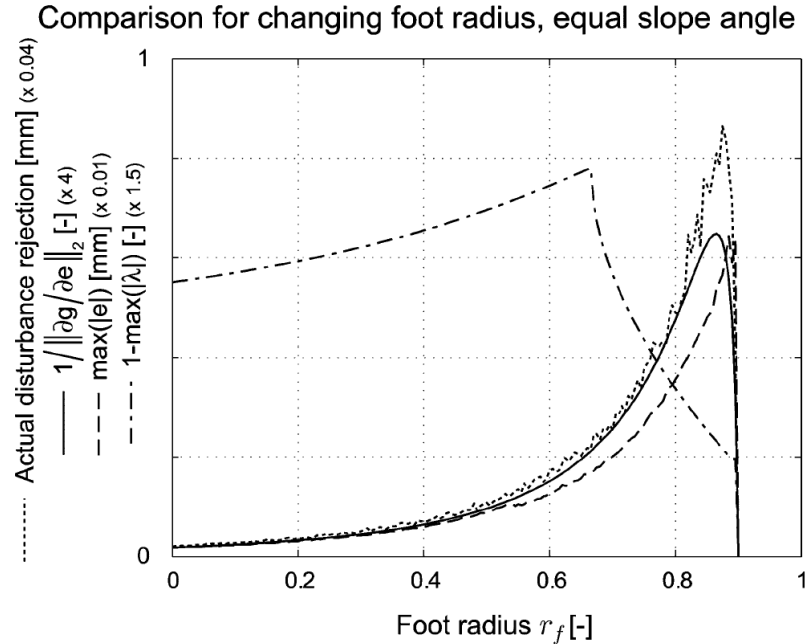


Figure 1.4: Disturbance rejection predicted by several gait robustness measures. (From [Hobbelen 2007], used without permission.) The model under consideration is [Garcia 1998]'s simplest walking model, with arc feet of radius r , walking down a slope of $\phi = 0.004$ rad. It is clear that eigenvalues correlate poorly with actual disturbance rejection, especially for large feet radii.

between a 'deep well' and a 'wide well', i.e. that having small eigenvalues implies a wide basin of attraction of the limit cycle.

Unfortunately, this does not seem to be the case for certain models with strongly non-linear behavior. [Hobbelen 2007] shows that there is rather poor correlation between actual disturbance rejection and the largest eigenvalue, especially as the foot radius gets larger. This graph is reprinted, without permission, in figure 1.4.

Similarly, [Schwab 2001] showed there is no direct relation between Floquet multipliers and disturbance rejection, which was measured as the area of the basin of attraction.

How is “actual disturbance rejection” usually measured?

In [Hobbelen 2007] and [Byl, Tedrake 2006], the “actual disturbance rejection” of a biped robot is computed via simulation. In both papers, an uncontrolled passive-dynamic biped is started from the particular state at which robustness is to be measured. The robot is then disturbed by a small amount each step, and the number of steps is counted until the robot falls down. The type of disturbance used in both experiments was varying the downhill slope slightly at each step. This type of disturbance obviously does not consider all possible

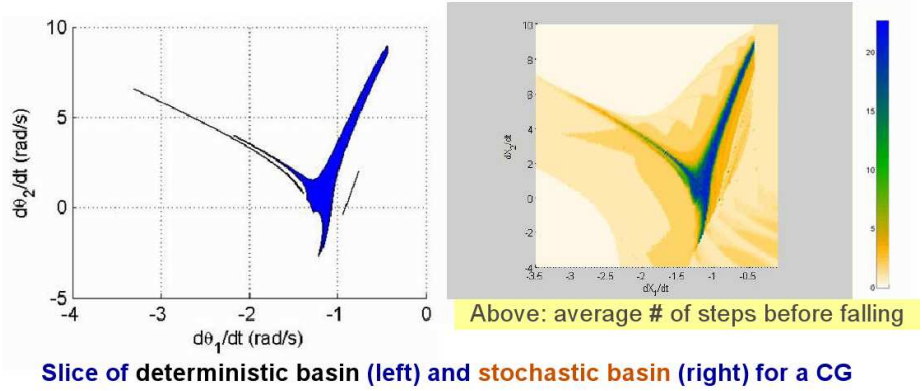


Figure 1.5: **Mean First Passage Time of a compass biped.** *Left:* A 2D slice of the 4D region of attraction of the limit cycle is plotted. *Right:* The same graph is plotted using the MFPT of each state. Reprinted from [Byl, Tedrake 2006] without permission.

disturbances, but is a reasonably good choice for reasons justified in [Hobbelen 2007]. This experiment is repeated many times for the same state, and the mean number of steps walked is then called “actual disturbance rejection” by [Hobbelen 2007]. There is some weak experimental verification that this measurement of robustness correlates well with the real world, presented in [Wisse 2004]

In this paper, this ‘multi-step, averaged’ gait robustness is not studied. Methods which require averaging are computationally intensive, not deterministic, and it can be difficult to calibrate the magnitude and type of the disturbance applied to the robots at each step. However, there seems to be some correlation between the metric of gait robustness proposed in this thesis and “actual disturbance rejection”. This is discussed further in Section 2.4.

Why are other metrics of gait robustness not ideal?

There are two recent pieces of literature which are related in spirit to the work of this thesis. [Byl, Tedrake 2006] present a metric of robustness called the Mean First Passage Time (MFPT). In words, it is the average time that it takes for a robot to fall, if it is perturbed a small amount once each step. The advantage of this simple measurement is primarily that it allows one to map out the robustness of many different starting points, both inside and outside the limit cycle’s region of attraction. Also, it can be calculated somewhat more quickly than would be expected thanks to a clever mathematical simplification. A figure from [Byl, Tedrake 2006] is reprinted in figure 1.5 for convenience.

The primary disadvantage of the MFPT may actually be that it provides too much information. One can look at figure 1.5 for a long time before being able to make any simple conclusions about the robustness of the robot, or even compare the robustness to other robots. Viewing the limit cycle basin of attraction in the angular velocity domain is similarly problematic, for reasons discussed in Section 2.2. Viewing the robustness of

robots with more than 2 degrees of freedom is nearly impossible, and comparisons between robots made with these metrics may be misleading. The physical meaning of the MFPT is also somewhat vague; should the average time be considered over the whole limit cycle, the basin of attraction, or just at one point? Obviously a longer walking time is better, but two robots could presumably have the same average walking time, but one robot might be much more sensitive to disturbances in a particular direction.

The other recent piece of related literature is [Hobbelen 2007], which presents a measure of robustness called the Gait Sensitivity Norm. The Gait Sensitivity Norm is a general method that is deterministic, can be calculated relatively quickly, and has good correlation with “actual disturbance rejection”.

However, using the Gait Sensitivity Norm to measure robustness requires careful thought; the researcher who uses this metric must carefully select gait stability indicators, as well as choose representative disturbances. The type of disturbance considered in [Hobbelen 2007] was varying the slope of the ramp, and the indicators of stability chosen included step length and step time. While these decisions were carefully considered and well justified, it is presumable that other disturbances – say, from the wind or friction at the hip joint – might affect the stability of some robots much more than others. Choosing representative disturbances and indicators might become very difficult as models become more complex.

Finally, a conservative engineer would prefer a worst-case robustness measurement rather than an average value, although both can certainly be useful measurements and will correlate to some degree. Unlike the metric described in this thesis, neither the MFPT or the Gait Sensitivity Norm are worst-case measurements. A worst-case measurement will be superior to averaged metrics especially when studying the effect of a controller on robots, because the number of experimental trials required to determine robustness is comparatively smaller.

What are the advantages of the metrics of gait robustness presented in this thesis?

The primary measure of gait robustness presented in this thesis is called the Impulse Disturbance Rejection radius, written r_{IDR} . Details of its definition and rationale are discussed in Chapter 2. Very briefly, it is the smallest, deterministic change of the momentum that moves a system from its limit cycle to an unstable region.

r_{IDR} has several advantageous properties as a metric of gait robustness.

1. It is a general metric applicable to any system which has a limit cycle with an attractive region, and another region in which states do not converge to the limit cycle.
2. It is applicable to systems both with and without control systems. In this thesis, however, only uncontrolled systems are studied.
3. It is a worst case metric suitable for conservative engineering practice. Once nondimensionalized, the robustness of robots with different mechanical structures or degrees of freedom can be fairly compared.

4. It provides information about the worst-case disturbances, specifically the direction and magnitude of the worst-case disturbance, so that robot designers can learn more about the reason for a particular stability or instability.
5. It is a one dimensional quantity that is easily graphed and has an easily understood physical meaning: the size of the worst-case disturbance of the generalized momenta of the system.
6. Although r_{IDR} is not a coordinate invariant quantity, it is closely related to a coordinate invariant measurement r_{EDR} . See Section 2.6.1.
7. Simulations results indicate a correlation between r_{IDR}^2 or r_{EDR} and multiple disturbance rejection such as the “actual disturbance rejection” mentioned in the previous section. See Section 2.4 for details.

There are two main problems with using r_{IDR} to measure robustness. First, it requires a rather large computational effort require to calculate. This discussed in Section 2.6.2. Second, it is very difficult to solve for the quantity analytically.

Finally, analyzing robustness by measuring the size of the worst-case, single-impulse disturbance is certainly not a new idea. Linear systems theory has used the concepts of gain/phase margins for decades. More recently, [Hobbelin 2007] even mention using some dimension of the basin of attraction to measure robustness, but dismiss it as being too computationally intensive or difficult to measure. In light of this statement, perhaps an important contribution of this thesis is to show that this measure of robustness is in fact not too difficult to approximately calculate using a modern computer.

1.4.2 Why are existing actuators not well suited for use in natural-dynamic machines?

The impedance of most actuators is too high for use in natural dynamic systems. As noted by [Hurst 2004] and [Pratt, Williamson 1995] rigid actuators dominate the dynamics of a system, especially during impacts. A new approach is needed to control natural dynamic machines. For this purpose, an actuator which controls torque is greatly preferred to one which merely position.

The author has great respect for the work of [Robinson 2000, Pratt et al 2001], who developed the Series Elastic Actuator (SEA). At low bandwidth, the SEA behaves very close to a perfect force or torque actuator; exactly the type of actuator needed for a natural-dynamics robot.

This thesis presents an extension of the SEA design. It is called the Variable Stiffness Series Elastic Actuator (VSSEA). The architecture of the two devices are related, although the VSSEA incorporates two antagonistically paired nonlinear springs and an additional motor. In this way, the VSSEA is related to the approach by [Hurst 2004], although a different topology of springs and motors was chosen for energy-efficiency considerations. The VSSEA is, as far as the author is aware, the only such linear actuator to use this particular topology. The details of the VSSEA design are described in Chapter 4.

The primary advantage of the VSSEA architecture is that it allows independent adjustment of position and effective spring stiffness. This could potentially greatly improve energy efficiency of a robot; most antagonistic actuators require the motors create large torques to create an effective high stiffness. In the VSSEA, a level of stiffness can be held mechanically and does not require any work.

A secondary advantage is that if the VSSEA motors are locked, a system which incorporates VSSEA actuators can be studied as a purely passive-dynamic system. These advantages are discussed in Chapter 4.

The utility of variable stiffness in passive-dynamic locomotion is also justified by the data in Section 3.8. It is shown that by varying the stiffness of the interleg spring, the passive-dynamics a biped can be adapted to walk both more efficiently and more robustly at a given forward velocity.

Chapter 2

METRICS OF GAIT ROBUSTNESS

This chapter introduces the Impulse Disturbance Rejection radius and Energy Disturbance Rejection radius, two metrics of gait robustness that are used extensively in this thesis.

2.1 Stability vs. Robustness

In this thesis, we make a distinction between *stability*, which is a yes/no value indicating whether a robot continues to walk or not, and *robustness*, which is a measure of *how* stable the robot is. Robustness is thus a quantifier, while stability is a property of the system. Stability is concerned with infinitesimally small changes near an orbit, and robustness is concerned with large disturbance rejection.

The stability and robustness of passive-dynamic robots has traditionally been examined via eigenvalue analysis of linearized models, such as in [McGeer, 1988]. It is generally thought that if the linearized model has eigenvalues that are significantly below one, the robot is thought to be more robust. Although linear analysis is relatively straightforward, such approximations only yield accurate results close to the linearization point, and may mislead us about the large-disturbance robustness of the robot. Other techniques to analyze stability such as Floquet multiplier analysis, which linearizes about points on an orbit, do not solve this problem. Measurement of stability via eigenvalues is a differential property around a point and in general may not be related to stability at other points; fundamentally asymptotic stability and large disturbance robustness are different quantities.

In contrast to the eigenvalue approach, which linearizes the system model, we investigate the full nonlinear equations of motion of a robot via simulation. Rather than look at the linearized system stability near the limit cycle, we instead investigate how far one can safely go away from the limit cycle in any direction and still return to it. We now proceed to define this quantity more precisely.

2.2 r_{IDR} and r_{EDR} : Name and Definition

The main definition of gait robustness used in this thesis is called the Impulse Disturbance Rejection radius, written r_{IDR} . In words,

r_{IDR} is defined as the length of the worst-case impulse which moves the system from any point on the limit cycle to any state which does not return to the limit cycle.

Mathematically, it can be defined for conservative Lagrangian systems as:

The Impulse Disturbance Rejection radius $r_{IDR} \in \mathbb{R}$ of a system with a Lagrangian \mathcal{L} and generalized coordinates q is defined as

$$r_{IDR} = \min \|p_x - p_y\|_2, x \in \mathbb{Q}_{NR}, y \in \mathbb{Q}_{LC}$$

where \mathbb{Q} is the configuration space of the system. Here $\mathbb{Q}_{LC} \subseteq \mathbb{Q}$ is the set of states passed through during a circuit of the limit cycle, and $\mathbb{Q}_{NR} \subseteq \mathbb{Q}$ are states which result in the system not returning to the limit cycle. The notation $(\dots)_x$ means evaluated at a point x . The norm is Euclidean.

It is also convenient to define the worst case impulse disturbance as

$$\begin{aligned} \Delta p_{IDR} &= p_{x'} - p_{y'} \\ \text{where } (x', y') &= \arg \min \|p_x - p_y\|_2, x \in \mathbb{Q}_{NR}, y \in \mathbb{Q}_{LC} \end{aligned}$$

Since the system momenta p define a great many cotangent bundles $\mathbf{T}_q^*\mathbb{Q}$, then $\Delta p_{IDR} \in (\mathbf{T}_q^*\mathbb{Q})_{x'}$. Now we can say that $r_{IDR} = \|\Delta p_{IDR}\|_2$.

Finally, we define one more quantity related to the worst-case change of kinetic energy induced by an impulse disturbance. We call it the “Energy Disturbance Radius” because it measures the length of an impulse disturbance in units of kinetic energy. First we define the worst case disturbance Δp_{EDR} as

$$\begin{aligned} \Delta p_{EDR} &= p_{x'} - p_{y'} \\ \text{where } (x', y') &= \arg \min (p_x - p_y)^T M^{-1} (p_x - p_y), x \in \mathbb{Q}_{NR}, y \in \mathbb{Q}_{LC} \end{aligned}$$

and use this to define

$$r_{EDR} = \frac{1}{2} \Delta p_{EDR}^T M^{-1} \Delta p_{EDR}$$

Here M is the inertial matrix (tensor) of the Lagrangian system. Since M is a metric tensor of the Riemannian space \mathbb{Q} and $\mathbf{T}_q^*\mathbb{Q}$ is a linear space, r_{EDR} is a coordinate invariant quantity. We could also have written $r_{EDR} = \frac{1}{2} \Delta \dot{q} M \Delta \dot{q}$ if we wished to express r_{EDR} in terms of generalized velocities.

Slightly more precisely, we can say that r_{IDR} is the shortest distance between the limit cycle and an unstable region, measured on the system’s cotangent bundle – the space defined by the generalized momenta of the system. Similarly, r_{EDR} is another shortest distance between the limit cycle and an unstable region, but this time its length is measured using the inertial (metric) tensor M of the system. r_{EDR} is a coordinate invariant quantity but r_{IDR} is not. See Section 2.6.1 for more information.

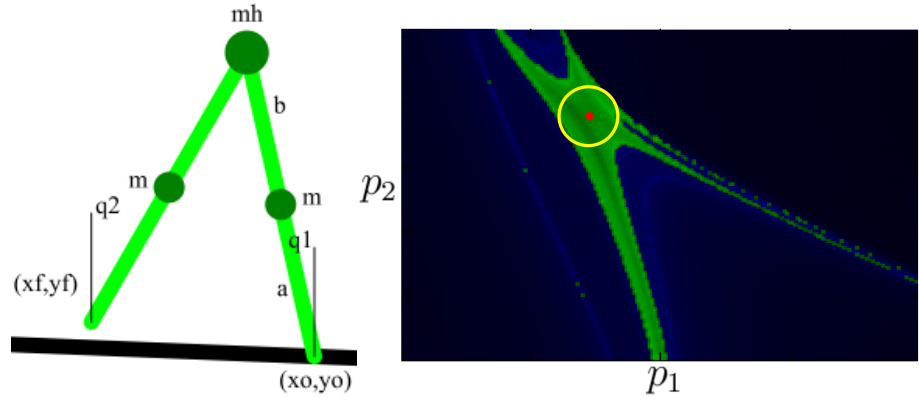


Figure 2.1: **Graphical interpretation of r_{IDR} .** *Left:* A compass biped. *Right:* A 2D slice of the 4D limit cycle basin of attraction of the compass biped. Specifically, this plane is the cotangent bundle $T_q^*\mathbb{Q}$ at the post-collision instant configuration. The green area is the attractive region of the limit cycle; darker green indicates it returns more quickly to the limit cycle. Blue states do not return to the limit cycle, and dark blue states indicate the states where the robot falls down more quickly. The red dot is where the limit cycle passes through this 2D section of the 4D space. The radius of the yellow circle r_{IDR} . This figure is for illustration purposes and measurements are not to scale.

The graphical interpretation of these metrics is to imagine a hypersphere expanding from the limit cycle, as is shown in figure 2.1. r_{IDR} is the largest such hypersphere that fits entirely in the basin of attraction, considered in the space defined by the system's generalized momenta. r_{EDR} is the largest hypersphere that fits entirely in the basin of attraction, considered in the Riemannian space defined by the metric tensor.

The physical interpretation of these metrics is simple: the robot's state at the limit cycle can be disturbed once by any impulse smaller than r_{IDR} or r_{EDR} , at any instant in time, in any direction, and the robot will not fall over.

The only difference between r_{IDR} and r_{EDR} is how the length of the impulse is measured. The former considers distance in terms of change in momenta, and the latter considers distance in terms of change of kinetic energy. This way distance in the generalized momenta space is measured is the only difference between the two. All simulation methods, experiments, and general philosophy of large-disturbance robustness is the same for both metrics, so frequently they will be both be referred to as simply r_{IDR} .

In this thesis, r_{IDR} is computed via numerical simulation. For details on why this measurement is analytically difficult to determine, refer to Section 2.5

2.3 Applicability, Properties, and Limitations of r_{IDR}

Because the definition r_{IDR} is rather loose, it is applicable to a large class of systems. It can be defined for any system with one or more limit cycles, as long as a distinction can be made between states which return to a particular limit cycle and states which do not. It is applicable to systems both with and without controllers, in a variety of different operating environments.

It is also important to note that r_{IDR} is a conservative measurement. It is entirely possible for a system to be very robust against the most common types of disturbances, but still have a small r_{IDR} because there are some (perhaps unlikely) relatively minor disturbances which move the system to a non-returning state.

Note that r_{IDR} is defined in terms of disturbances to the generalized momenta of the system. This is a better choice than joint velocities; two robots with different distributions of leg mass may require impulses of different magnitude to disturb their joint velocities by the same value. Therefore, the physical meaning of the length of the worst-case disturbance would vary based on the model being studied. By using momenta, this problem is resolved; impulse magnitudes are a fair comparison of disturbance rejection for different models, assuming that the system coordinates for two models are defined in the same way.

Similarly, r_{EDR} has a physical meaning that can be shared even between models which do *not* have coordinates defined in the same way. The change in kinetic energy created by an impulse disturbance is a quantity that may be used to fairly compare the robustness of any two models of similar mass.

There are several objections to using r_{IDR} or r_{EDR} to quantify robustness. The most severe objection is that they consider only disturbances to the generalized momenta p , and not the configuration q of the robot. It is conceivable that the robot might be very sensitive to impulsive disturbances in some postures and less sensitive in others. A full analysis of disturbance rejection would therefore have to assess all possible disturbances from all possible postures, meaning that r_{IDR} is in some ways an incomplete measurement of the gait robustness.

This objection can be restated as a question, “Does r_{IDR} , which considers disturbance rejection against single perturbations, also correlate well to rejection of continuously varying disturbances or disturbances in other postures?”

This is a good question, and the answer to this question is addressed in Section 2.4. However, this objection may not be as bad as it seems; in fact, it is likely that there will be a rather good correlation between the system’s robustness to single impulsive disturbances and the robustness to disturbances in the entire state space, at least for the class of dynamic systems which exhibit limit cycle walking. Let us consider the compass biped model for a moment to explain.

Assume that the compass biped is most sensitive to disturbances at the instant immediately following heelstrike – i.e. the start of a new step. It is most sensitive at this moment because this is the instant that is furthest from the only stabilizing event in this passive-dynamic system: the heelstrike, the instant in which energy is gained or dissipated depending on the specifics of the collision.

If we perturb the generalized momenta of a robot walking at the limit cycle at this

instant, the next step will be a different step length, and presumably the robot at this posture is less robust to disturbance. However, because the definition of r_{IDR} consider stability over several steps, in a sense we are also measuring the size of the limit cycle's attractive region in the momenta planes defined at this new posture, as well as any other postures the robot goes through on its way back to the limit cycle. Because of this, we should be able to reasonably assume that if we see a large basin of attraction on the $\mathbf{T}_q^*\mathbb{Q}$ plane at the limit cycle, this will correspond to a large basin of attraction on \mathbb{Q} .

Said another way, for passive-dynamic walking systems similar to the compass biped with an $2n$ -dimensional state space $\mathbb{Q} = (p_1, \dots, p_n, q_1, \dots, q_n)$, we should expect to see a strong (scaled) correlation between the hypervolume of the basin of attraction in n -dimensional momenta space $\mathbf{T}_q^*\mathbb{Q} = (p_1, \dots, p_n)$ and the hypervolume of the limit cycle's basin of attraction in \mathbb{Q} . This assumption was visually confirmed via examining cotangent space graphs created via simulation, but is not proven here.

Finally, another limitation of r_{IDR} is that it says nothing about how fast convergence to the limit cycle occurs. Presumably, some sort of gradient, contraction, or eigenvalue-based analysis might yield insight into this information, but such approaches are not investigated here.

2.4 Does r_{IDR} correlate well with multiple-disturbance robustness?

Excellent work has been done by [Hobbelen 2007] related to verifying that a particular metric of robustness is actually measuring the robustness of a system.

In [Hobbelen 2007], good correlation is shown between the largest single deterministic disturbance and the “actual disturbance rejection” of the robot. The definition of r_{IDR} is essentially similar to what [Hobbelen 2007] refer to as measuring a single deterministic disturbance. However, in [Hobbelen 2007], only a single type of disturbance is studied – that of changing the ramp angle. In this thesis, we use a disturbance to the system momenta, which is a more general type of disturbance.

Interestingly, although r_{IDR} and [Hobbelen 2007]’s ‘actual disturbance rejection’ measurements are not strictly equivalent¹, there appears to be good correlation between r_{IDR} and “actual disturbance rejection”. A visual comparison between [Hobbelen 2007]’s metric and r_{IDR} for the same model, shown in figure 2.2, may be convincing.

The experiment results shown in figure 2.2 are very simple. For a constant slope of $\phi = 0.04$ rad, using values of $a = 0.0, b = 1.0, m = 0.005, mh = 0.99$ for the compass biped, the effect on r_{IDR} was studied. The only difference between the parameters used to measure r_{IDR} and the those studied in [Hobbelen 2007] are that in this simulation the feet are not completely massless. Thus, the model differs very slightly from the simplest walking model studied in [Garcia 1998]. This difference is required for practical reasons; without mass at the feet, the simulator cannot measure r_{IDR} .

¹Strictly speaking, for some there are some states $(q_1, \dots, q_n, p_1, \dots, p_n) \in Q$ which cannot be reached merely by adding a single impulse at the limit cycle and letting the system’s time dynamics unfold. Therefore, it is not strictly accurate to compare [Hobbelen 2007]’s metric and r_{IDR} ; the former is a measure of multiple disturbance rejection and the latter is a measure of single disturbance rejection.

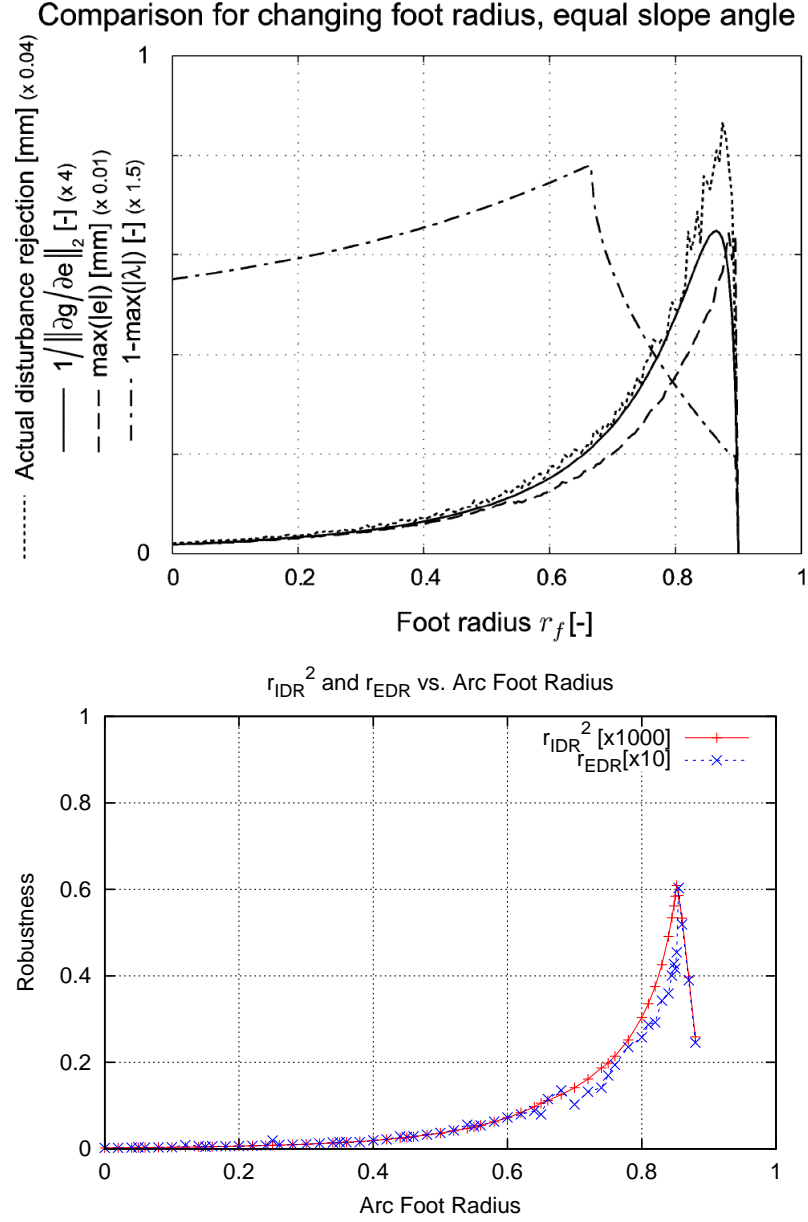


Figure 2.2: **Correlation between r_{IDR}^2 and the Gait Sensitivity Norm.** *Top:* Various gait robustness metrics plotted against actual robustness. (From [Hobbeln 2007], used without permission.) *Bottom:* r_{IDR} and r_{EDR} values for essentially the same experiment, although with leg masses that are not truly massless – they have a combined mass of about 1 percent of the hip mass. Regardless, measurements of robustness appear to correlate well with [Hobbeln 2007]'s metrics, although . Please forgive the slight amount of numerical noise present in the simulation measurement of r_{EDR} . Given sufficient simulation time, the curve becomes smooth like the r_{IDR} curve.

Looking at the two figures, we can see a reasonably good correlation between the gait sensitivity norm, r_{IDR}^2 , and r_{EDR} for a range of feet radii. This suggests that all three metrics are measuring something akin to the same physical quantity, and adds further support to the claim that eigenvalue-based measures of robustness are very likely misleading researchers about the robustness of certain highly nonlinear systems.

2.5 On the Difficulty of Finding r_{IDR} Analytically

The concept of measuring the size of the worst-case single impulse disturbance to a dynamic system is not a new idea, although the author is unaware of any prior research applying the concept to the robustness of bipedal robots. Unfortunately, r_{IDR} is a difficult quantity to derive analytically for most systems, especially hybrid systems with switched dynamics such as those found in walking systems.

As an alternative to using r_{IDR} , the author considered using contraction theory[Slotine 2004] to take the first variation of the Poincare map, and find the region that a robot's basin of attraction is contracting. At the end of the day, however, using contraction theory in this way is different than the property of returning to the limit cycle; one is a differential property, the other is a distance on a manifold. It seems possible, even probable, that many passive dynamic robots when disturbed may move away from the limit cycle at some instants, then move closer to it at other instants. Contraction theory is a very strong property, a form of asymptotic convergence. However, it is unclear whether most nonlinear biped systems converge asymptotically or not; worse, you cannot examine asymptotic stability on just the cotangent bundle $\mathbf{T}_q^*\mathbb{Q}$, because this plane is different for each step length and disturbances result in the robot taking a variety of step lengths as it returns to the limit cycle!

Perhaps if a distance $d_{LC}(q, p)$ between the limit cycle and an arbitrary state (q, p) could be defined, a coordinate system could be found where the distance to points on the limit cycle does indeed contract. However, a formal treatment of this would go deep into the theory of manifolds, functionals, and differential geometry, and computational feasibility would still be an issue.

Worse, even if this is possible, there is still a fundamental difference between such 1-step asymptotic stability, which considers the robot stable if and only if the state space contracts each step, and the more general r_{IDR} , which considers the stability of the robot over several steps. A quote, taken slightly out of context but very applicable here:

“The key insight is that stability does not necessarily need to be obtained within a single step (the trajectory control approach), as long as the walking motion is stable over the course of multiple steps. In other words, the walking motion must be regarded as a cyclic motion which only needs to be stabilized in its entirety.” – [Wisse 2004]

Certainly, the concept of ‘asymptotic stability’ is very powerful and guarantees stability and convergence to a trajectory if phase space contraction and boundary conditions are met. However, for bipedal robots, the concept of stability as being ‘states which return to the limit cycle’ is more appropriate, and may be applicable to a larger class of systems. Unfortunately, it is also much more difficult to treat analytically.

In conclusion, somewhat sheepishly the author must admit that he sees no way of analytically deriving r_{IDR} , given the limited nonlinear analysis methods currently available to him. This is the reason that r_{IDR} is computed exclusively via simulation in this thesis.

2.6 Common Questions and Answers

2.6.1 Are r_{IDR} and r_{EDR} coordinate invariant measurements?

Although not analytically shown, based on simulation results the author believes that r_{IDR} is not a coordinate invariant measurement, but r_{EDR} is. This was determined by simulating two identical compass bipeds using equations of motions derived in two different generalized coordinate systems. Although the resulting disturbances Δp_{IDR} for each coordinate system were very similar, they did not refer to the exact same physical disturbance. That is, the worst-case disturbance in one generalized coordinate system did not match the worst-case disturbance in the other coordinate system, when a coordinate transform was used. Thus, the Δp_{IDR} calculated via simulation for both of these coordinate systems were found to be different, and the resulting length of r_{IDR} was also markedly different.

However, it is thought that the quantity r_{EDR} is coordinate invariant. When the above-mentioned experiment was repeated using r_{EDR} , results showed that the disturbances Δp_{EDR} refer to the same physical disturbance regardless of the generalized coordinates they are measured in. That is, the two disturbances are related by a simple coordinate transform. The length of r_{EDR} was also identical to the appropriate number of significant digits.

The invariance of r_{EDR} is not proven here. However, based on the facts that it is a measure of change in kinetic energy, it uses a metric tensor to measure a distance in a linear space, and also that simulation results suggest invariance strongly, it seems likely that it is indeed an invariant quantity.

The fact that r_{IDR} is not coordinate invariant is one reason that all of the bipeds considered in this thesis have the generalized coordinates q defined in the same way, and have only two degrees of freedom. In more complex experiments, it is more likely that r_{EDR} is the more useful quantity.

2.6.2 What is the computational cost of measuring r_{IDR} ?

On a single 2.4Ghz Pentium 4 with 1G of RAM, the simulation takes approximately 150 seconds to compute r_{IDR} or r_{EDR} for models with a two generalized momenta. With a more sophisticated search algorithm, perhaps the computation could be performed faster. The simulation used to find r_{IDR} uses an unsophisticated two-stage search algorithm described in Appendix D.3.

2.6.3 What happens to the robot when it is disturbed by Δp_{IDR} or Δp_{EDR} ?

The robot takes several steps and falls forward. None of the robots studied in this thesis fell backward when disturbed by these worst-case impulses. This is because immediately surrounding the boundary of the basin of attraction of the limit cycle is a region of states

which result in the robot falling forward. This is a effect has been described before in [Wisssse 2004], and is caused by the robot taking too small a step relative to its forward velocity.

It is difficult to describe verbally what the robot's gait looks like when the worst case disturbance is simulated, especially for more complex models. However, if we view the behavior of reference biped described in Section 3.4 when perturbed this way, we can make a qualitative statement about its motion when perturbed by Δp_{IDR} . After perturbation, the reference biped takes a large step followed by several small steps, and then falls forward. The small steps have very little ground clearance and the foot nearly scrapes the ground. Indeed, looking at the foot clearance of the non-stance foot may be an easy way to visually tell whether or not a robot is about to fall.

2.6.4 How many steps does it take for the robot to fall when disturbed by Δp_{IDR} or Δp_{EDR} ?

Theoretically, if the robot is disturbed by exactly r_{IDR} , it will be right on the boundary of stability, neither falling down nor returning to the limit cycle. In practice, it depends on simulation accuracy and how long the simulation searches for r_{IDR} using the procedure described in Appendix D.3. Since the simulation artificially restricted the number of steps considered, generally this resulted in about 15-20 steps before the robot fell. A graph of the total system energy when disturbed by the worst-case impulse Δp_{IDR} is shown in figure 2.3. The total energy approaches some tipping point gradually, crosses it, and then falls over a few steps later.

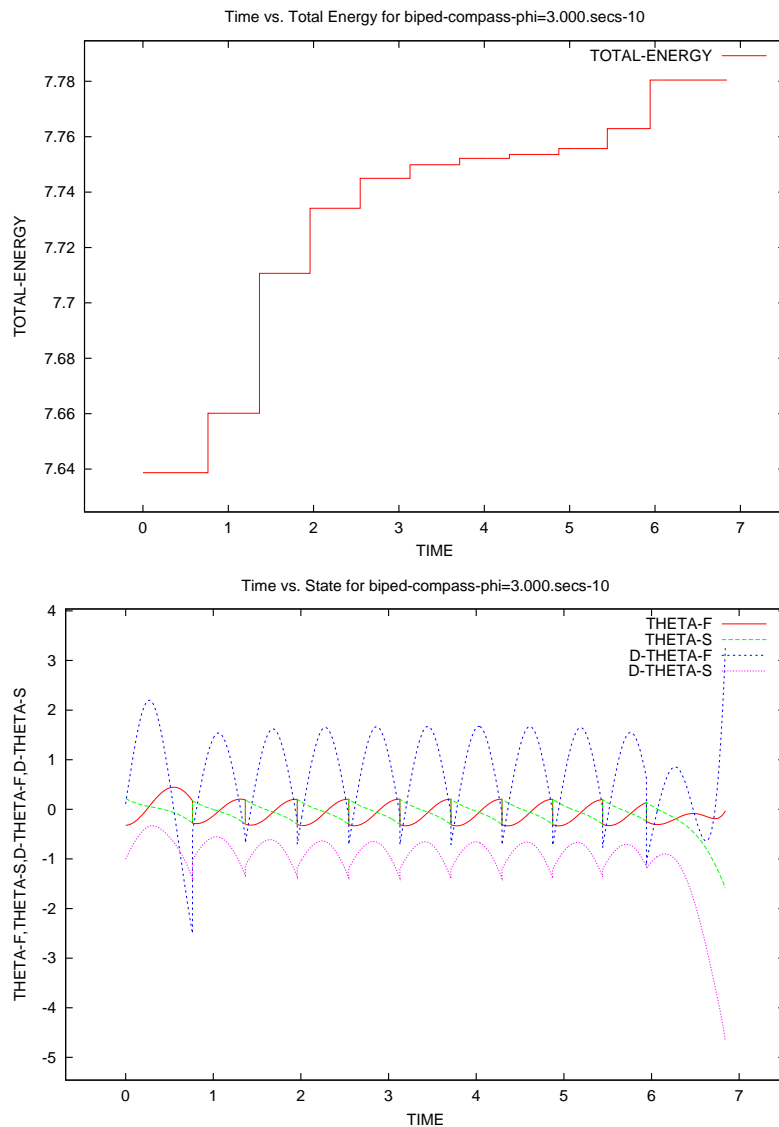


Figure 2.3: **Total system energy of reference biped disturbed by Δp_{IDR} .** *Top:* Total system energy as a function of time when a compass biped is disturbed by the worst-case impulse Δp_{IDR} . Energy rises slowly, approaches some unstable value, crosses the value, and then falls. *Bottom:* The states of the system during the disturbance. It is very difficult to tell visually that the biped is actually close to falling.

Chapter 3

OPTIMIZING THE GAIT ROBUSTNESS OF PASSIVE-DYNAMIC BIPEDS

In this chapter, we present simulation results which use the definitions of r_{IDR} and r_{EDR} developed in the proceeding section. Using these metrics we quantitatively measure the effect that various mechanical structures have on the robustness of purely mechanical limit cycle walking.

With an infinite energy budget and perfect actuators, we can obviously make any robot as robust as we desire by controlling the dynamics of the robot very strongly. But with a finite energy budget, is there always a tradeoff between robustness and energy consumption? Or are some robots not only more stable but also more efficient? Can we have our cake and eat it too?

As with [Srinivasan 2006], this thesis advocates an approach of gait synthesis, rather than gait analysis, towards understanding legged locomotion more deeply. However, the results in this paper are concerned primarily with the details of robot construction rather than understanding animal locomotion. The predictive power of these simulations may not be significant.

Starting with a compass biped, one of the simplest biped robot models that is physically realizable,¹ we add various mechanical features to the robot and monitor the effect of the features on the nondimensionalized velocity and robustness of the limit cycle walking. The focus of this chapter is restricted to models with only two degrees of freedom, because disturbances to the generalized momenta can be easily graphed and visualized.

In this thesis, the mechanical structures studied are limited to a few very simple foot shapes, different mass distributions, a kinematically constrained torso, and linear springs at the hip and ankle. Knees are not considered in this thesis.

There have been several observations by various researchers that certain mechanical features improve the gait robustness of physical robots, but there has been little research into *why* certain features are more beneficial. [McGeer, 1988] informally comments that a human-like ratio of 45/55 upper/lower leg lengths resulted an experimental knee-walker walking more robustly. One wonders why this particular ratio is good, if it is optimal or not, and if the mechanical structure of humans is optimized for mechanical robustness in some way. It seems plausible that evolution would naturally select for animals with legs that move with good energy efficiency, robustness, and controllability, so we end this introduction with the question:

How much of human walking is purely mechanical? How much of a robot's gait

¹ Assuming, that is, that you can solve the foot-scuffing problem with some sort retracting foot. [Garcia]'s 'simplest walking model' may be simpler, and is very beautiful theoretically, but it is a model that is meant to capture the essence of walking, not to model a physical robot.

can be made purely mechanical?

3.1 Froude Number and Cost of Transport

The Froude number F_r is a dimensionless number comparing inertial and gravitational forces. It may be used to compare the velocities of objects of different sizes.

$$F_r = \frac{\text{'centrifugal force'}}{\text{'gravitational force'}} = \frac{mv^2l^{-1}}{mg} = \frac{v^2}{gl}$$

By measuring the forward velocity of a bipedal robot in terms of the Froude number and not ms^{-1} , we can more accurately compare the relative speed of locomotion of robots and animals of various sizes.

Another useful dimensionless quantity is the Cost of Transport c_t . It is a measurement of the energy that a particular machine or animal uses to move a certain amount of mass a certain amount of distance. It is generally calculated after nondimensionalization, using dimensionless distance and weight, and motion at a constant velocity is generally assumed. It is defined as

$$c_t = \frac{\text{energy}}{\text{weight} \cdot \text{distance}}$$

In some literature, the meaning of the ‘energy’ part of c_t is more precisely specified. For example, does c_t mean the metabolic energy expended by the animal, or the mechanical work done? Antagonistic muscles may co-contract in a walking animal, using energy but performing no mechanical work. Similarly, actuators may have internal friction which consumes energy but not count toward any external mechanical work that can be used for forward locomotion.

In this thesis, we follow the lead of [Collins, et al 2001] and define the mechanical cost c_{mt} to be the purely mechanical work done. The specific energy cost c_{et} is defined to be the total energetic cost required as measured by metabolic energy or battery drain.

The word “efficiency” is used a great deal in this chapter. This word will refer to the inverse of c_{mt} . That way, the words “high energetic efficiency” mean that c_{mt} is very low.

Also, it is important to note that the efficiency of a biped is often related to the speed a robot moves down a given slope. This is because there is a general relationship between step size and collision loss; longer steps result in harder collisions and more energy loss at the collision. Thus we can say for robots descending a given slope, the ones that move faster and with longer steps very likely have higher mechanical efficiency.

We will now compare the energetic efficiency of several robot systems using the proceeding definitions. It is assumed in this chapter that a downhill slope is a suitable way of comparing the control-free gait robustness of various passive-dynamic systems.

3.2 Energetic Efficiency of Passive Dynamic Systems

Arguably the most important reason to study passive- and natural-dynamic robots is their superior energetic efficiency. As should be clear from reading Section 1.3.5, at present

passive-dynamic robots have few clear advantages over the stiff, fully-actuated conventional position control approach except for their better efficiency and presumably better safety.

Therefore, we should carefully establish exactly why this increase in energetic efficiency is worth the tremendous research effort being expended. Table 3.1 is based on a similar table presented in [Collins, et al 2001]. Refer to figures 1.1 and 1.3 for photographs of selected robots.

Table 3.1: Energetic Efficiency of Various Robots

Name	Reference	c_{et}	c_{mt}
Asimo	[Kajita et al 2002]	3.2	1.6
Denise	[Wisse 2004]	5.3	0.08
Spring Flamingo	[Pratt et al 2001]	2.8	0.07
Monopod II	[Ahmadi 1998]	0.22	-
Cornell Biped	[Collins et al 2005]	0.20	0.055
Human Walking	[Collins et al 2005]	0.20	0.05
Dynamite	[McGeer, 1988]	-	0.04

Asimo, the only robot in this list which uses conventional stiff actuation systems, clearly has a much higher mechanical cost of transport than any of the other robots. This is most likely due to its stiff actuation via harmonic gearboxes, which are very precise but not particularly efficient. On the other hand, difficulties encountered when actuating passive dynamic robots seems to have prevented the researchers from actually achieving high c_{et} . This is a problem of engineering and not theory; the engineering resources of a university are dwarfed by the tremendous amount of money and labor poured into Asimo, and the quality of engineering is not as high.

We now speculate on the reason for the relatively high c_{et} of the bipeds based on passive-dynamic robots. In the case of Denise, low-efficiency pneumatics seem to be the culprit. In the Spring Flamingo, high actuator friction and a lack of concern in energy efficiency may be the reason. On the other hand, the Monopod II is an excellent example of the benefits of carefully designing the mechanical and control systems to complement each other. Its low cost of transport is due to careful use of springs and natural oscillations to improve running efficiency.

3.3 On the Choice of Mechanical Structures Studied

The decision of which mechanical structures to study – such as knees, feet, or a torso – is somewhat arbitrary. The relatively common addition of arc-shaped feet to robots, for example, is in the author’s opinion largely a holdover from the original passive dynamic walking research of [McGeer, 1988], which likened a walking robot rolling wheel. In nature, there are no animals that have arc-shaped feet, and only a few animals such as birds have feet

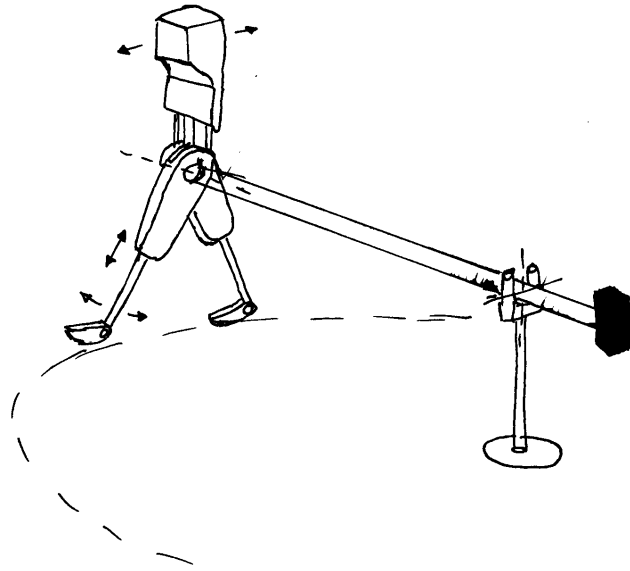


Figure 3.1: Sketch of proposed robot built from four VSSEA actuators. This sketch shows a proposed robot with two actuators in the torso that control the angles of the legs relative to the torso, and two more actuators placed in each telescoping leg. The motion of this concept robot is approximately planarized via a long boom, similar to the Spring Flamingo[Pratt et al 2001] or BiMASC[Hurst 2004].

which protrude both forwards and backwards. Such feet are also very likely not optimized for efficient walking.

The mechanical structures studied in this chapter – specifically arc feet, springs at the hip and foot, and a constrained torso – were selected because they were relatively simple mechanical additions to the compass biped model. They also could be implemented in a robot constructed using VSSEA actuators, which will be described in detail in Chapter 4. For now, assuming that four linear actuators of equal mass and length – though not necessarily spring stiffness – were used to build a robot, one natural configuration for the robot is the sketch shown in figure 3.1.

When the VSSEAs are controlled to provide energy for the system, such a robot would have a mechanical model roughly like that shown in figure 3.2(a). However, when the motors were locked, the VSSEAs would act merely as springs and the robot model would reduce to that of figure 3.2(b). There are two advantages to being able to reduce the model like this.

1. The mechanical robustness of the robot can be simply analyzed separately from its control system, by locking the actuators and treating the mechanics as a passive dynamic system.

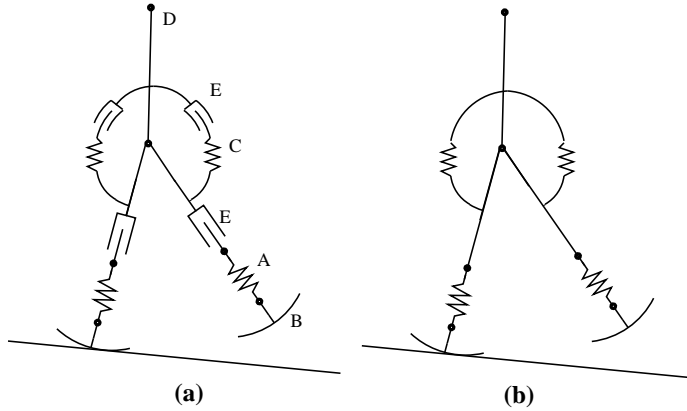


Figure 3.2: Functional models of proposed biped. (a): The functional model of the robot shown in figure 3.1 Beware: the symbols marked E that resemble dampers are actually linear actuators which change length and apply a force. When the VSSEA actuators are locked, (a) reduces to a simple passive-dynamic robot, shown in (b). More details on the VSSEA actuator can be found in Chapter 4.

2. If the mechanical system is stable enough by itself, we do not need to design a control rule that stabilizes the robot. Rather, the purpose of the control system becomes simple: keep the mechanical oscillation going. There are several techniques which can accomplish this, such as virtual gravity [Asano, Luo 2006], constant-energy control [Goswami et al 1996], and other methods such as those by [Spong 1999]. None of these systems are really stabilizing control systems; they merely keep the mechanical oscillation going.

In summary, selection of mechanical features studied in this thesis was based primarily on a particular mechanical design concept sketch shown in figure 3.1.

3.4 The Reference Biped

In the remainder of the chapter, we present data on the effects of various mechanical features. As a reference point, we start with the compass biped, shown in figure 3.3. The design parameters of this biped are $m = 0.25$, $m_H = 0.5$, $a = 0.5$, $b = 0.5$, $\phi = 3.0$, which are the leg mass, hip mass, lower leg length, upper leg length, and downhill slope, respectively. Using this arbitrary model as a departure point, we study the effects of adding more complexity to what we will call this “reference biped”.

Again, this model is just an arbitrary point to start from. It is certainly not a very robust model, and there is much that can be done to improve upon it.

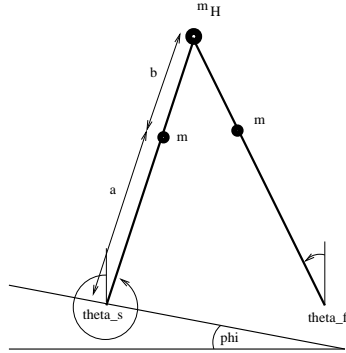


Figure 3.3: **Reference biped model.** This is the compass biped model we will use as a departure point for the experiments presented in this thesis. It has the parameters $m = 0.25$, $m_H = 0.5$, $a = 0.5$, $b = 0.5$, $\phi = 3.0$.

3.5 Notes on Numeric Methods, Graphs

Random search methods used in the simulation resulted in the possibility that true values of r_{IDR} and r_{EDR} may be slightly lower than those presented in this thesis. Therefore, assuming proper numerical integration accuracy, these simulation values are possibly only an upper bound; the exact values may lie below these curves. For more details on the techniques by which r_{IDR} was measured, please refer to Appendix D.3

Data in this chapter, unless otherwise noted, were taken on a slope of $\phi = 3.0$ degree slope (about 0.0524 rad). Robustness is measured using r_{IDR} and r_{EDR} . Walking velocity is measured using the Froude number F_r .

Some graphs exhibit rather chaotic behavior after some limit is reached. This data was removed according to the author's best judgment. It was generally too noisy to interpret anything useful from it. Therefore, these searches are only for the deterministic data, before extensive bifurcation or chaotic effects occur. Bifurcation is described further in section 3.6.2. Although chaotic solutions had in general very low r_{IDR} values as measured by the simulation, it is not clear if the numerically measured values are valid for such systems. True robustness for chaotic gaits may be higher or lower than simulation results would lead us to believe, and so are not included here.

All r_{IDR} and r_{EDR} measurements were taken by searching the post-collision instant cotangent space \mathbf{T}_q^*Q for the unstable point nearest the limit cycle. This is in accordance with the definition of r_{IDR} described in Section 2.2.

3.5.1 Explanation of Figures and Significance

There are several rather unusual graphs shown in this thesis that may require some explanation as to their significance. In general, the smaller the figure, the more the figure is intended to be used for qualitative rather than quantitative analysis. Please refer to figure

3.4 for some examples.

- **Robustness vs. Velocity Graphs:** Plotting the robustness values and F_r as we vary a parameter is difficult. Although we could graph r_{IDR} , F_r , and ϕ on a single 3D graph, finding the proper 3D perspective that expresses the information in an easy to understand form can be difficult. In the experiments in this thesis, almost all parameters resulted in r_{IDR} , r_{EDR} and F_r varying monotonically, so it was preferable to just use two 2D plots to express the data. Thus, one graph shows the change of r_{IDR} as the parameter is varied, and the other shows r_{IDR} vs F_r . An example of a pair of these graphs is Figure 3.6.
- **Cotangent Bundle:** These graphs show $(p_1, p_2) \in \mathbf{T}_q^*\mathbb{Q}$ for the post-collision instant posture. The yellow region corresponds to the basin of attraction of the limit cycle. The small circle or oval shows the size of r_{IDR} , and the cross at the center of the oval is the limit cycle generalized momenta state that passes through this cotangent space. Looking at the cotangent bundle is most useful for developing an intuitive feel for how robustness was affected by a particular mechanical structure and investigating which boundary of the basin of attraction is limiting or constraining the value of r_{IDR} . An example of this type of graph is shown in Figure 3.4:*Upper Left*. The horizontal axis defines the momenta of the free leg, and the vertical axis is the momenta of the stance leg.
- **Limit Cycle Projection:** The limit cycle for a biped with two degrees of freedom actually traces out a curve in 4D state space $(q_1, q_2, p_1, p_2) \in \mathbb{Q}$. However, at the limit cycle, because the gait is symmetric, we can project this 4D space onto a 2D plane without loss of information. The horizontal axis expresses position and the vertical axis expresses velocity. If gait bifurcation occurs and the gait becomes multi-period, it is obvious when looking at this plane; two or more loops will appear instead of one. An example of this type of graph is shown in Figure 3.4:*Upper Right*.
- **States vs. Time:** Showing the system state vs time shows the period of the gait of the robot. The length of the robot's step can be roughly computed by observing the size of the jump of the generalized position of the robot at the heelstrike. Similarly, the size of the jump of generalized velocities yields information about the amount of energy lost during the impact. An example of this type of graph is shown in Figure 3.4:*Lower Right*.
- **Total System Energy vs Time:** This shows the accuracy of the numerical integration. For most robots, constant system energy can be seen – or at least constant to smaller than 10^{-10} J per step – by looking at the scale of the vertical axis and realizing how tiny the variations in energy really are. However, if bifurcation is occurring or a disturbance occurs, the total system energy will vary from step to step. An example of this type of graph is shown in Figure 3.4:*Lower Left*.

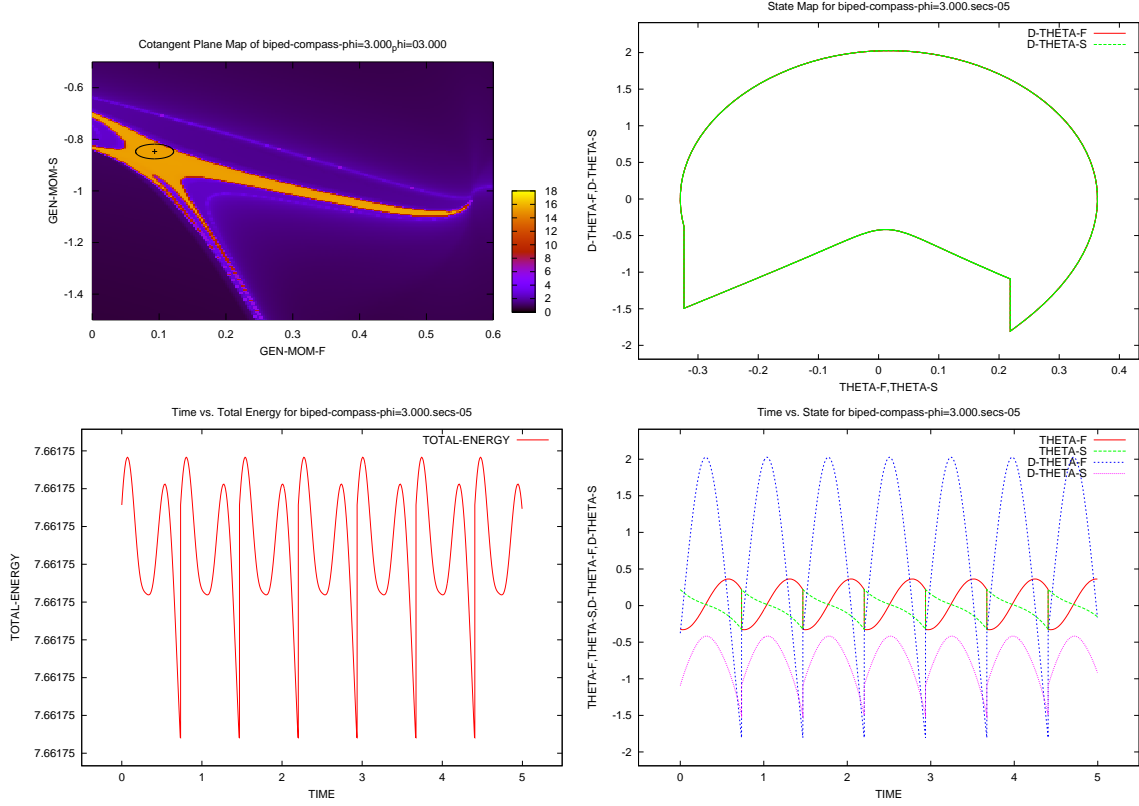


Figure 3.4: Reference Biped Data Graphs. *Clockwise from upper left:* The post-collision instant cotangent space graph, the limit cycle projected onto 2D space, a graph of states vs. time, and a graph of total system energy vs. time.

- **Robot Posture:** Finally, it can be useful to visually see what the robot looks like at the instant the cotangent bundle picture was taken. Step lengths and slope can be quickly visually confirmed. Examples of these automatically created pictures are shown in figure 3.5.

3.5.2 Is the post-heelstrike instant really the most unstable instant?

No. This was a surprise to the author and was discovered only just before this thesis was completed.

Throughout this thesis, it is assumed that size of the basin of attraction would be smallest at the instant immediately after heelstrike. This assumption was based on the observation that, for a biped robot walking down a hill, the only stabilizing event during the walking cycle is the impact between the foot and ground. It seemed reasonable to assume that the

post-collision instant would be the most unstable point in the limit cycle because it is the instant farthest away in time from the next stabilizing event. Disturbances at this instant would have the most time in which to move the system away from the limit cycle.

However, this hypothesis seems to be incorrect. In fact, the mid-stride instants were more sensitive to disturbances than instants proceeding or following the collision. Figure 3.5 shows several the evolution of the reference biped cotangent spaces as it takes a single step. Clearly, the shape of the basin of attraction of the limit cycle is very complex and changes shape throughout the stride. Also, it is obvious that the size of the basin of attraction of the limit cycle is smallest in the middle of the stride rather than near the beginning or end. This visual inspection is supported by computation of r_{EDR} and r_{IDR} .

Due to time constraints the author cannot analyze this problem further, except to say that the results in this paper are thus very likely overestimating robustness. The measurements presented are thus truly accurate only for momenta disturbances around the heelstrike collision. This is not as bad as it may sound; by far the largest disturbing event during each step is the collision. In the end, the author feels that the results in this paper are still valid and are essentially measuring the same physical quantity as the Gait Sensitivity Norm defined by [Hobbelin 2007], which does not consider disturbances that occur mid-stride.

3.6 Effect of Slope

3.6.1 Experiment Description and Motivation

In this experiment, the slope that the robot walks down is changed from $\phi = 0.1$ degrees to 5.2 degrees. The effect of this change on the gait robustness of the reference biped is examined.

The motivation for this experiment is the observation that the forward speed of a passive dynamic robot is easily adjusted by varying the downhill slope. How fast can the reference biped go before walking begins to become unstable? At what speed is the reference biped most stable? We pursue these questions in this experiment.

Data from this experiment is presented in several figures, which we now introduce for convenience.

- Figure 3.6 shows r_{IDR} and r_{EDR} plotted against values of F_r and also against values of ϕ .
- Figure 3.7 shows data for several representative data points. Specifically, it shows the cotangent bundle spaces $T_q^*\mathbb{Q}$, phase planes, and state spaces and total energy over time for robots at slopes of $\phi = 1.5, 3.0, 4.5$ degrees. These data points correspond to the reference biped moving at slow, medium, and fast speeds.

3.6.2 Discussion

What happens to the gait robustness and forward velocity of a robot as the slope changes? Increasing slope improves r_{IDR} , r_{EDR} and F_r approx-

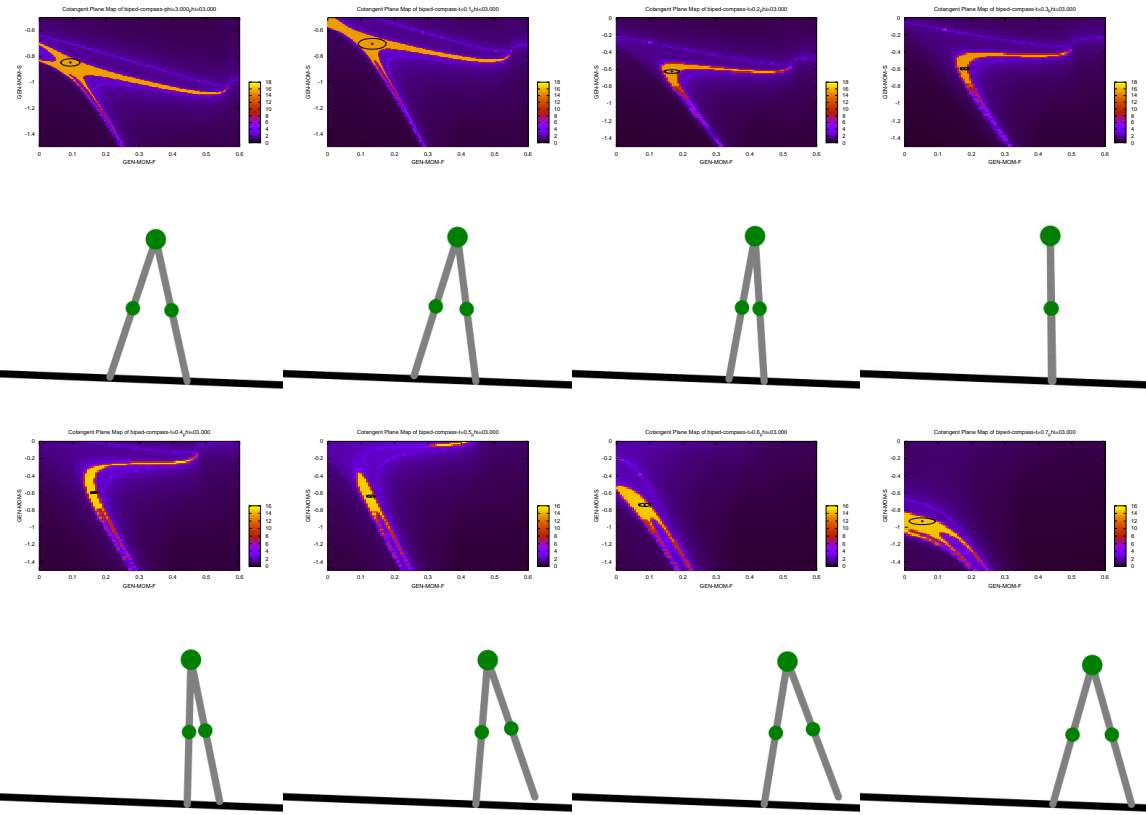


Figure 3.5: Cotangent spaces of the reference biped during a step at the limit cycle. The cotangent spaces of the reference compass biped at $t=0.0, 0.1, 0.2, 0.3, 0.4, 0.5, 0.6, 0.7$. Contrary to expectation, the moment most sensitive to disturbances was not the post-collision instant, but appears to be between $t = 0.4$ and $t = 0.5$.

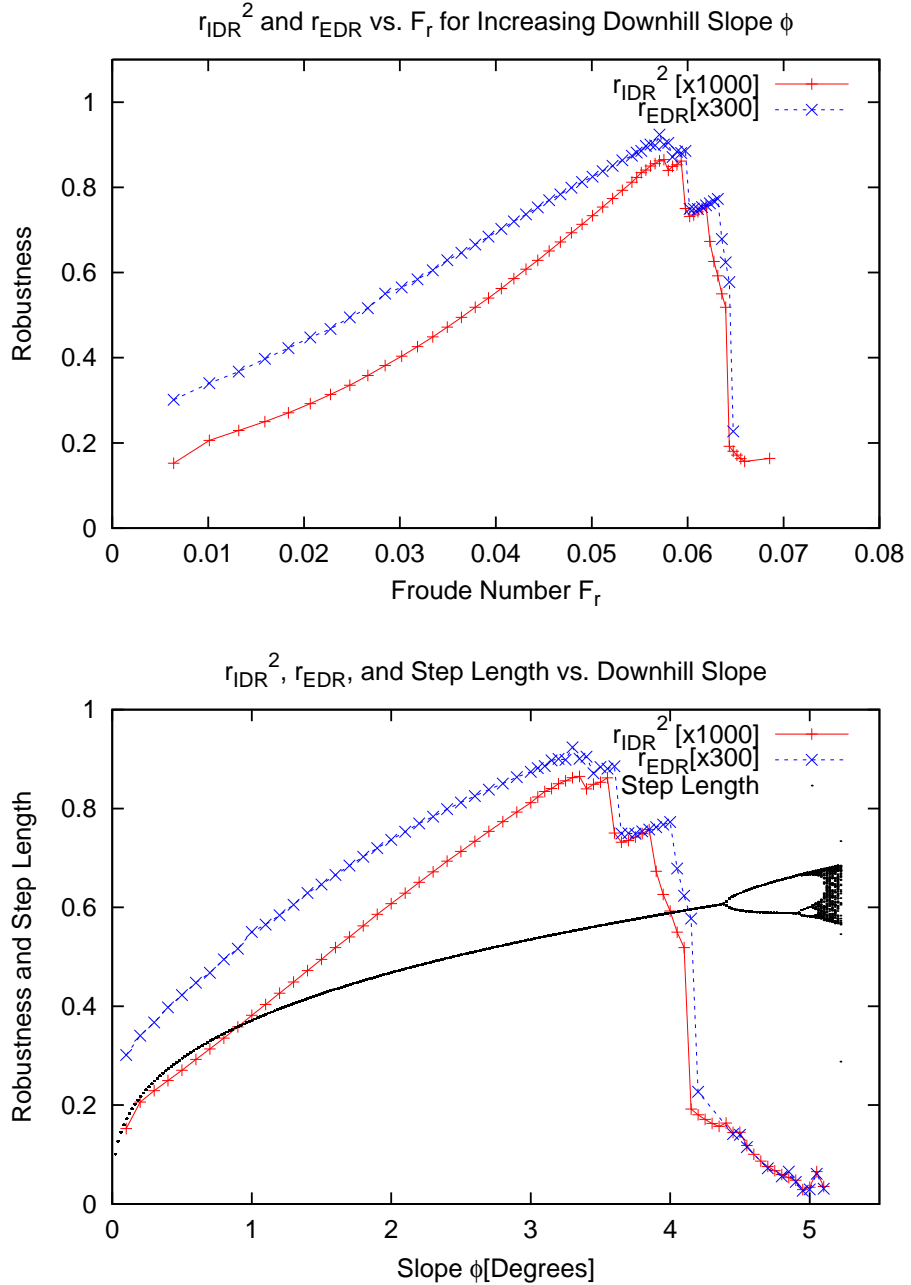


Figure 3.6: **Effect of changing the slope ϕ .** *Top:* r_{IDR} vs. Froude number for $0.1 \leq \phi \leq 4.4$ degrees. *Bottom:* r_{IDR} shown vs. ϕ for $0.1 \leq \phi \leq 5.2$ degrees. The step length of the robot when walking at the limit cycle is also shown. As can be seen, above 4.4 degrees, the step length has bifurcated, and the robot takes alternating large and small steps.

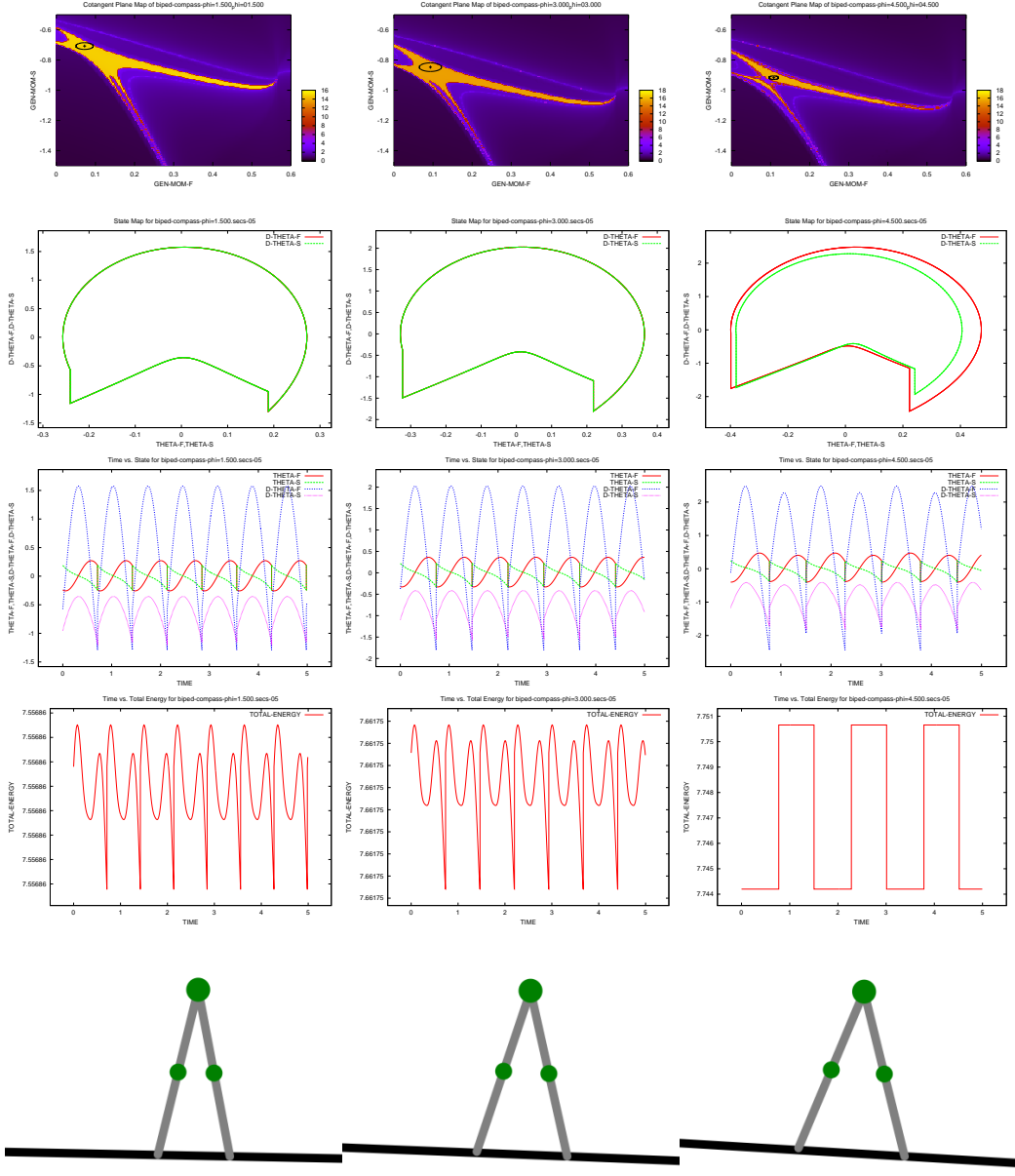


Figure 3.7: Data from robots at selected values of ϕ . From left to right, several quantities for 1.5, 3.0, and 4.5 degree slopes. From top to bottom, the graphs shown are the cotangent space, the projected state space plane, (q, p) vs time, and total system energy. In the phase plane graph of the $\phi = 4.5$ degree robot there appear to be two limit cycles. This is because the limit cycle has bifurcated at this slope, and it now takes two steps to complete one circuit of the limit cycle. In other words, the robot takes alternating small and large steps at this slope.

imately linearly until some threshold is reached and the system begins to become unstable.

We will now be slightly more precise about what this means. Consider the data shown in figure 3.6. Figure 3.6:*Top* shows r_{IDR} vs the dimensionless Froude velocity, and 3.6:*Bottom* shows r_{IDR} versus ϕ .

We can see a general trend of increased robustness and walking speed as the slope increases. Robustness peaks between a slope of 3.4 and 3.9 degrees, and then begins to decrease, dropping suddenly at 4.1 degrees. Robustness continues to decrease until no limit cycles exist at a slope of approximately 5.2 degrees.

We can see that the choice of $\phi = 3.0$ degrees for the reference biped is a fairly aggressive value. It corresponds to a rather high walking velocity, and increasing the slope much further than this will make the robot move faster but with less robustness.

On Gait Bifurcation

Passive dynamic walking robots exhibit gait bifurcation phenomena for certain sets of parameters. Bifurcation, in the context of this thesis, refers to some parameter of the limit cycle taking on more than one value during several steps. For example, when we say that “step length has bifurcated”, what this means is that period of the limit cycle is now more than one step; the robot is taking alternating large and small steps.

To understand this graphically, examine the figure 3.6:*Bottom*. The step length of the reference biped when walking at the limit cycle is plotted. For slopes $0 \leq \phi \leq 4.3$ degrees, the limit cycle has only one period. Each step at the limit cycle is the same length. However, for slopes steeper $\phi > 4.3$ degrees, the robot begins taking a large step followed by a small step. This is a two-period gait; the dynamics of the limit cycle require two steps to make a complete cycle. At $\phi = 5.0$ degrees or so, the step length parameter has bifurcated several times and it is now very difficult to predict how long the next step will be. Such gaits are called chaotic, because even though the robot is moving at its limit cycle, it is nearly impossible to predict the next step length.

Clearly, just before the first gait bifurcation begins, the value of r_{IDR} decreases sharply. As bifurcation continues and the step length becomes more chaotic, the robustness continues to decrease and eventually reaches zero when the limit cycle no longer exists.

The fact that bifurcation is occurring at the slope of $\phi = 4.5$ degrees can also be verified by carefully looking at any graph in the right column of figure 3.7.

For the remainder of this paper, we ignore bifurcation and what happens to gait robustness for multi-period gaits. The vast majority of the walking gaits studied here did not bifurcate; if they did, the data was thrown out because of the difficulty of finding r_{IDR} and F_r for robots with gaits of variable step length. To calculate the Froude number for a chaotic gait would require averaging the forward velocity over several steps, and introduce unnecessary complexity into the simulation. For this reason, limit cycles which have bifurcation are not shown.

3.7 Effect of Mass Distribution

3.7.1 Experiment Description and Motivation

In this experiment, the masses on the legs are moved about and made heavier and lighter relative to the hip mass. Specifically, in the first experiment, the lower leg length a is varied from 0.4 to about 0.9, and the effect on gait robustness is measured. The masses are held constant at $m = 0.25, m_H = 0.5$.

In the second experiment, the lengths a, b are held constant, and the mass m_H is varied from 0.05 to 0.95.

In both experiments, lengths and weights are normalized so that $a+b = 1, 2m+m_H = 1$, and the downhill slope is fixed at $\phi = 3.0$ degrees.

The motivation for this experiment is the question: what can we do to the mass distribution to make the robot as robust and energy efficient as possible?

Data from this experiment is presented in several figures which we now introduce.

- Figure 3.8: Top shows the effect of varying a on r_{IDR} and r_{EDR} , plotted against nondimensionalized forward velocity F_r . The bottom of the graph shows the same graph, but plotted against a .
- Figure 3.9: Top shows the effect of varying m_H on the values of r_{IDR} , plotted against m_H . The bottom of the graph shows the effect on r_{IDR} of varying m_H , plotted against m_H .
- Figure 3.10 shows data for several representative values of a . It shows the cotangent spaces $\mathbf{T}_q^*\mathbb{Q}$, phase planes, and state spaces and total energy over time for robots with lower leg lengths of $a = 0.52, 0.63, 0.82$. These three data points were selected because they lie on the ascending, peak, and descending values of r_{IDR} shown in figure 3.8.
- Figure 3.11 shows data for several representative values of m_H . It shows the cotangent spaces $\mathbf{T}_q^*\mathbb{Q}$, phase planes, and state spaces and total energy over time for robots with lower leg lengths of $m_H = 0.05, 0.35, 0.82$. These three data points correspond to very light, average, and heavy hip masses.

3.7.2 Discussion

What happens to the gait robustness and walking velocity of a robot as we move the masses up and down the leg? *Changing the relative lower leg length greatly affects r_{IDR} , r_{EDR} and F_r , which increase and decrease approximately linearly, with a peaking behavior. This peaking effect is presumed to be due to the change in natural pendular frequency of the swing leg, and some optimal swing period appears to exist for a given forward speed.*

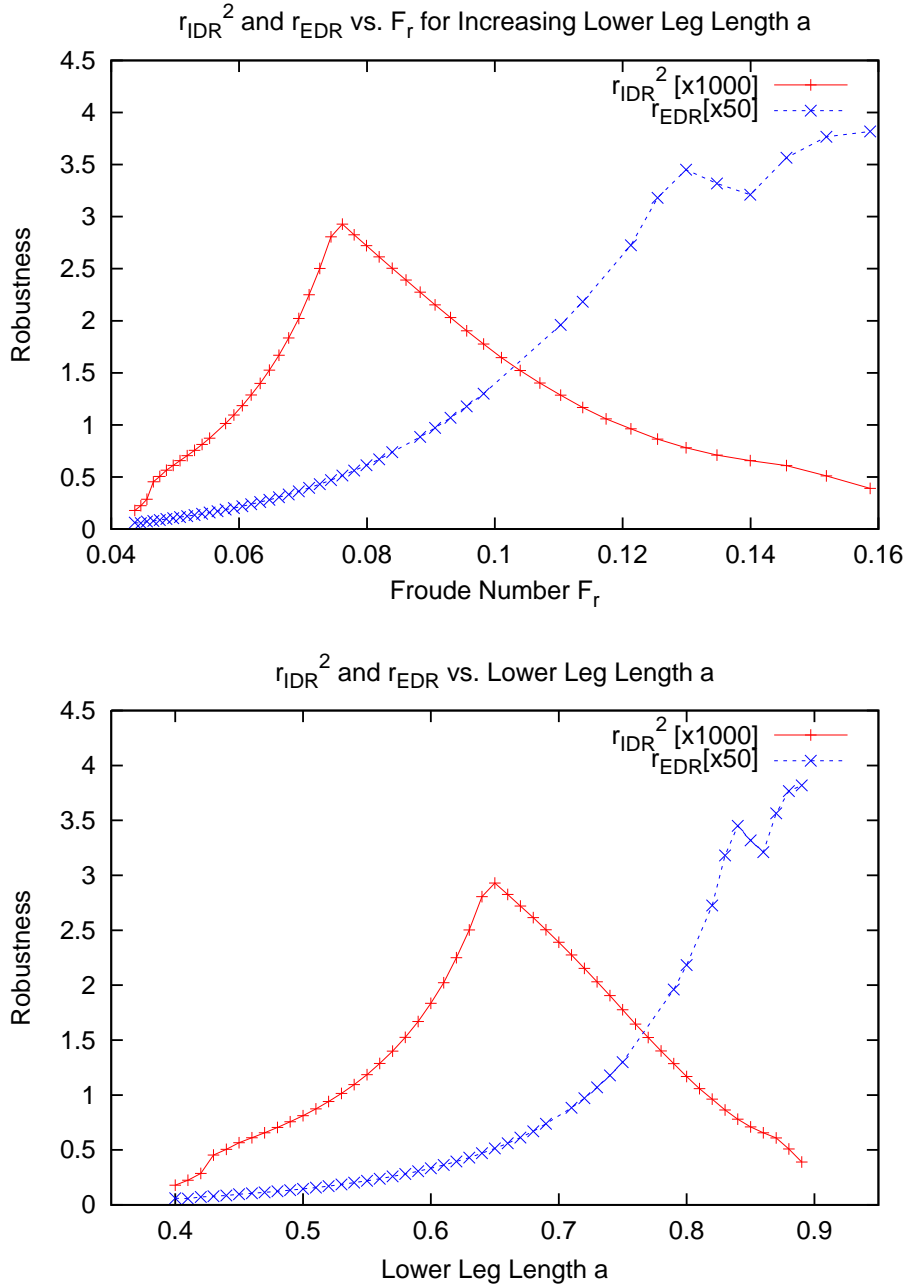


Figure 3.8: **Effect of varying lower leg length a .** *Top:* r_{IDR} vs F_r for $0.4 \leq a \leq 0.9$. There seems to be an optimally robust value at about $a = 0.63$, when $m = 0.25, m_H = 0.5$. *Bottom:* The same values shown vs. a .

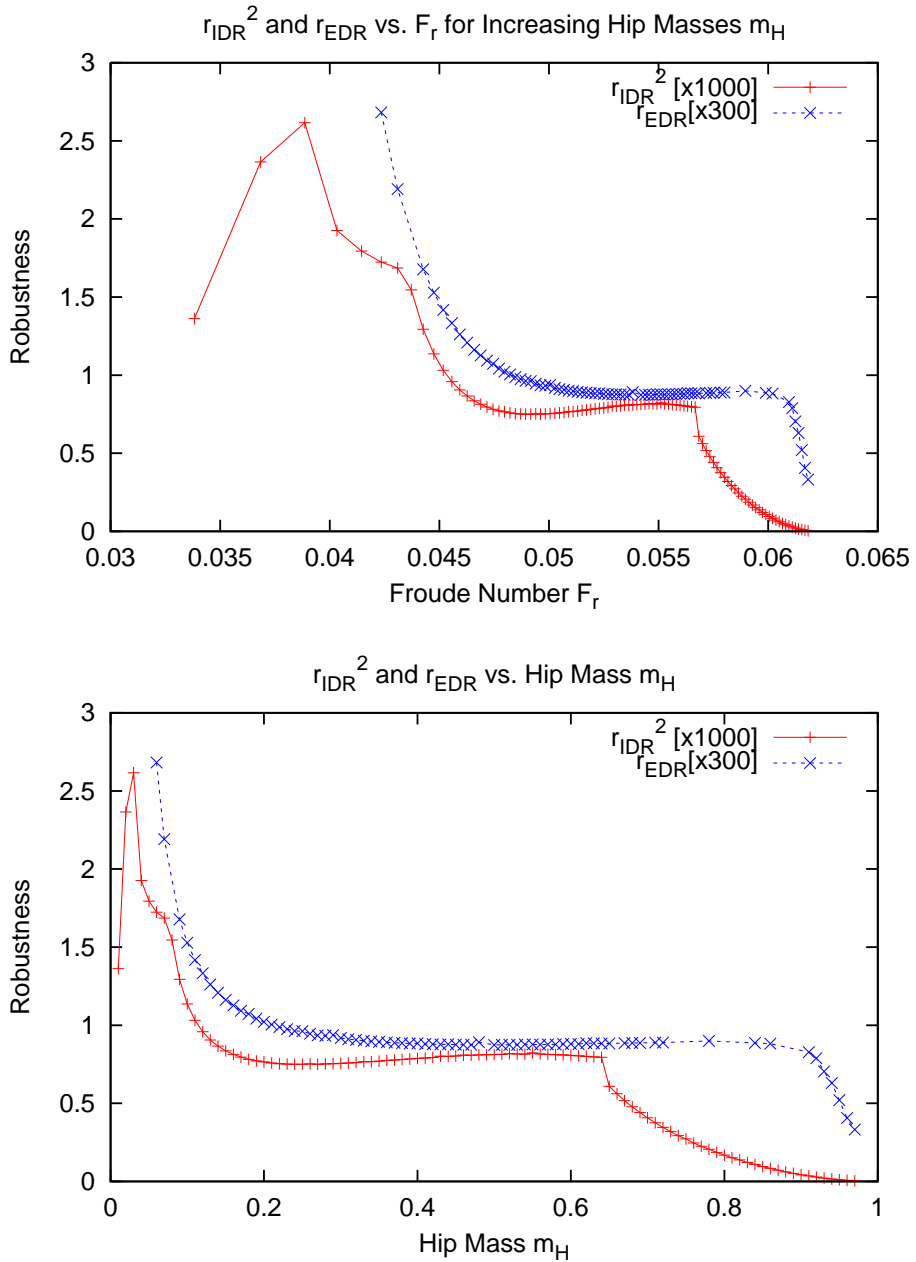


Figure 3.9: **Effect of varying hip mass m_H .** *Top:* r_{IDR} vs F_r as m_H is varied from 0.05 to 0.95. Having extremely heavy legs compared to the hip mass appears to be more robust, albeit this is somewhat unrealistic for practical robots. For most practical values, the ratio of hip mass to leg mass affects robustness very little. On the other hand, once leg masses become lighter than some threshold, robustness decreases. *Bottom:* The same values shown vs m_H .

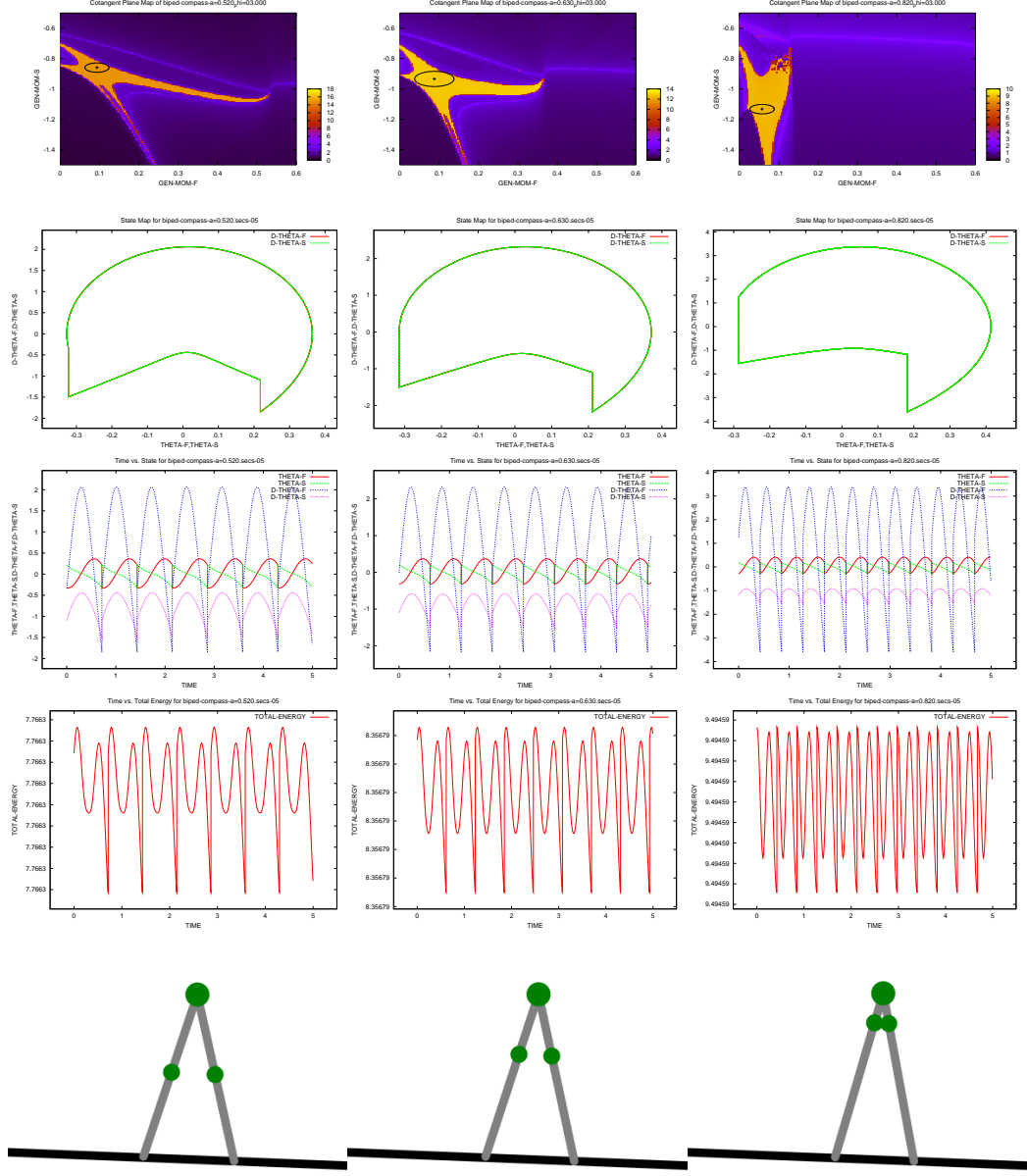


Figure 3.10: **Data for selected values of a .** Left to right: $a = 0.52, a = 0.63, a = 0.82$. The most stable value is approximately $a = 0.63$. Looking at the cotangent planes, we can see that the size of r_{IDR} is limited by the top boundary of the basin of attraction for $a = 0.52$, and by the lower-left boundary for $a = 0.82$. $a = 0.63$ is the sweet spot where both boundaries limiting the size of r_{IDR} .

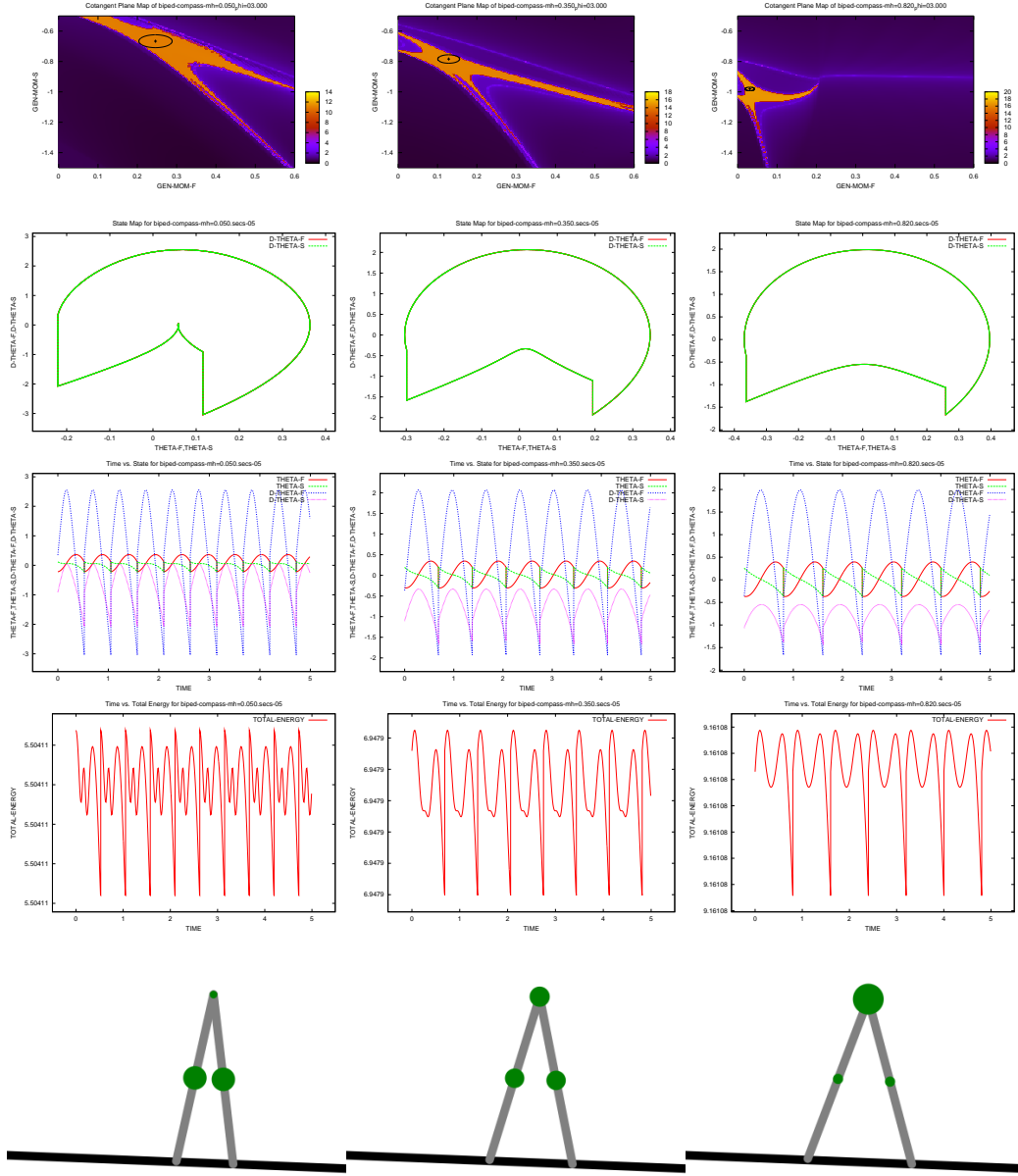


Figure 3.11: **Data for selected values of m_H .** Left to right: $m_H = 0.05, m_H = 0.35, m_H = 0.82$. Note how the constraining boundary on the basin of attraction is different for each robot.

This is one of the few graphs in this thesis where the qualitative behavior of r_{IDR} and r_{EDR} do not agree very well. The values of r_{EDR} seem to suggest that it is much better for robustness to have the leg masses as close to the hip mass as possible. More study is needed to determine if this is a simulation artifact or not. We therefore base our conclusions off of the values of r_{IDR} only.

Changing the natural period of the leg swing by moving the leg mass up and down the leg has a great effect on the robustness of the robot. Robots with too slow a leg swing will have their hip mass fall forward before their foot has swung forward to catch the robot's descent. Thus we see great changes in gait robustness as this natural pendular period changes.

The changes in walking velocity are easily understood. For a given step length, if the center of mass of the system is higher, the angle between the ground and the direction the center of mass is moving at heelstrike is decreased. The smaller this angle, the less energy is lost and the faster the robot will move. This effect is well explained in [Ruina et al 2005].

What happens to the gait robustness and speed of a robot as we change the ratio of hip mass to leg mass? *Changing the ratio of hip mass to leg mass has in general little effect on the r_{IDR} and F_r . However, at one extreme, robots with very heavy legs move more slowly but are more robust. At the other extreme, robots with lightweight legs move faster but are less robust.*

We now provide several hypotheses for the results seen in figure 3.9. Extremely light legs would be very unstable, because small disturbances to their momenta would make them move wildly. Though they could be controlled by a control system for a vanishingly small energy cost, a heavier leg might simply absorb the disturbances energy and 'take it in stride', so to say. To rephrase this, while a control system for a very light leg would have to resist nearly full force of a disturbance to keep the legs of the robot cycling properly, it is conceivable that a well-designed mechanical structure could presumably accept the disturbance without any additional energy cost. Therefore, heavier legs will likely be more robust. This behavior was seen for very heavy legs.

3.8 Effect of Hip Spring

3.8.1 Experiment Description and Motivation

In this experiment, an interleg spring (often called 'hip spring' in this thesis) is introduced to the reference biped model ($a = b = m_H = 0.5, m = 0.25, \phi = 3.0$ deg). This spring acts on both legs with a torque that is proportional to the angle between the legs. That is, the torque from the spring which tries to force the legs together is

$$\tau_{\text{hip}} = k_{\text{hip}}(q_f - q_s)$$

where q_s and q_f are the angles of the stance and non-stance legs, relative to the vertical.

Motivation for this experiment was the observation of [McGeer, 1988] that humans take faster steps than is predicted by a purely passive model. Adding a hip spring is a simple way to improve the step speed. We now study its effect on robustness and locomotion speed.

Data from this experiment is presented in several figures which we now introduce.

- Figure 3.12 shows the effect of varying hip spring stiffness k_{hip} on the r_{IDR} and r_{EDR} , plotted against nondimensionalized forward velocity F_r . The bottom of the graph shows the same graph, but with r_{IDR} plotted against k_{hip} .
- Figure 3.13 is the same as figure 3.12, but performed at a slope of $\phi = 1.0$ degrees.
- Figure 3.14 shows data for several representative values of k_{hip} on a slope of $\phi = 3.0$. It shows the cotangent spaces $\mathbf{T}_q^*\mathbb{Q}$, phase planes, and state spaces and total energy over time for robots with lower leg lengths of $k_{\text{hip}} = 0.5, 2.2, 5.5$. These values correspond to weak, medium, and stiff interleg springs.

3.8.2 Discussion

What happens to the gait robustness and forward velocity of a robot as we stiffen an interleg spring? *An interleg spring increases nonstance leg swing frequency. Thus it has similar effects as increasing lower leg length a ; robustness increases until some optimal point is reached for a particular forward speed. Increasing stiffness past this point results in a decrease of robustness. Forward velocity continues to increase as the hip spring is stiffened.*

Springs attached at the hip greatly affect the nonstance leg swing period, and therefore show the same sort of beneficial effect on robustness and efficiency that we noticed when lower leg length a was varied.

Performing the same experiment at a slope of $\phi = 1.0$ degrees resulted in the same qualitative effect. This lends support to the claim that there is an optimal interleg spring stiffness for a given robot walking at a given speed. If we could change the interleg spring stiffness, we could optimize the robot for walking at a variety of speeds. Such a variable stiffness mechanism is presented in Chapter 4, and would make it possible to tune the passive dynamics to better match a range of desired gait speeds.

We make a comparison to human walking. Research by [Kuo 2001] indicates that humans may actuate their hip muscles in a way that is roughly equivalent to having a spring at the hip. Also, from [Donelan 2002], we see that humans prefer to take smaller steps than would be predicted by mechanical models. Presumably this is because it reduces the fourth-order relationship between step length and energetic loss present in human locomotion [Kuo 2001]. This also suggests that a bipedal robot with a hip spring will be more energy efficient, and thus move faster given a constant slope. This phenomenon is exactly what we saw.

This effect is also described in another paper, [Ruina et al 2005], where simple collisional mathematics applicable to all legged models show that decreasing step size improves energetic efficiency because collisional losses are reduced. That is, for a given velocity, a robot with a hip spring takes shorter, faster steps than one without. Halving the step length reduces mechanical collisional energy loss per step to one fourth.

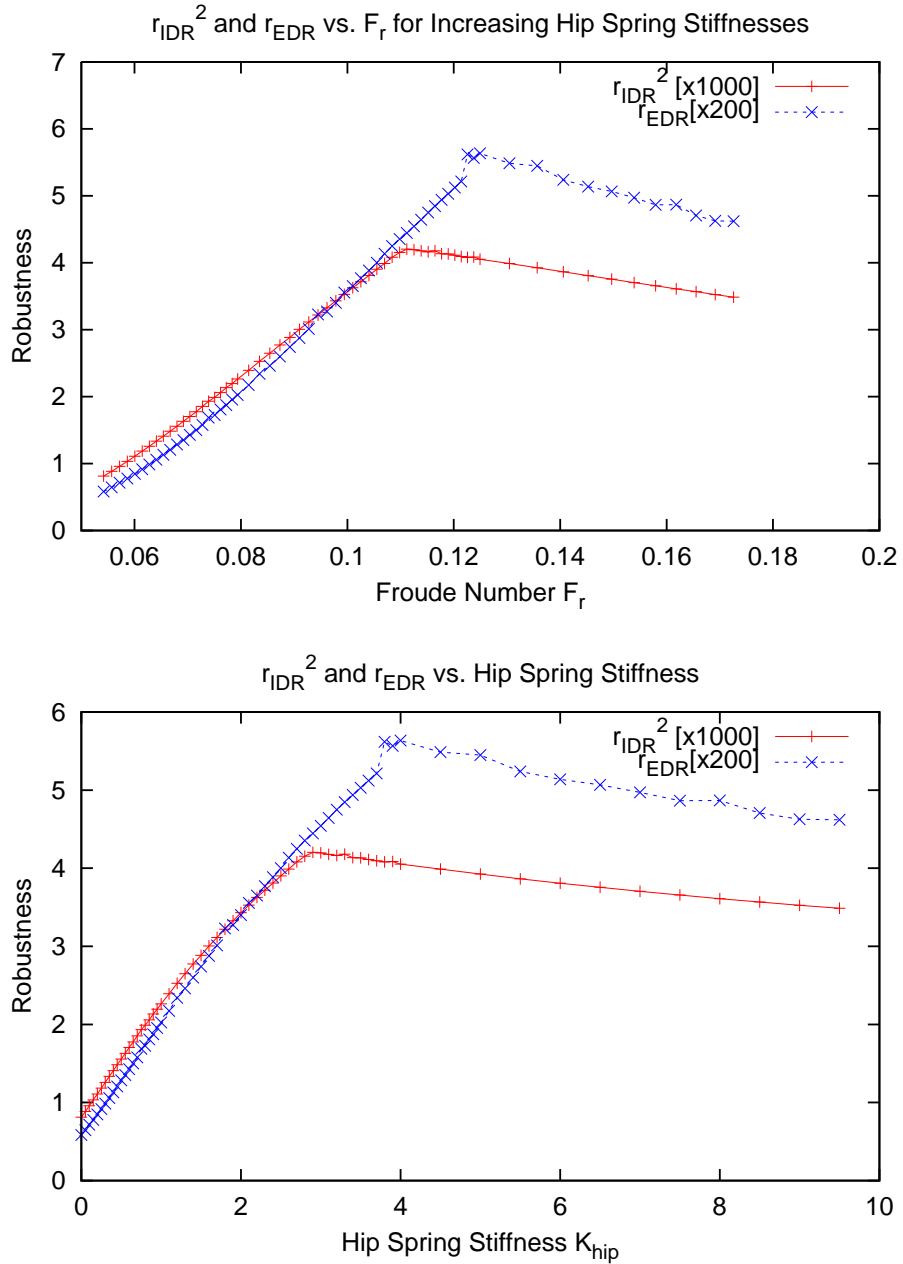


Figure 3.12: **Effect of varying interleg spring k_{hip} on a slope of $\phi = 3.0$ degrees.** Top: r_{IDR} and r_{EDR} vs F_r for $0.0 \leq k_{\text{hip}} \leq 10.0$. There seems to be an optimally robust value at roughly $k_{\text{hip}} = 3.0$, when $a = b = m_H = 0.5, m = 0.25$. Bottom: The same values shown vs. k_{hip} .

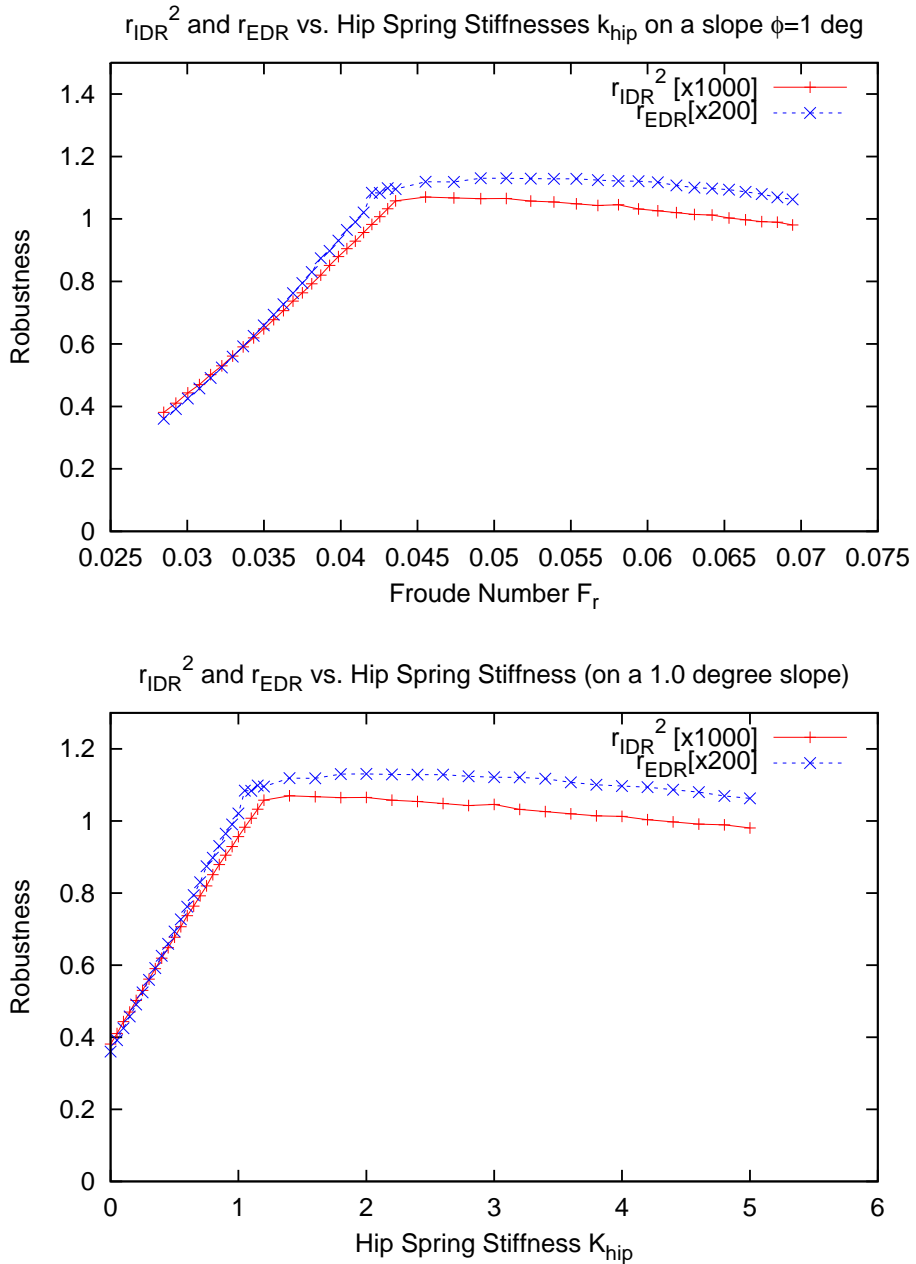


Figure 3.13: Effect of varying interleg spring k_{hip} on a slope of $\phi = 1.0$ degrees.
Top: r_{IDR} vs F_r for $0.0 \leq k_{\text{hip}} \leq 10.0$. There seems to be an optimally robust value at about $k_{\text{hip}} = 1.2$, when $a = b = m_H = 0.5, m = 0.25$. *Bottom:* The same values shown vs. k_{hip} . Essentially this is the same as figure 3.12, but at a different slope. Note that the optimal stiffness is different. Therefore, if we had a variable stiffness spring, a robot could adapt its intrinsic behavior to improve gait robustness. Such a variable stiffness mechanism is described in chapter 4.

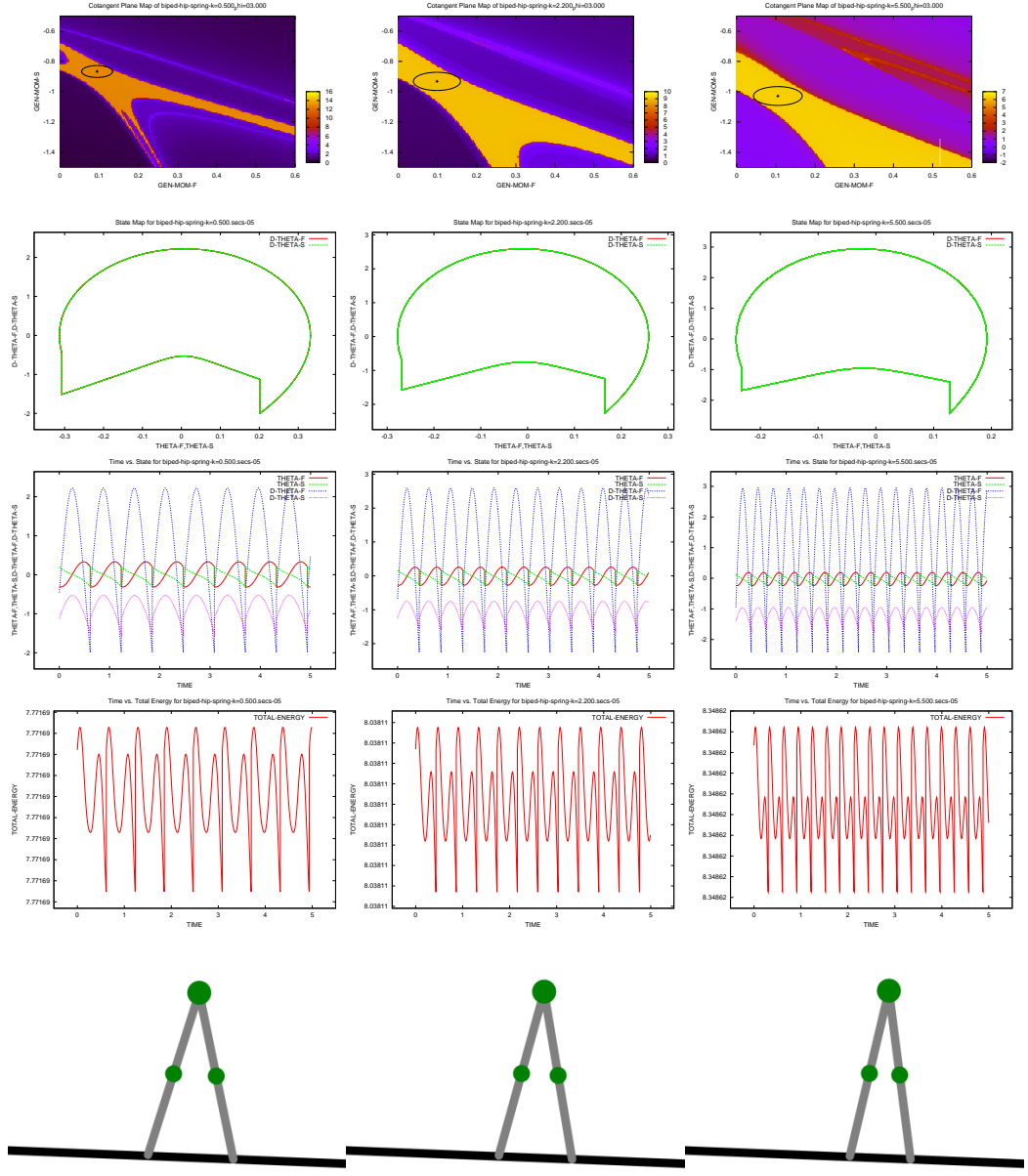


Figure 3.14: **Data for selected values of k_{hip} on a $\phi = 3.0$ degree slope.** Left to right: $k_{\text{hip}} = 0.5, 2.2, 5.5$. Note the differences in cotangent space basin of attraction, and step length and periods.

3.9 Effect of Ankle Springs

3.9.1 Experiment Description and Motivation

In this experiment, a spring is added to the stance leg of the reference biped model ($a = b = m_H = 0.5, m = 0.25, \phi = 3.0 \text{ deg}$). This spring applies a torque to the leg which works to restore the stance leg to an angle perpendicular to the floor. That is,

$$\tau_s = k_{\text{ankle}}(\phi + q_s)$$

where q_s is the angle of the stance leg, measured counterclockwise relative to the vertical, and ϕ is the downhill slope, measured clockwise with respect to the horizontal.

The motivation for this experiment is to examine if the effect of round feet, studied in Section 3.10, provide a similar stabilizing effect as a flat foot with an ankle torque created by a spring.

This kind of ankle torque is actually somewhat unrealistic, especially as the spring stiffness increases; it is not immediately obvious how one would design a purely mechanical foot and spring that would apply a torque in this manner. However, with sufficiently wide flat feet and some mechanical linkage or pulley system between the support and non-support foot, this type of torque could presumably be recreated mechanically. There are, of course, practical restrictions on how large an ankle torque is physically realizable. Foot size is one obvious restriction. Such problems are not considered here.

Data from this experiment is presented in several figures which we now introduce.

- Figure 3.15: Top shows the effect of varying k_{ankle} on r_{IDR} and r_{EDR} , plotted against nondimensionalized forward velocity F_r . The bottom of the graph shows the same graph, but with r_{IDR} plotted against k_{ankle} . Increasing ankle spring stiffness improves locomotion speed and robustness.
- Figure 3.16 shows data for several representative values of k_{ankle} . It shows the cotangent spaces $\mathbf{T}_q^*\mathbb{Q}$, phase planes, and state spaces and total energy over time for robots with ankle stiffnesses $k_{\text{ankle}} = 1.0, 3.0$.

3.9.2 Discussion

What happens to the gait robustness and forward velocity of a robot as we stiffen an ankle spring? *An ankle spring improves the robustness and forward velocity of a robot. As with the hip spring, there appears to be an optimally stable value for a given slope and mass distribution.*

We now present an intuitive hypothesis for why the gait robustness improves. If we made the hip spring very very stiff, the robot would not walk at all, or if it did take steps they would be very short. The stance leg would be supported by the spring's ankle torque and be essentially unable to fall down; as it falls, the restoring ankle torque would become greater than the gravitational force pulling it down, and the robot would bounce back up

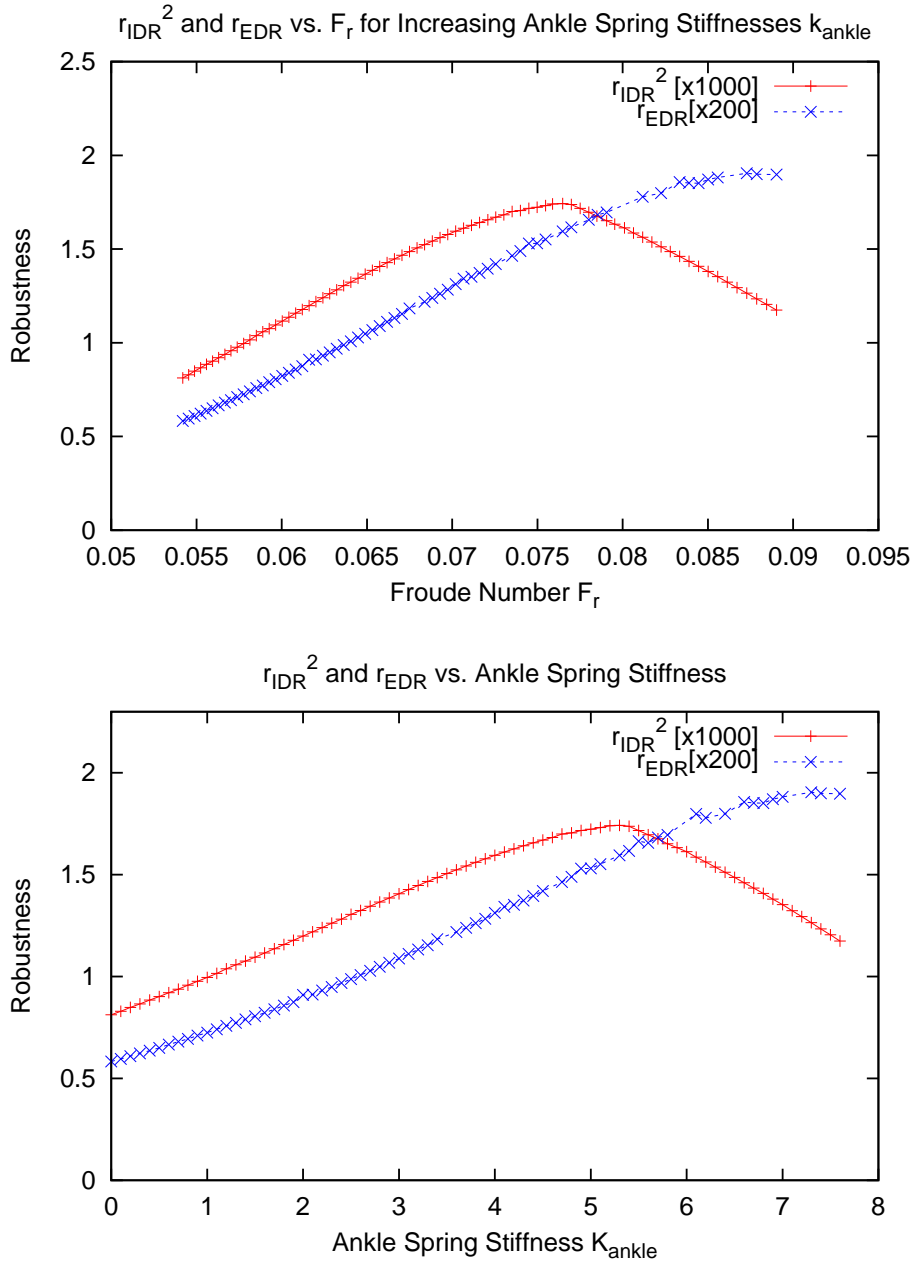


Figure 3.15: **Effect of varying ankle spring k_{ankle} at $\phi = 3.0$.** Top: r_{IDR} vs F_r for $0.0 \leq k_{ankle} \leq 10.0$. There seems to be an optimally robust value at about $k_{ankle} = 5.3$, when $a = b = m_H = 0.5, m = 0.25$. Bottom: The same values shown vs. k_{ankle} .

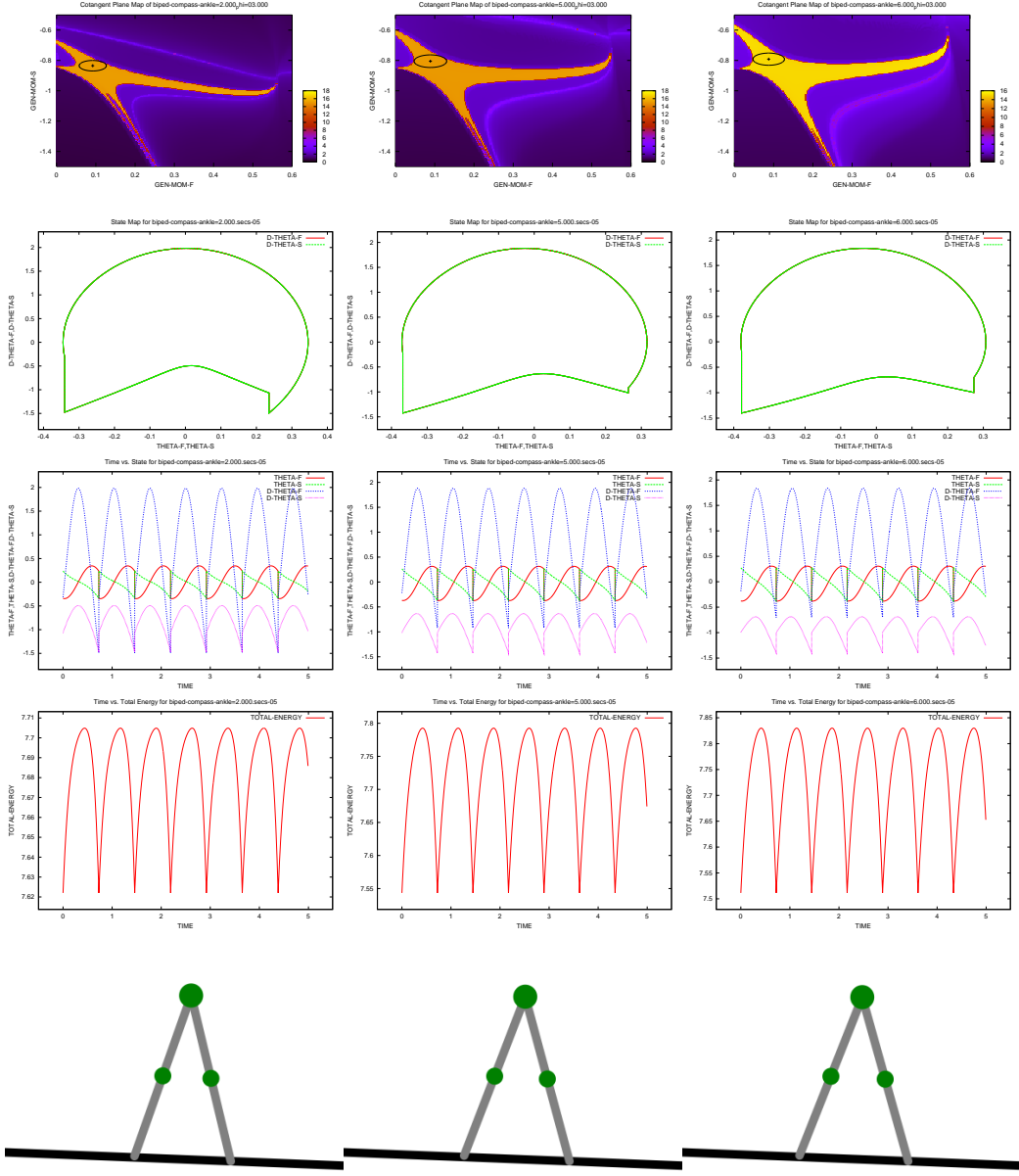


Figure 3.16: **Data for selected values of k_{ankle} .** *Left to right: $k_{ankle} = 2.0, 5.3, 6.0$.* Because the ankle torque was implemented via a controller, when we look at the total system energy graph, we see the potential energy stored in the spring affect system energy because controllers are treated as external energy sources in simulation. By looking at the areas of the cotangent spaces, the robustness of robots can be visually inspected.

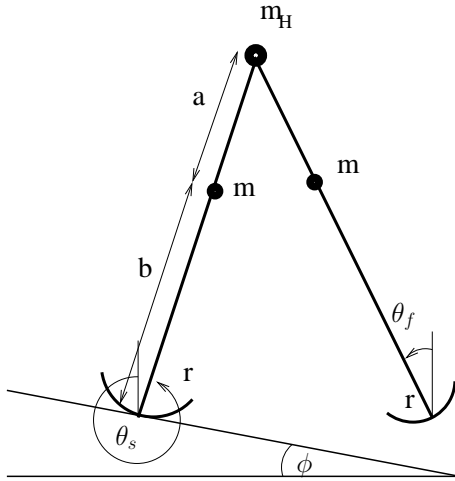


Figure 3.17: Picture of robot with arc-shaped feet, showing dimensions.

again. This actually happens in simulation for values of k_{ankle} above approximately 5.3 or greater.

The more interesting question is, why did the robustness decrease at all above $k_{ankle} = 5.3$? The author is uncertain as to the answer. The spring at this stiffness is creating a very large torque, almost enough to support the hip mass by itself, so perhaps it is an unrealistic effect that has no physical meaning.

Also unusual is that r_{EDR} does not agree with r_{IDR} . We present no explanation for this phenomenon.

The reason that ankle springs improve gait speed is somewhat more clear. The ankle torque speeds motion through the swing, and the higher average angular velocity of the stance leg is thought to account for the improved gait speed.

3.10 Effect of Arc Foot Radius

3.10.1 Experiment Description and Motivation

In this experiment, arc-shaped semicircular feet are added to each leg of the reference biped ($a = b = m_H = 0.5$, $m = 0.25$, $\phi = 3.0$ deg). Arc feet are a commonly studied addition to the compass biped model. In this experiment, heel and toe effects are not considered. The arc feet are assumed to be large enough that the stance leg is never supported by a single point on the heel or toe of the arc, but instead is always rolling on the rounded arc foot sole.

The motivation for this experiment is to examine whether or not the effect of round feet provide a similar stabilizing effect as a flat foot with an ankle torque, studied in Section 3.9.

Data from this experiment is presented in several figures which we now introduce.

- Figure 3.18: *Top* shows the effect of varying r on the values of r_{IDR} and r_{EDR} , plotted against nondimensionalized forward velocity F_r . The bottom of the graph shows the same graph plotted against r .
- Figure 3.19 shows data for several representative values of r . It shows the cotangent spaces $T_q^*\mathbb{Q}$, phase planes, and state spaces and total energy over time for robots with arc radii of $r = 0.3, 0.56, 0.68$.

3.10.2 Discussion

What happens to the gait robustness and forward velocity of a robot as we add arc feet of increasing radius? The larger the radius of the foot, the more robustly and faster the robot will move.

Arc feet greatly improved the robustness and walking velocity of the robot, up to extremely large radii. The improvement in walking velocity is well known. For example, [Ruina et al 2005]’s work argues that the effect of feet is to reduce the downward component of the velocity of the center of mass at the instant of heelstrike. In effect, it shortens the effective step length, reducing energy loss. The rolling motion also improves walking velocity by moving the robot forward slightly during each step.

The beneficial effect of arc feet on robustness has been weakly experimentally verified by [Wisse 2004]. Arc feet were found to improve robustness the larger the arc was.

There have been several reasons proposed why arc feet will improve walking robustness. [Asano, Luo 2006] argue this is because of a slight torquing affect by the foot on the stance leg. However, the results presented in this thesis seem to reject the hypothesis that flat feet with an ankle spring produce a similar effect to arc feet. The relative sizes of the effects seems to be markedly different, as will be shown in Section 3.13.

[McGeer, 1988] mentioned that the eigenvalues of the linearized model suggest an optimal value foot radius of approximately 0.3. Our results contradict this and suggest that in regards to arc feet, bigger is better.

[Kuo 2002] finds experimentally that if humans are made to walk wearing ski boots with arcs on the bottoms, a radius of about $r = 0.3$ is most comfortable. Presumably this must be because of other reasons than improved robustness; if the results in this thesis are correct, to improve robustness it is advantageous to have as large a foot arc as possible. An alternative explanation is that this model is too simple to capture the essential dynamics of human walking.

Finally, [Ringrose 1997]’s experiments with dynamically stable running robots show that, for some range of radii, arc feet can make a running robot self-stabilize. It would be interesting to investigate how the radius of arc feet could be selected to improve both walking and running motions in bipedal robots.

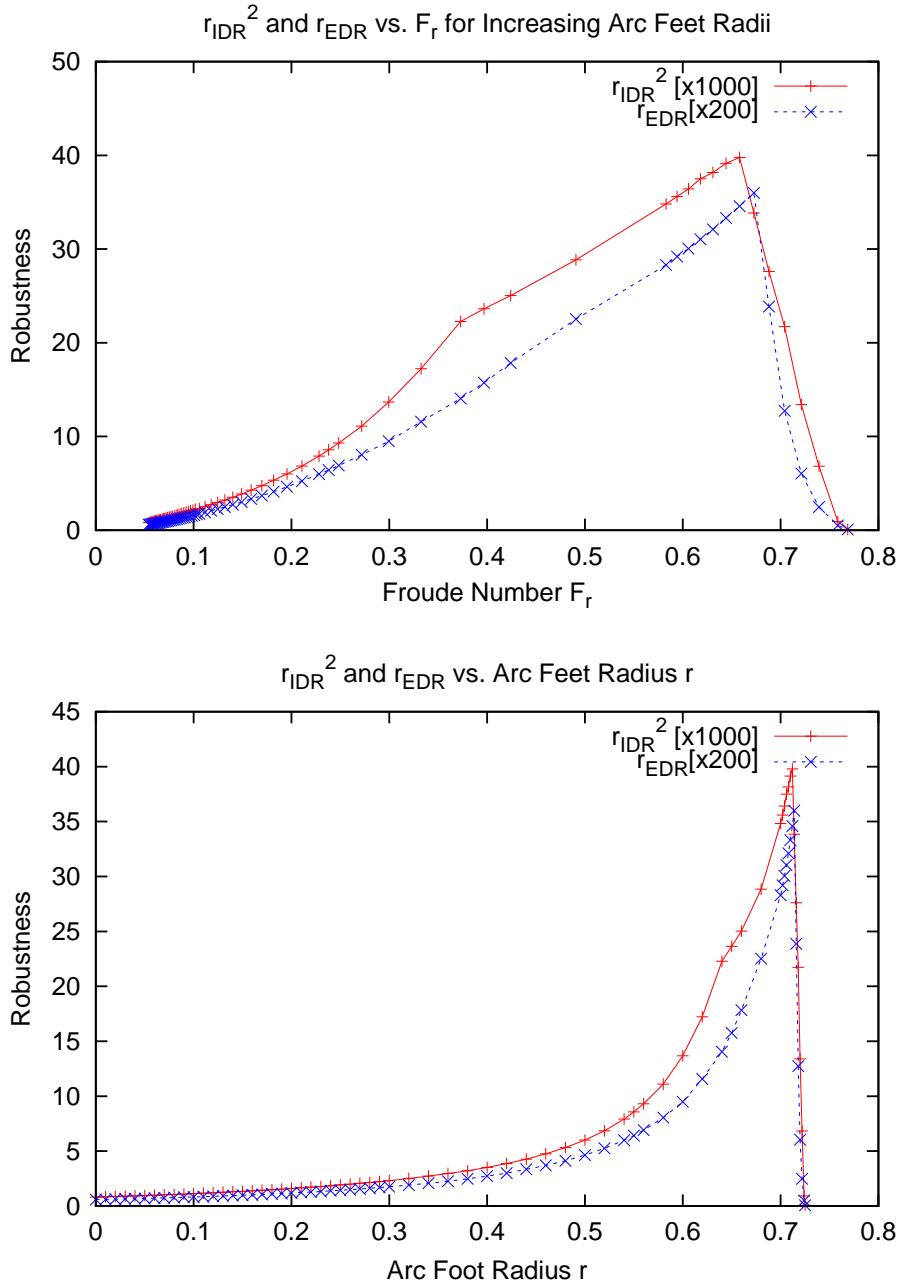


Figure 3.18: **Effect of arc foot radius r .** *Top:* r_{IDR} and r_{EDR} vs F_r for $0.0 \leq r \leq 0.725$. Robustness increases until about 0.8, after which it drops off very sharply. *Bottom:* The same graph, but r_{IDR} is plotted vs r .

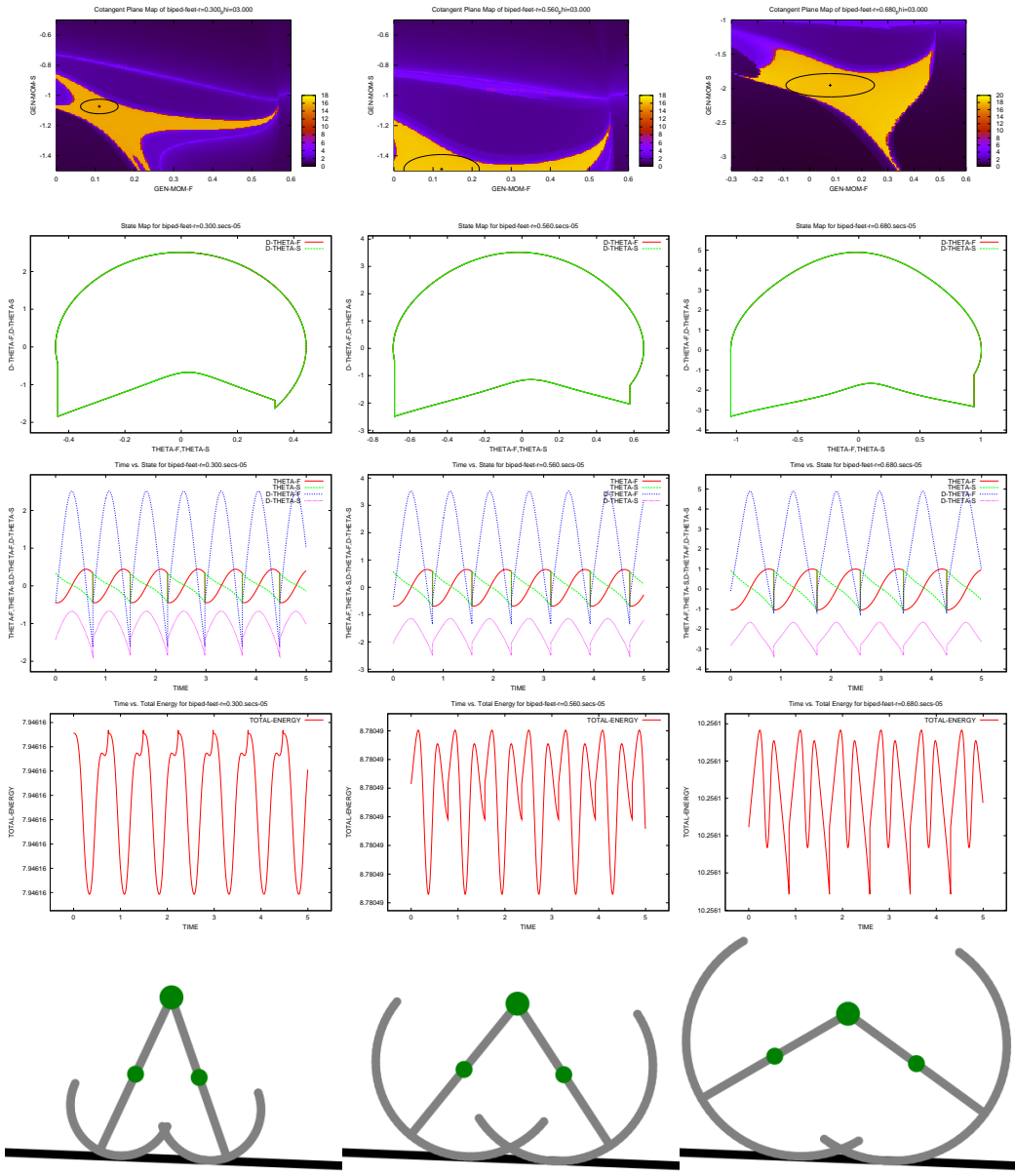


Figure 3.19: **Data for selected feet radii r .** *Left to right:* $r = 0.3, 0.56, 0.68$. Note that the scale of the axes is different for the $r = 0.68$ cotangent space graph so that it was centered more properly.

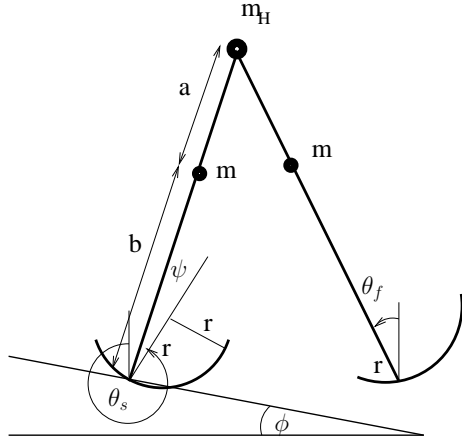


Figure 3.20: **A biped with forward-pointing feet.** Note that ψ , the angle between the center of the arc foot and the shank of the leg, is measured from the tip of the leg link. Positive values of ψ make the center of the arc feet move more and more forward.

3.11 Effect of Forward-Pointing Feet

3.11.1 Experiment Description and Motivation

In this experiment, arc-shaped semicircular feet, such as the ones presented in the previous experiment, are tilted forward. That is, the center of the arc foot's radius is moved forward, outside of the leg, by a small amount. This means that the robot's effective leg length – the distance between the support point and the hip mass – could actually increase as the robot rolls forward near the end of the step. This is impossible in the previous experiment, where the effective leg length decreases as the robot rolls forward. As before, the arc feet in this experiment are assumed to be large enough that the stance leg is never supported by a single point on the heel or toe of the arc, but instead is always rolling on the rounded arc bottom.

Specifically, the feet are moved forward by an amount ψ , which is the angle between the lower leg segment and the center of the foot arc, measured from the bottom of the lower leg. Please refer to Figure 3.20 to see this graphically.

In this experiment, the arc foot radius is held constant at $r = 0.2$.

The motivation for this experiment is the observation that humans and most walking animals have legs which protrude in the front of the leg further than the back. Is this because forward-pointing feet improves passive robustness?

[Wisss 2004] and [Srinivasan, Ruina 2005] observe that forward-pointing feet may tend to counter the most common mode of falling for passive dynamic robots: falling forward. Indeed, in every robot presented in this thesis, applying a worst-case disturbance Δp_{IDR} or Δp_{EDR} always resulted in the robot falling forward, never backward.

There is also some anecdotal evidence that humans are more robust to preventing forward

falls than backward falls. Experienced martial artists often attest to the fact that it is much easier to trip an opponent and make him fall backwards rather than forward; once the heel slips, there is almost nothing the opponent can do to stop the backward rotation of their body. The situation is similar to why unskilled ice skaters routinely fall on their tailbone more than they fall forward. Perhaps the reason for both of these tendencies is related to forward-pointing feet.

Data from this experiment is presented in several figures.

- Figure 3.21: Top shows the effect of varying ψ on the values of r_{IDR} and r_{EDR} , plotted against nondimensionalized forward velocity F_r . The bottom of the graph shows the same graph plotted against ψ .
- Figure 3.22 shows data for several representative values of ψ . Due to a mistake realized late in this thesis, the cotangent spaces $T_q^*\mathbb{Q}$ are not shown. However, we do show the phase planes, state spaces, and total energy over time for robots with a forward tilt of $\psi = 2.0, 5.0$ degrees.

3.11.2 Discussion

What happens to the gait robustness and forward velocity of a robot as we make the foot protrude more and more forwards? The robot will move slower. Robustness will increase slightly, then begin to decrease. Bifurcation begins for relatively small values of ψ .

The slowing effect of the forward-pointing feet was unexpected. The author hypothesizes that the effect has to do with the rolling and rising motion that the feet create, and this subtle effect slows the overall step time of the robot.

The reason for the improved robustness and then decreased robustness is not clear to the author and so no speculation is presented here. Above $\psi = 10.0$ degrees, bifurcation begins to occur.

Due to time constraints, little r_{EDR} data was taken, and results are inconclusive.

3.12 Effect of a Mechanically Constrained Torso

3.12.1 Experiment Description and Motivation

In this experiment, a massive torso is added to the robot. This torso is mechanically constrained so that it is fixed relative to the line which bisects the angle between the legs. This constraint does not increase the degrees of freedom of the robot. It does, however, add three new design parameters: a new torso mass m_t , a distance from the hip to the torso d , and an amount ξ to lean the torso forward or backward relative to the bisecting angle.

Specifically, the angle of the torso relative to the vertical is $\theta_t = \xi + \frac{1}{2}(q_f + q_s)$. Please refer to Figure 3.23 to see this graphically.

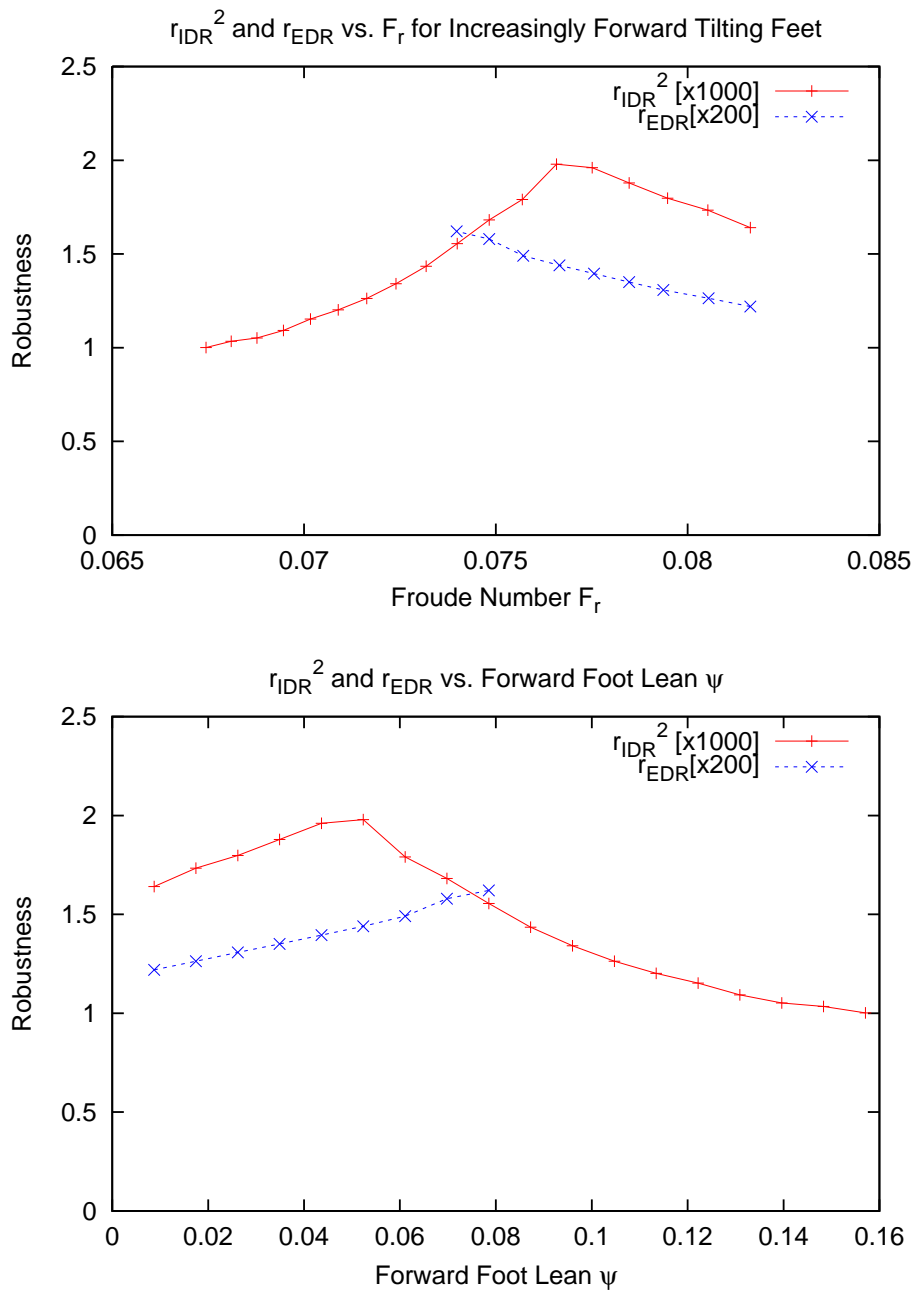


Figure 3.21: **Effect of tilting $r = 0.2$ radius arc feet forward by ψ .** Top: r_{IDR} vs F_r for $0.0 \leq \psi \leq 10.0$ degrees. Robustness increases until about 0.05 radians, after which it begins to decrease. Forward velocity decreases as ψ increases. Bottom: The same graph, but r_{IDR} is plotted vs r .

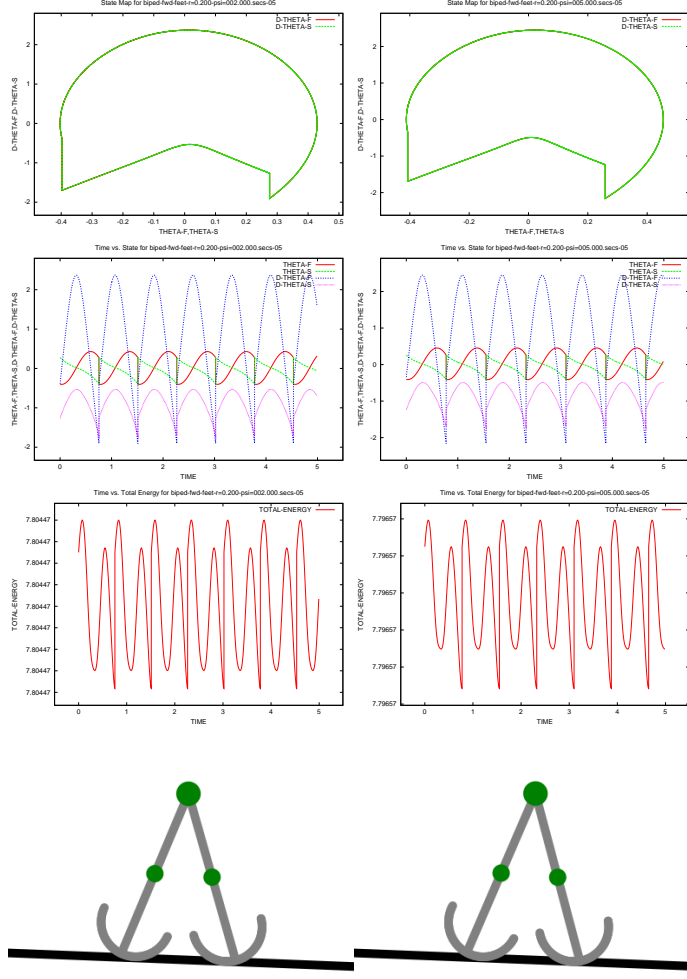


Figure 3.22: **Data for selected values of ψ .** Due to time constraints, the cotangent space pictures are not included. *Left to right:* $\psi = 2.0, 5.0$ degrees. Clearly, the effect of the forward tilting is very subtle, and visually distinguishing the robots with and without forward tilt of this type is difficult. Bifurcation begins at approximately $\psi = 10.5$.

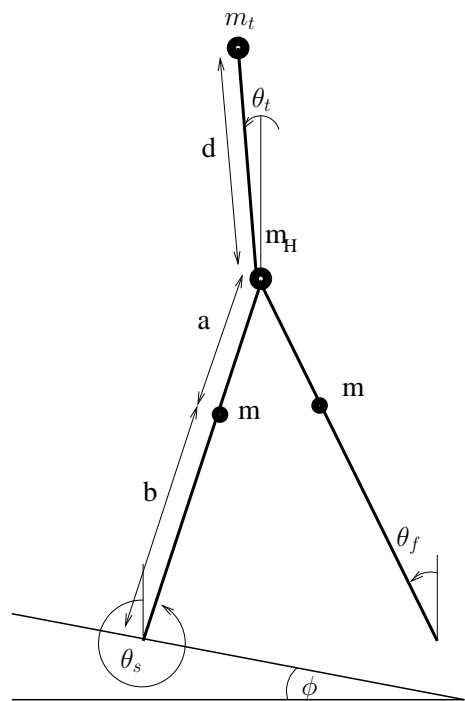


Figure 3.23: A biped with a torso constrained by the rule $\theta_t = \xi + \frac{1}{2}(q_f + q_s)$.

In this experiment, the hip mass is split into two. Half of the mass goes into the torso. That is, for this experiment $m = m_H = m_t = 0.25$, and we vary d and monitor the effects as the torso gets longer.

The motivation for this experiment is the observation that humans, animals, and most robots have torsos. Torsos of this kind have been studied by [Wisse 2004] and found to have beneficial effects on gait robustness and gait efficiency. It was similarly studied by [McGeer, 1988], who also found it to have beneficial effects.

Data from this experiment is presented in several figures which we now introduce.

- Figure 3.24: Top shows the effect of varying d on the values of r_{IDR} , plotted against nondimensionalized forward velocity F_r . The bottom of the graph shows the same graph, but with r_{IDR} plotted against d .
- Figure 3.25 shows data for several representative values of d . It shows the cotangent spaces $\mathbf{T}_q^*\mathbb{Q}$, phase planes, and state spaces and total energy over time for robots with torso lengths of $d = 0.04, 0.1, 0.16$.

3.12.2 Discussion

What happens to the gait robustness and forward velocity of a robot as we move the torso mass farther from the hip? *Robots with torsos had decreased robustness and forward speed. This may have several causes. Perhaps the slope is too steep for this model. Perhaps the mass distribution was poorly selected. Perhaps this model of a torso is too artificial.*

Rather surprisingly to the author, adding a torso decreased forward speed and gait robustness, exactly the opposite of what was expected.

A constrained torso was expected to improve gait robustness and walking speed. Torsos are generally thought to improve energetic efficiency because the center of mass will be moved higher, so the heelstrike collisional loss will be smaller for a given step length. Higher energetic efficiency leads to higher speeds on a fixed slope.

The robustness was also expected to improve because the higher center of mass will take longer to fall, giving the swing leg more time to move forward and catch the robot after a disturbance.

However, both of these hypotheses were incorrect. The author surmises that this is too steep a slope for these particular design parameters, and that the torso might improve gait robustness and efficiency on shallower slopes.

It is also possible that constraining the torso according to the rule $\theta_t = \xi + \frac{1}{2}(q_f + q_s)$ is simply never beneficial to robustness. Let us consider the effect of this type of torso at the collision. For most angles, the torso will continue moving forward, and because of the constraint locking it to both legs, this momentum will naturally kick the old support leg out backwards, making it more difficult for the non-stance leg to swing forward and catch the robot's forward fall. If so, this constrained torso is not advantageous to gait robustness unless other mechanisms are added, such as a hip spring.

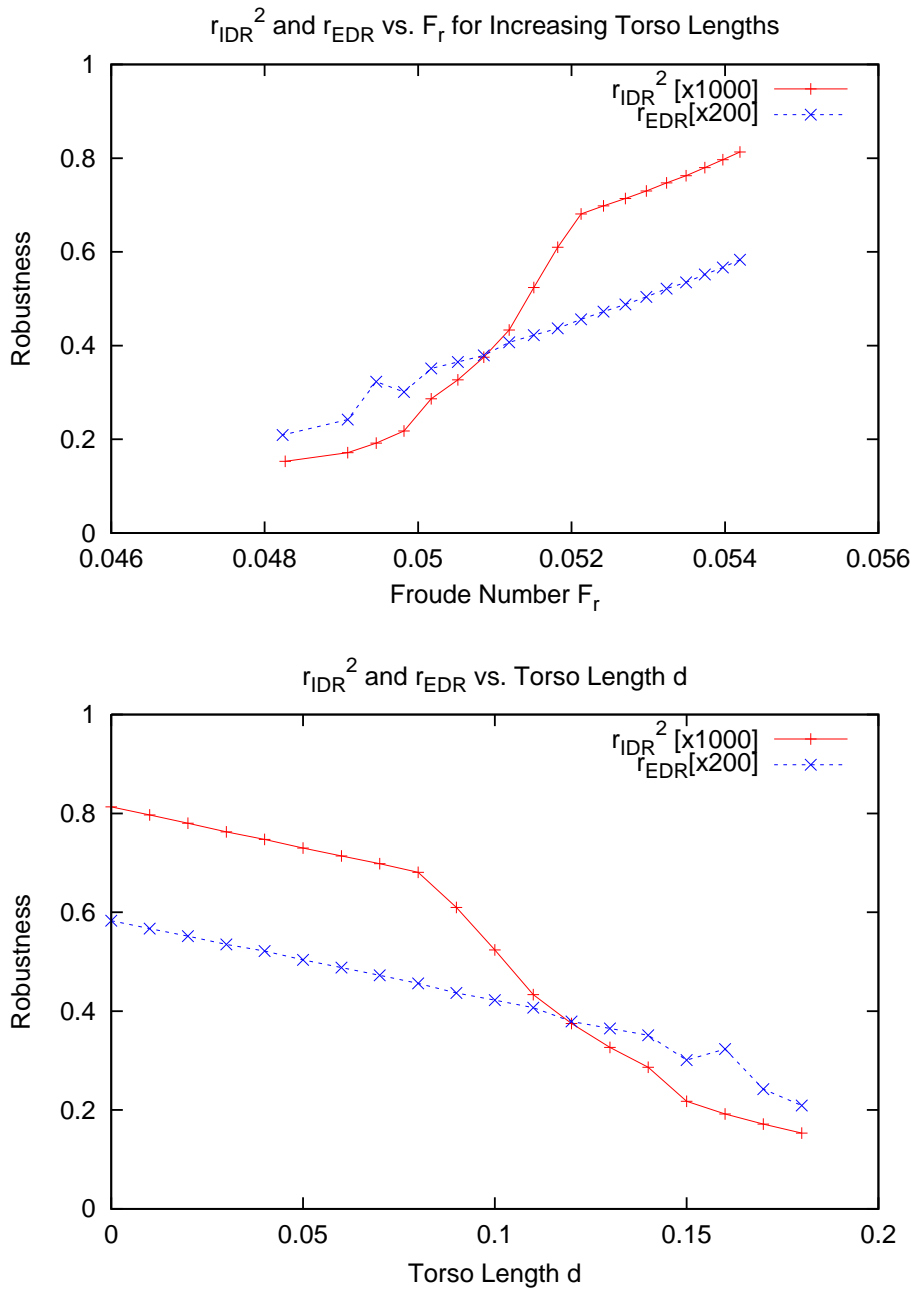


Figure 3.24: **Effect of increasing torso length d .** *Top:* r_{IDR} and r_{EDR} vs F_r for $0.0 \leq d \leq 0.3$. As can be seen here, adding any torso at all decreases the robustness of the robot. *Bottom:* The same values shown vs. d .

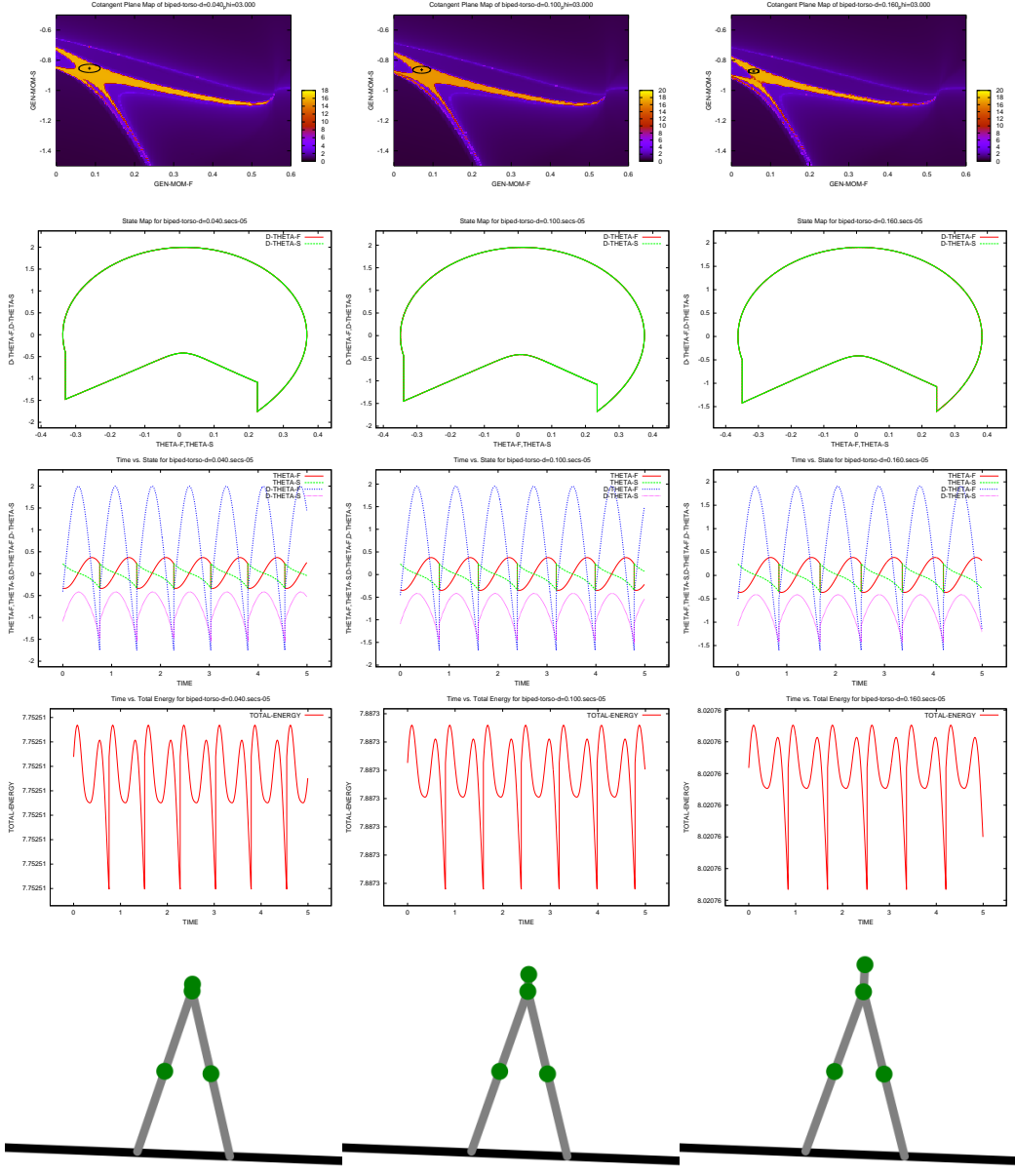


Figure 3.25: **Data for selected values of d .** *Left to right:* $d = 0.04, 0.10, 0.16$. By looking at the cotangent space, it can be seen that the $d = 0.16$ robot is nearing a point where bifurcation will begin. When bifurcation occurs, the post-heelstrike instant cotangent space will have two separated yellow regions, as was seen in figure 3.7:right.

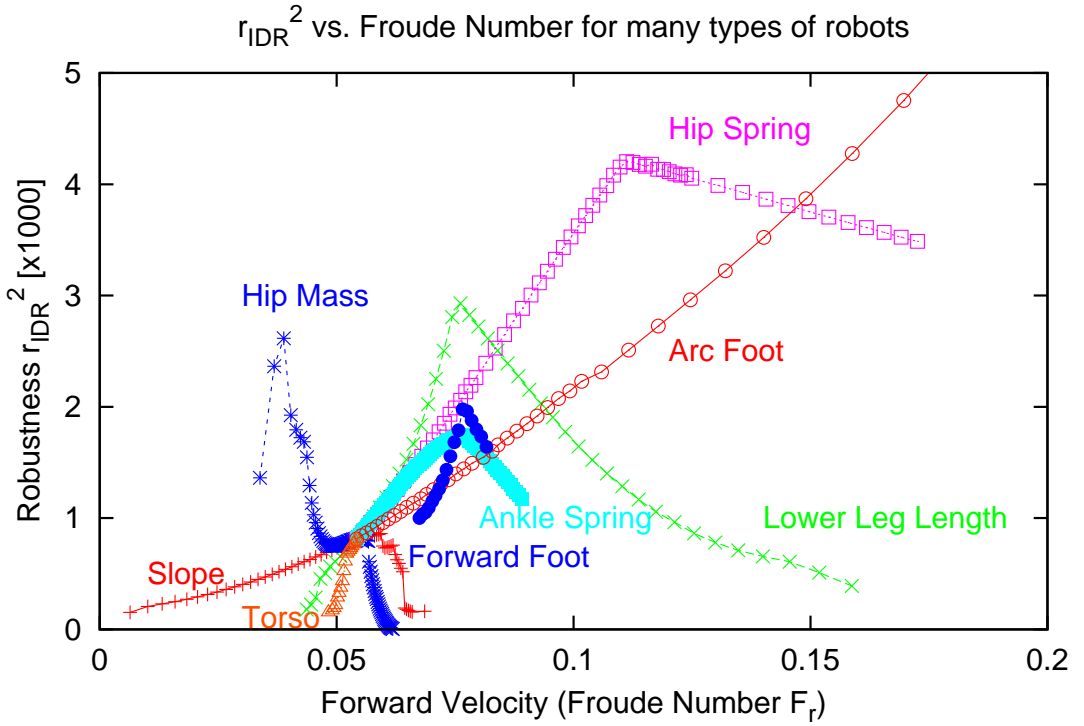


Figure 3.26: **Combined data for experiments thus far.** r_{IDR}^2 vs F_r for various model parameters. A visual comparison of the effects of adding various mechanical structures to the compass biped yields this graph. Clearly, adding a hip spring, feet, or increasing a would yield immediate improvement in gait velocity and robustness. Though not shown, the major difference between using r_{IDR}^2 or r_{EDR} is the scaling.

Because the effect of d was detrimental, experiments to vary ξ or m_t were canceled. Perhaps the effects of a torso are advantageous for different mass distributions at different slopes, but that would stray too far from the reference model studied in this thesis. Unfortunately, this experiment was rather inconclusive, except for the realization that this type of constrained torso is not always beneficial to robustness.

3.13 Comparison of Effects of Mechanical Additions to Reference Biped

We now replot all of the r_{IDR} graphs from the previous experiments in figure 3.26.

From this graph, we can say that

- Stabilizing additions to the reference biped include feet, a hip spring, and moving the leg mass up the leg slightly.

- Position of masses of the leg masses m was more important than their mass relative to the hip mass m_H .
- Ankle springs and rounded feet do not have similar effects; rather, hip springs and ankle springs have similar effects for low stiffnesses. However, hip springs quickly become much more advantageous.
- Contrary to popular wisdom, adding a torso to the reference biped using the constraint $\theta_t = \xi + \frac{1}{2}(q_f + q_s)$ is not always a good thing, and may have a destabilizing effect for certain parameters.
- There seems to be a free-leg oscillation period which is optimal for some forward velocity. Robustness plots exhibited peaking behavior for all parameters for which the non-stance leg oscillation period varied.

3.14 Future Engineering Goal

Many of the topics presented in this thesis began as part of an engineering goal: to design a robust bipedal robot which walks and runs, moves at speeds comparable to that a human, and does so as efficiently and robustly as possible. Although this thesis did not see this ambitious goal to conclusion, or even through the design phase, that goal remained in mind throughout forays into other research areas.

There are a few criteria that the robot was intended to be designed to meet. Specifically, those criteria are:

1. **Walking Speed:** The robot is desired to walk with a velocity corresponding to $0.15 \leq F_r \leq 0.20$. $F_r = 0.2$ corresponds to a comfortable walking gait in humans.[Donelan 2002] For a person with a leg length of 85cm, $0.15 \leq F_r \leq 0.20$ corresponds to a walking velocity of about 1.1-1.3m/s (4.0-4.6kph).
2. **Cost of Transport:** An average human walking at $0.15 \leq F_r \leq 0.20$ has a cost of transport of $c_{et} \approx 0.2$, and the mechanical efficiency of $c_{mt} = 0.05$. [Collins, Ruina 2005]
3. **Slope Choice:** The cost of transport corresponds directly with the angle of the slope that a purely passive-dynamic robot walks down. Assuming an efficiency $c_{mt} = 0.05$, and

$$\phi \approx c_{mt}$$

we thus pick $\phi = 3.0$ degrees, for a $c_{mt} \approx 0.0524$ rad.

4. **Step Length and Frequency:** The step length and step frequency of the robot is desired to be comparable to that of a human or animal unless circumstances strongly suggest a reason to do otherwise.

5. **Gait Robustness vs. Efficiency:** Mechanical gait robustness should take priority over energetic efficiency. This is a practical consideration; it is easy to buy more powerful motors but hard to invent stabilizing controllers for bipeds.
6. **Realizability:** Mechanical features which are physically unrealistic or impossible to build will be discarded.

3.15 Evolution of a Robust Passive-Dynamic Biped

As a first step towards the engineering goal presented in the previous section, we now consider the design space for a robot using the features we have presented in this thesis. This design space that needs to be searched is 8-10 dimensional, depending on if we want to use flat feet or arc feet and whether we vary slope ϕ . These design parameters are $\psi, a, m_H, k_{hip}, k_{ankle}, r, \psi, d, m_t, \xi$. Note that ankle torques are not considered a valid design parameter when arc feet are used.

Searching such a high dimensional space for robust, stable robot designs presents many challenges, especially when we know so little about the space. Still, evolutionary optimization methods could be used. We now present the results of one simple search, and explain how the same methods might be used to design a complex biped with high mechanical robustness.

3.15.1 An Evolved Compass Biped

This section is an illustrative example of how we might optimize the mechanical structure of a compass biped using an evolutionary procedure, and the human brain to help assist optimization.

In this experiment, we created three generations of a compass biped. We created the first generation of compass bipeds by randomly picking values of a, m_H , the two ‘design parameters’ considered in this experiment. When we had found 33 combinations of parameters that resulted in robots with stable limit cycles, we tested each robot and measured its r_{IDR} and F_r .

Examining this data, we then selected 5 well-performing robots of the first generation. The design parameters of these robots were recorded, giving us a range of parameters which resulted in relatively robust bipeds. From this narrowed range of values, the second generation of robots was created. This second generation of robots were generally more robust and walked faster than the first generation. Generations 1 and 2 are marked ‘gen1’ and ‘gen2’ in figure 3.27. There are many possible robots which might result in the same r_{IDR} and F_r , so please do not assume that two data points near each other necessarily have the same structure.

For the third generation, a single robot that it was felt represented a good balance between robustness and walking speed was selected. To this robot, two variations were tested. One variation was to add increasingly large arc feet, shown in figure 3.27 as ‘Gen3a-R’. In the second variation, a hip spring was added instead of feet, and various increasing spring stiffness were tested for their effect on gait robustness and velocity. These robots are marked Gen3b in figure 3.27.

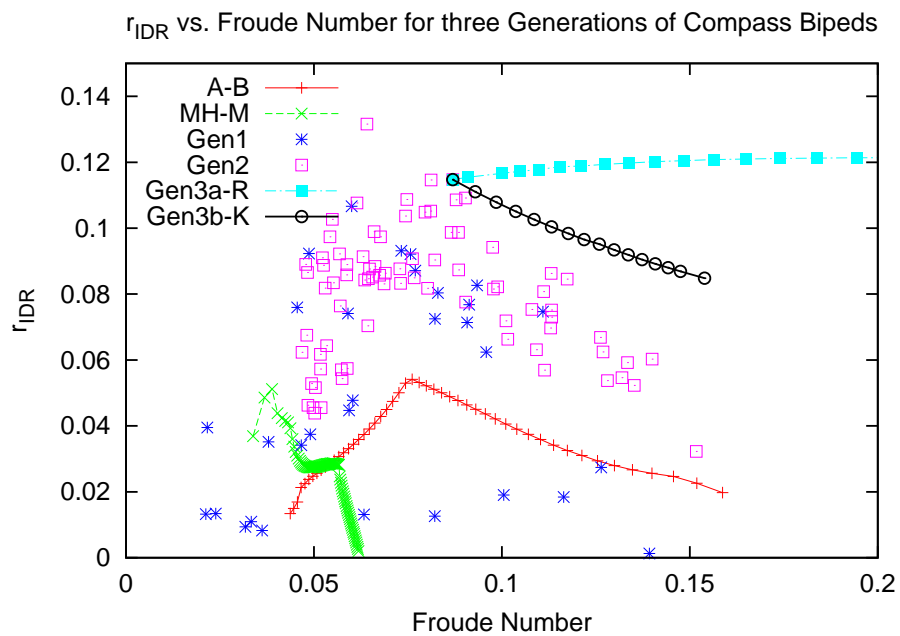


Figure 3.27: **Three generations of compass bipeds.** Generation 1 consists of 33 randomly selected points. Generation 2 consisted of 50 points, also also randomly selected, but over a smaller range of parameters. Generation 3 are variations on a single robust robot, showing the effect of adding a hip spring and an arc foot. The hip spring slightly lowered robustness, and arc foot scarcely improved robustness. Both additions increased gait velocity. The green and red lines are the results of varying a and m_H from the experiments earlier in this chapter, and are shown for comparison.

Figure 3.27 shows the results of evolving three generations of compass biped robots. The parameters of the robot selected for generation 3 for its good balance between gait robustness and forward speed are $a = 0.787$, $m_H = 0.154$. This robot walked with a forward speed of $F_r = 0.08$ and with a robustness of $r_{IDR} = 0.115$.

As would be predicted by the qualitative analysis of the parameters a, m_H that was presented in this chapter, the center of mass is quite high and the legs are relatively heavy. The high center of mass improves forward velocity and the relatively heavy legs improved robustness.

The relatively long lower leg length a may be the reason a hip spring had little effect; the natural swing period of the leg was likely already faster than the optimal value.

Other than requiring additional generations and trials as the dimensionality of the design space increases, the author does not see any reason why this type of design parameter optimization could not be used for the design of more complex bipeds. The the results of this experiment was a relatively robust and efficient walking robot. Although only two design parameters were studied, m_H and a , followed by k_{hip} and r , using this same procedure we could presumably design a robot with all of the features presented in this thesis.

Chapter 4

VARIABLE STIFFNESS SERIES ELASTIC ACTUATOR

In Section 3.8, it was shown via simulation that the optimal hip spring stiffness is different for two different forward velocities. This suggests that a physical robot with a variable stiffness spring could adapt its passive dynamics to better match the desired forward speed and increase the gait robustness.

Yet even if a passive dynamic robot has the ability to adjust its passive dynamics to better suit its environment, it is useless in the real world without actuators. The real world does not have infinitely long downhill slopes; we must provide energy to the robot using actuators. Practical considerations require the actuator have good force or torque capabilities, and not interfere with the mechanical passive dynamics of a robot like those analyzed in the previous chapter.

This chapter presents a novel actuator called the Variable Stiffness Series Elastic Actuator (VSSEA). The actuator is uniquely well-suited for use in natural dynamic robots. It is more versatile than many other compliant actuators, and the variable stiffness springs allow the possibility of maximizing a robot's passive-dynamic robustness to disturbances given a particular gait velocity.

4.1 Motivation for a New Actuator

As was mentioned in Section 1.3.1, traditionally actuators are designed to be very stiff machines so that position can be controlled accurately. Stiff machines have very good zero motion force bandwidth; that is, they can develop forces very quickly without much internal effort or movement. Compliant machines necessarily have lower zero motion force bandwidth. This is because it takes time for the compliant element to be displaced and for a force to develop.

Although being stiff is an advantage for position control systems – control systems for which the ideal actuator is a machine that is able to control position perfectly – being stiff is a disadvantage for natural dynamic systems. In natural dynamic systems, the ideal actuator is a machine that is able to control torque perfectly.

Excellent work outlining the advantages of compliant actuation has been done by [Pratt, Williamson 1995], [Pratt et al 2001], and [Robinson 2000]. A quote may illustrate their advocacy of the subject:

“We propose that for natural tasks, zero motion force bandwidth isn't everything, and incorporating series elasticity as a purposeful element within an actuator is a good idea.” – [Pratt, Williamson 1995]

It may be worth considering human muscle for a moment; human muscle is very close to a perfect force actuator in many ways. In today's marketplace, there exists no simple,

slow-speed, high-torque actuator which approaches a perfect force actuator. Since there are no simple actuators as good as human muscle, engineers who wish to have good force control accuracy are forced to introduce complex transmissions, compliant elements, load cells and related sensors.

Although so-called “direct-drive”, high torque electric motors exist and would seem to be a good candidate as a perfect force actuator, generally the torque of these motors is still one or more orders of magnitude lower than is needed for a mobile robot, and the power-to-weight ratio is low. For the foreseeable future, for most compliant actuation systems, it seems better to use an electric motor, geartrain or ballscrew, and a compliant transmission system.

One such compliant actuation system is the SEA (Series Elastic Actuator), developed by [Pratt et al 2001] and later [Robinson 2000]. It is simple, robust, and has good performance at low bandwidths. Indeed, the actuator presented in this thesis is named after the SEA and shares many similar design features. We now proceed to describe the VSSEA design.

4.2 Overview of the Variable Stiffness Series Elastic Actuator (VSSEA)

The actuator presented in this paper is named the Variable Stiffness Series Elastic Actuator (VSSEA), because it is essentially similar to the standard Series Elastic Actuator (SEA) design of [Robinson 2000][Pratt, Williamson 1995], but with the additional capability of variable stiffness. It uses two antagonistic nonlinear (quadratic) springs to effectively create a linear spring. This can be shown as follows, referencing figure 4.1 or 4.2:c for relevant measurements.

Assume we have an output mass sandwiched between two antagonistic compression springs A and B. Let x be the displacement of the mass from the equilibrium point. Here l_0 is the natural length of the spring, and l_{eq} is the length of the spring when in equilibrium with the antagonistic spring (at no-load conditions on the output mass). We assume that the springs are always under compression, (i.e. that $l_0 \geq l_{eq}$, $x \leq l_0 - l_{eq}$).

If the force-distance relationship for each spring when displaced from its natural length l_0 by a distance x is equal to

$$F(x) = K_l x$$

where K_l is the linear stiffness constant for that spring in units of N/m, then the force on the output mass is

$$\begin{aligned} F &= F_A - F_B \\ &= K_l[(l_0 - l_{eq}) - x] - K_l[(l_0 - l_{eq}) + x] \\ &= -2K_l x \end{aligned}$$

The precompression term ($l_0 - l_{eq}$) has no effect on the force the output mass sees, so a system which uses linear springs is not adjustable.

However, if the reactive force from the spring when displaced from its natural length l_0 by a distance x is equal to

$$F = K_n x^2$$

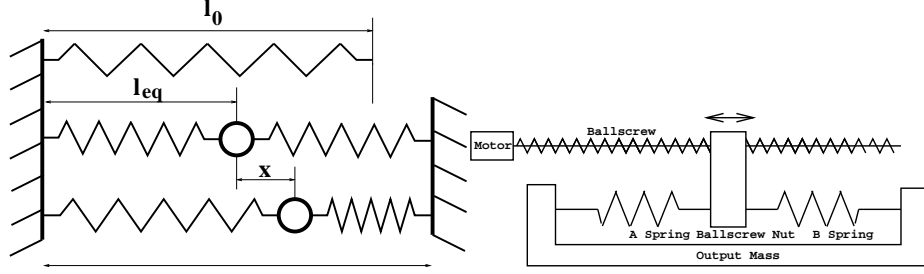


Figure 4.1: **Schematics for the VSSEA.** *Left:* Mechanical configuration of two compression springs used in the VSSEA, emphasizing spring lengths. *Right:* A functional schematic of the VSSEA design.

where K_n is the nonlinear stiffness constant for that spring in units of N/m^2 , then the force on the output mass is

$$\begin{aligned}
 F &= F_A - F_B \\
 &= K_n[(l_0 - l_{eq}) - x]^2 - K_n[(l_0 - l_{eq}) + x]^2 \\
 &= K_n[l_0 - l_{eq} - x][l_0 - l_{eq} - x] \\
 &\quad - K_n[l_0 - l_{eq} + x][l_0 - l_{eq} + x] \\
 &= K_n[l_0^2 - 2l_0l_{eq} - 2l_0x + l_{eq}^2 + 2l_{eq}x + x^2] \\
 &\quad - K_n[l_0^2 - 2l_0l_{eq} + 2l_0x + l_{eq}^2 - 2l_{eq}x + x^2] \\
 &= K_n[-4l_0x + 4l_{eq}x] \\
 &= -4K_n[l_0 - l_{eq}]x
 \end{aligned}$$

We now define $K_{eff} = -4K_n(l_0 - l_{eq})$ to be the effective linear spring constant in units of N/m . This gives us $F = K_{eff}x$, which is a linear spring that obeys Hooke's Law.

Notice that the effective stiffness K_{eff} , can be adjusted through the equilibrium pre-compression term ($l_0 - l_{eq}$).

In summary, the combination of two quadratic rate springs results effectively in a linear spring with a variable stiffness.

The concept of using two antagonistic nonlinear springs to produce a variable stiffness effect seems well known by many other researchers investigating variable-stiffness mechanisms, such as [Hurst 2004]. The maximum dynamic range of stiffness for two antagonistically paired quadratic springs is easily shown to be limited to a 2:1 ratio [Bicchi et al 2001], but we believe this range to be sufficient for the purposes of tuning the dynamics of a passive-dynamic robot.

Most researchers working on variable-stiffness mechanisms, such as [Migliore 2005], [Zinn et al 2004], and [Bicchi et al 2005], use actuators and quadratic springs in a different component topology than the VSSEA. They follow the principle that actuating antagonistic motors in common mode changes stiffness, and differential actuation changes position. In the VSSEA

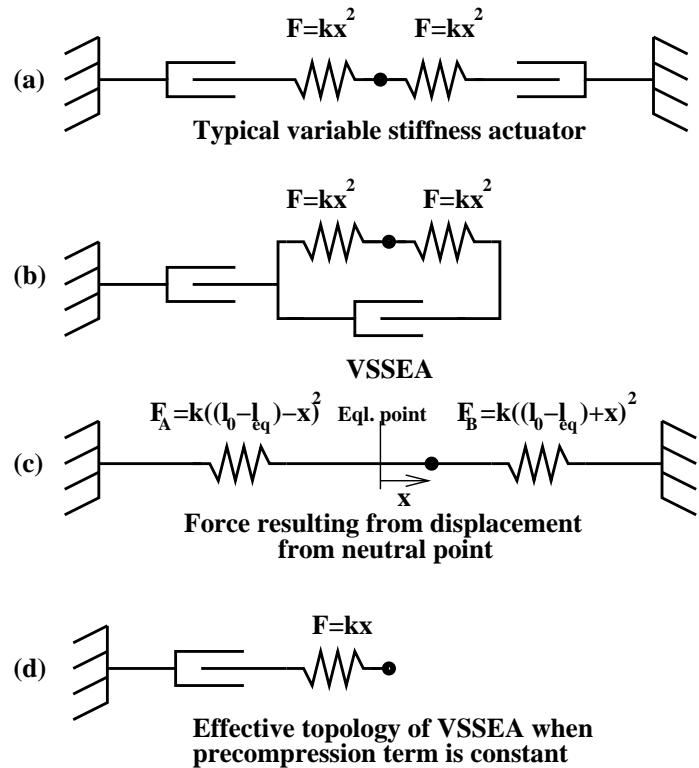


Figure 4.2: **A comparison of variable stiffness actuator topologies.** Warning: the elements drawn as dampers are in fact rigid, high stiffness electrical motors connected to leadscrews or ballscrews; i.e. stiff linear actuators. The black dots denote the mass being controlled relative to the fixed end of the VSSEA actuator. (a) shows a common topology used by many variable stiffness researchers. (b) shows the VSSEA topology. (c) shows the force on the output mass when both linear actuators are locked. (d) shows the effective VSSEA topology when only the precompression actuator is locked. This is the same as the SEA design by [Pratt, Williamson 1995].

design, the stiffness and position are actuated independently, similar to [Hurst 2004]. Graphically, the difference between the VSSEA and these other variable-stiffness mechanisms can be seen in figure 4.2(a) and 4.2(b).

The reason for the different topology is due to a different goal. Most researchers desire for the stiffness of the actuator to be varied quickly and continuously throughout a motion, and use this stiffness change as an essential part of the control system (for, say, the purposes of safety [Bicchi et al 2005], [Zinn et al 2004] or for bio-mimetic reasons [Migliore 2005]). In contrast to this, when using the VSSEA actuator in passive-dynamic robot models such as those presented in this paper, rather than *vary* the effective stiffness, we desire to *hold the stiffness close to some optimal value* corresponding to some stable, efficient limit cycle, while still being able to add energy to the system via actuation.

The benefit of the VSSEA topology is that, without any mechanical changes, and assuming that the motor/ballscrew combination is very stiff when unactuated or can be locked, a robot built with the VSSEA design could become a purely dynamic walker simply by removing power from the actuators. This was shown in figures 3.1 and 3.2. Another benefit of this topology is that control and analysis of the system are very close to linear, provided the stiffness is not changed quickly during operation, since the actuator model reduces to the simple SEA design shown in 4.2(d) when the precompression motor is kept a constant length.

While other robots have been built using SEAs[Pratt, Pratt 1998], unlike the approach presented in this paper, the mechanical design and control systems used on such robots did not generally focus on exploiting the great energetic efficiency found when operating near a passive-dynamic limit cycle.

4.3 Advantages of the VSSEA

We begin with the advantages most relevant to this thesis: the advantages of the VSSEA when used in natural dynamic systems. Assume for a moment that we have a passive-dynamic robot that we wish to actuate and make it walk at a range of speeds. As was shown in Section 3.8, the optimally robust spring stiffness value varies depending on the forward speed of the robot. Therefore, including a variable stiffness spring increases the range of speeds at which a passive-dynamic robot can robustly locomote.

The general limitations of passive dynamic robots to a single speed has been noted before by other researchers:

“Since the passive walking pattern is determined by the natural frequency of the mechanical system, changing the limit cycle can only be achieved by: 1. applying an additional force or torque, 2. actively changing the intrinsic system parameters.” – [van der Linde 1998]

“At this moment the passive walkers are restricted to one walking speed due to the eigenfrequency, which is fixed by the mechanical constructions.” – [Van Ham et al 2005]

Unlike the SEA, the VSSEA is not limited to a single eigenfrequency. By changing the effective stiffness of the actuator, a range of natural eigenfrequencies can be achieved. The

intrinsic mechanical oscillation of the system can be changed by varying the precompression on the springs.

Another problem common to all compliant actuators is that they only work for relatively low control bandwidths.

“While a compliant actuator or drive train can enhance safety characteristics, the performance of such systems is limited. The flexible modes of the compliant system prevents control bandwidths greater than about one-third of the fundamental resonant frequency.” – [Zinn et al 2004]

The VSSEA design could therefore improve control bandwidths of comparable SEAs up to a factor of two – as was mentioned earlier, the effective stiffness of the VSSEA can only be varied by a factor of two. However, if for some reason zero motion force bandwidth is really needed to be used in some situation, there is a way of adjusting the VSSEA for this task. One interesting feature of the VSSEA that is of debatable utility is the ability to fully compress the springs. When the springs are fully compressed, there is no longer any compliance between the input and output, and the VSSEA reduces to a normal, stiff actuator suitable for position control.

It may be that for some tasks such as running, looser springs with longer travel are better, but for other tasks such as walking, stiffer springs have superior robustness. Or vice versa. The important point to note is that the VSSEA design is flexible and capable of working over a range of such operational modes.

4.4 Disadvantages of the VSSEA

There are several disadvantages to the VSSEA as it is currently implemented. Most are related to engineering considerations and not a flaw in the conceptual design itself.

The greatest problem with the VSSEA design is the level of friction in the prototype, even after lubrication and adjustment. The problem is innate to compressive designs; similar to the problem present in motorcycle fork shock absorbers, any bending of the VSSEA during operation results in the bushings binding slightly, which greatly increases friction.

The current implementation of the VSSEA is also much too heavy to be used in a mobile robot; this design was intended as a proof-of-concept prototype. Another design revision is required, although it is unclear as to how the one of the heaviest parts, the ballscrew, could be lightened significantly.

Another engineering problem with the VSSEA is the accuracy of the load cells used. They turned out to be relatively fragile and inaccurate due to the friction problems mentioned earlier. Indeed, they probably contribute to the friction problem a great deal due to the way they were attached. They tend to cause a slight twisting or bending moment when force is applied. For most tasks, very accurately measuring the length of each spring is probably the better approach to follow.

Finally, a weakness common to all compliant actuators is the relatively low control bandwidths. Although two-actuator systems such as those presented by [Zinn et al 2004] can solve the bandwidth problem, this thesis ignores this problem entirely and assumes that

an appropriately well designed natural dynamic system will not even *need* high bandwidth control.

4.5 Mechanical Description

A CAD representation of the actuator is shown in figure 4.3. A prototype has been manufactured, and is shown in figure 4.4. The mechanical properties of the prototype are listed in table 4.1. More detailed schematics can be found in Appendix C.

Table 4.1: Parameters of Prototype Actuator

Parameter	Value	Units
Max length	89	cm
Overall mass	4.5	kg
Spring stroke	20	cm
No-force stroke	>10	cm
Max. K_{eff}	6400	N/m
Min. K_{eff}	3200	N/m
Main Motor	90	W
Precompression Motor	5	W
Max. Force	>320	N

We now describe the details of the VSSEA design, referring to the components labeled in figure 4.3 as necessary. At the heart of the actuator is the “main” motor (A) connected to a ballscrew (B). The ballscrew nut (C) is sandwiched between two variable-rate quadratic springs (not shown), which themselves are put under some variable amount of precompression by what we will call the “precompression” motor (D) and leadscrews (E). Two load cells (F) measure the compressive force acting on each spring. To determine the position of the output link (connected at D), length sensors (not shown) measure the length of each spring. The length sensors can also be used to verify the accuracy of the forces measured by the load cells, because the force-compression characteristics of the springs are known. A dust cover (G) keeps the actuator interior clean.

The prototype is composed mainly of aluminum and steel. Currently, most of the weight is from the ballscrew and long round guide tubes that run the length of the actuator.

Force-control is accomplished through PID feedback control of the ballscrew, using a quadrature encoder with 1024 counts per revolution. Applied force is calculated from measurement of the lengths of the springs, as well as the overall length and position of the actuator ballscrew nut and output mass.

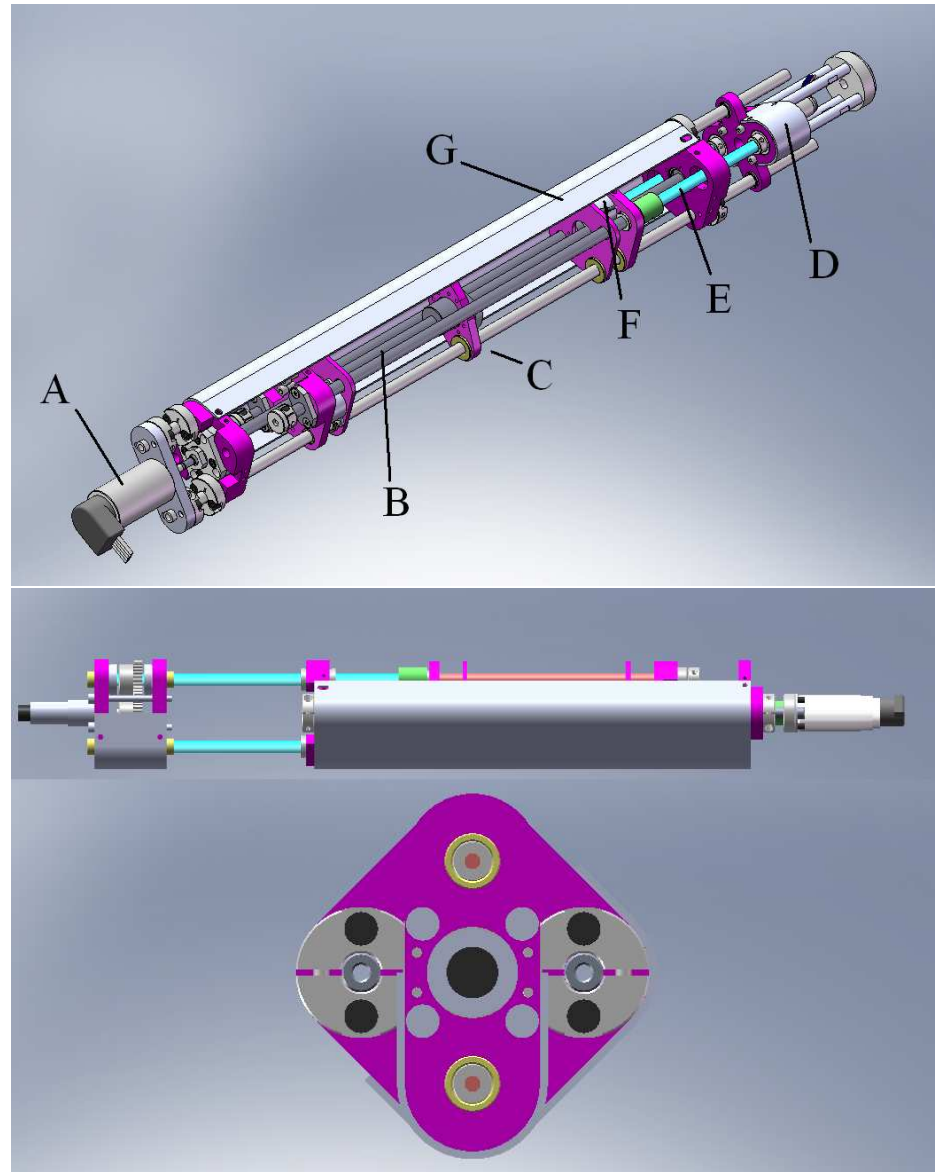


Figure 4.3: A computer rendered image of the VSSEA.



Figure 4.4: **Photos of the VSSEA.** *Left:* The VSSEA on a table. Extra sensors have been fitted to the VSSEA for testing. *Right:* The VSSEA in a vertical-hang test configuration. Two other configurations are possible: horizontal and “hopping” modes.

4.6 Electrical System and Control System Details

The VSSEA uses one relatively high torque 24V Faulhaber motor which draws up to 10A at stall, and a much smaller motor with a gearbox which adjusts the antagonistic spring precompression. Power is supplied by two motorcycle batteries as a simple and portable source of large amounts of current. Motors are controlled via the Faulhaber MCDC 3603 motor controller, used in current-control mode.

Sensors are measured using a custom designed 16-bit A/D board based on the Microchip MAX1270. This A/D board is interfaced to a hobbyist FPGA kit – the ‘Dragon’ board from www.fpga4fun.com – which is inserted into the PCI slot of a computer. The FPGA is responsible for taking sensor measurements, counting encoder pulses, and performing local PD control. A simple custom RTLinux kernel module responds to interrupts triggered by the FPGA and performing high-level computation and computing desired force control torques.

There are 6 sensors which are monitored regularly by the FPGA: two load cells which measure the compressive force on each spring, two potentiometers to measure the length of each spring and the length of the entire actuator, and two quadrature encoders with 1024 counts/revolution of the ballscrew. Additionally, two limit switches detect the limits of travel for the precompression leadscrews.

Chapter 5

CONCLUSIONS AND FUTURE RESEARCH

5.1 Conclusions

In this thesis, two metrics of gait robustness, r_{IDR} and r_{EDR} , were defined and studied via simulation. Both measurements predict qualitatively similar behavior when a particular design parameter is varied, although they do not agree on the magnitudes and specifics of the effect. For example, when either metric of robustness is used to analyze the stability of a biped with an interleg spring, we see a peaking behavior with an optimal value. However, the particular optimally robust spring stiffness is different depending on which metric is used.

This opens up an important question: which of the two measurements is more physically relevant to the robustness of a passive dynamic biped? Change in generalized momenta, using r_{IDR} , or change in kinetic energy, using r_{EDR} ? This can only be answered by experimentation.

A method for evolving a complex passive dynamic biped has also been presented.

Finally, a novel actuator suitable for not only actuating a passive dynamic robot, but adapting its intrinsic passive dynamics to better match the environment has been presented. The actuator would work well with the design concept presented in section 3.3.

5.2 Future Research

This section outlines some interesting directions that later research could build upon this thesis. In no particular order, we present a laundry list of possible interesting future work.

- **Experimental Work:** Currently, a great weakness of this thesis is that r_{IDR} and r_{EDR} have not undergone significant experimental or statistical analysis to see if they correlate well with physical experiments. Also, the problem of the most unstable instant not being the post-collision instant, as mentioned in Section 3.5.2, has not been fully addressed. Verifying the physical meaning of r_{IDR} and r_{EDR} experimentally would be very supportive to this thesis and to the greater passive-dynamics community.
- **Further Model Optimization Work:** Towards the end of Chapter 3, a compass biped was optimized for robustness and forward velocity. Using the existing models present in the simulator, it would be a simple matter to spend a few weeks of computer time to perform a wide search of the 10 design parameters considered in this thesis. On a 2.4Ghz single core computer with sufficient RAM, approximately 500-600 models can be thoroughly tested per day. Several thousand or perhaps tens of thousands of

data points with an evolutionary method would likely be sufficient for a rough search of the 10-dimensional search given some reasonable constraints on the range of each parameter.

- **Further Model Experiments:** How do the r_{IDR} values of biped models with more than 2 degrees of freedom compare to the results in this paper? What is the effect of knees on gait robustness? How do running robots compare? Such models could be integrated into the simulator with very little additional work.
- **Programming Work:** The current version simulator is written in a rather general manner, already uses OpenGL for 3D visualization, and could be extended to support 3D models with a few weeks of work. Specifically, supporting 3D models would require additional simulation constraints such as friction and perhaps certain nonholonomic constraints.
- **Theoretical Work:** The energy-distance method of simultaneously measuring robustness and developing optimal controllers presented in the following section (5.3) is a further extension of the concept of robustness. This distance would not only consider the generalized momenta of the system, but also the generalized coordinates.
- **Engineering Work:** The VSSEA actuator is fine as a prototype, but needs significant weight reduction and less friction before it is suitable for use in a practical mobile robot. Revising the design, measuring control bandwidths experimentally, and constructing a 2D bipedal walker such as the one shown in figure 3.1 would help support the practical nature of the ideas presented in this thesis.

5.3 Mechanical/Control System Design in a Natural Dynamics Biped

This section discusses a design method applicable to natural dynamics systems. Whether a passive-dynamic robot with a control system is still truly passive-dynamic or not is an issue of terminology, so we will avoid this philosophical problem and use the more general term “natural-dynamics” to mean a passive-dynamic system with a controller. I believe this is appropriate given the loose definition discussed in Section 1.3.4.

How does one control a natural dynamics biped without destroying its passive-dynamic behavior? What is the objective of the control system? These are difficult questions with a multitude of answers. As was unfortunately noted by another researcher,

“There is still no general design strategy for [natural dynamic robots] and their controllers...” – [Buchli et al 2006]

Still, in perhaps naive opposition to this quote, this section outlines a general design strategy for natural dynamic robots and their controllers, assuming they are near a limit cycle. The author warns that much of this section is merely conceptual, and mostly conjecture without data or mathematics to support it. It is also likely that this design strategy

is well known by other researchers. However, it is an interesting area of future research that the author wished to outline a little more clearly. With these admissions out of the way, we will now describe a method of designing mechanical structure and a controller simultaneously.

5.3.1 Types of Controllers

In the following sections, we artificially divide controllers into three categories, depending on the function of the controller. These classifications are rather arbitrary and are made purely to help clarify the distinction between energy used for forward locomotion and energy used to reject disturbances.

Oscillation-Sustaining Controllers

The majority of previous research into passive-dynamic robot control focuses upon what we will term “oscillation-sustaining” controllers. They will be called this because they provide no stabilizing influence on the mechanical-environmental interaction of a passive-dynamic robot. Rather, they merely provide energy keep the mechanical-environmental interaction going in environments other than a downhill slope; in essence, an oscillation-sustaining controller merely replaces the gravitational gradient as an energy source, while keeping the mechanically efficient limit cycle. This allows a robot to walk up a hill, down a hill, or on the flat. Stabilization of gait still occurs exclusively via mechanical effects, as with purely passive-dynamic robots.

Controllers such as those by [Goswami et al 1996], [Spong 1999], and [Asano, Luo 2006] fall into this category of controllers. Such controllers are probably a good first step towards making practical bipeds. At the very least, they provide some forward speed control and slightly decouple the robot from its environment. In many ways all three of these controllers are equivalent; they add torques to the system which maintain a constant level of total system energy from step to step.

The flaw with using only these controllers in a robot is that they leave the task of stabilization entirely to the mechanical effects. From reading the chapter 3 it should be clear that even optimized passive-dynamic robot mechanical systems are only mildly robust to disturbances.

Stabilizing Controllers

The second class of controllers we will call “stabilizing controllers”, for the simple reason that this class of controllers provides stabilizing effects to the robot which improve upon the natural mechanical gait robustness.

There is little we can say in general about such controllers. The task of designing this type of controller is made especially difficult if we follow the philosophical approach outlined in Section 1.3.4. That is,

The controller must not force the robot to move in a certain way, but must work with the passive dynamics of the system.

As far as the author is aware, the only general method to date which can be used to stabilize a biped using the natural dynamics design approach is Virtual Model Control, proposed by [Pratt et al 2001]. The method, however, provides no hints as to how an optimal minimum-energy use controller might be designed.

Arbitrary Trajectory Controllers

A third class of controller might be called the “arbitrary trajectory tracking” controller. A controller of this type could make a robot arm follow any trajectory. However, this type of controller is not particularly relevant to the concept of natural dynamics, since the core idea of natural dynamics is to exploit some mechanical behavior for greater efficiency in a certain class of movements or when there are few constraints on motion, not to move at some prescribed velocity along a trajectory. We do not consider this type of controller further.

Therefore, let us focus only on the problem of keeping a bipedal robot walking and use only stabilizing and oscillation-sustaining controllers.

5.3.2 The Mechanical/Control Design Concept

Let us assume for this remainder of this chapter that we desire to design a bipedal robot that walks at a fixed speed, consumes as little energy as possible, and is very robust against disturbances. Now assume we want to design the mechanics and controller of the robot to complement each other. We ask three natural questions:

Looking at the figure 3.27, there seems to be a tradeoff between mechanical robustness and mechanical efficiency. If more data points were plotted, is very likely we would see a Pareto front. On such a front, the mechanical structure of the robot can be made more stable, or more efficient, but not both.

If we build a robot and plan to use only an oscillation-sustaining controller and rely on mechanical effects for our stabilization, we obviously want to choose the mechanical structure which maximizes gait robustness. A metric such as the ones presented in this thesis could be used for this purpose.

On the other hand, if we somehow also knew how to design a stabilizing controller, a more fruitful approach might be to separate the design into two parts. First, design the mechanical system and oscillation-sustaining controller to create a marginally stable limit cycle, and as low cost of transport as possible. Then, use the stabilizing controller to make this limit cycle robust against disturbances. Theoretically, one could stabilize even a marginally stable limit cycle a vanishingly small energy cost. The situation would be similar to balancing an inverted pendulum; if you keep the pendulum close enough to vertical it requires almost no energy to keep stable. Larger disturbances, of course, would need to be fully resisted by the controller.

But wait a moment! It is presumable that small disturbances might be resisted by a robust mechanical system with no controller energy cost. This suggests some sort of balance between mechanical stability and controller-achieved stability might in some circumstances be optimal, depending upon the operating environment and expected magnitude of disturbances.

Now we are faced with two very difficult questions:

1. How do we decide whether gait robustness is achieved mostly via mechanical effects or via a control system?
2. How do we decide how much energy should be expended sustaining the mechanical oscillation and expended rejecting large disturbances?

Imagine for a moment that we could measure large disturbances to the mechanical system not in terms of r_{IDR} or r_{EDR} , but in terms of controller energy consumed. Any type of controller could presumably be used, but let us assume that we have somehow developed the energetically optimal 1-step stabilizing controller. This hypothetical optimal controller uses the minimum amount of actuator energy to return the robot from any state to the stable region of the mechanical limit cycle each step.

Much like the way that r_{IDR} and r_{EDR} are a scalar measurement of distances on $T_q^*\mathbb{Q}$, we could use the energy consumed by this hypothetical optimal controller to define a distance between any two states on \mathbb{Q} . That is, we could use the hypothetical optimal controller to measure the ‘energy consumed’ distance on the state space manifold. Let us call this ‘controller energy distance’ d_e .

This opens a powerful approach for measuring the purely mechanical robustness of a robot. We can now measure the distance between two states in terms of d_e . Disturbances could also be measured in terms of d_e . And since d_e is measured in units of energy, we could also compare the work done by the oscillation-sustaining controller and the stabilizing controller. This lets the designer use a common currency when deciding on the optimal tradeoff between robustness and gait efficiency.

An example may clarify. Consider two robots, A and B, walking on even ground and powered completely by their oscillation sustaining controllers and stabilizing controllers. Robot A has expends 1.0 joules of energy sustaining its mechanical oscillation each step, but can reject 0.8 joules worth of disturbances each step using mechanical effects. Robot B is more efficient on flat surfaces and expends 0.7 joules of energy sustaining its oscillation each step, but is much less mechanically robust and has only 0.2 joules worth of mechanical disturbance rejection.

Let us continue this contrived example and pretend that the environment the robots will operate in is slightly bumpy and introduces a disturbance of about 1.2 joules each step. In this environment, robot A is energetically the winner, consuming 1.0 joule of energy to sustain its mechanical oscillation, dissipating 0.8 joules of the 1.2 joules of disturbance energy mechanically. It thus requires $1.0 + (1.2 - 0.8) = 1.4$ joules of energy per step. Robot B will consume $0.7 + (1.2 - 0.2) = 1.7$ joules of energy per step. However, on a very flat smooth surface with no disturbances, robot B would require less energy.

This example is meant to illustrate that there may be a tradeoff between robustness achieved mechanically and robustness achieved via stabilizing control, but we can compare the two if we measure everything in terms of energy. Admittedly, it sounds somewhat strange to measure the robustness of a purely mechanical system in terms of the energy used by some hypothetical controller. On the other hand, perhaps it is fitting that this situation

occur when designing a controller and mechanical system at the same time; otherwise too much may be assumed by the designer and the design will be suboptimal.

Designing an Optimal Minimum-Energy-Use Controller

We now stop ignoring the elephant in the room and turn to the problem of designing the hypothetical optimal controller.

We approach the design of such a controller from the perspective of the calculus of variations. The calculus of variations can be used to derive Lagrange's equations by formulating it as a variational problem of minimization, and using the local property that the physical trajectory is the one where the differential 'action' is assumed to be zero, i.e. that $dqMdq = 0$.

When that local property $dqMdq = 0$ does not hold, it often becomes much more difficult to analytically derive the equations for how a rigid body moves. Indeed, the problem of finding the functional which minimizes the action integral between two points is essentially the same as Pontryagin's minimization principle; minimizing the path integral of the action results in the optimal control trajectory. This branch of mathematics was also extensively studied by Bellman, who founded the field of Dynamic Programming.

Although no general analytic methods exist for finding such functionals in general, there are many optimization methods which can be used numerically using various minimization principles. In [Tedrake 2004], for example, a controller for a passive dynamic biped was developed using such numerical methods.

Obviously, using numerical methods to design an optimal controller for every single mechanical model under consideration is prohibitively computationally intensive. After all, making an optimal minimum-energy-use controller using numerical methods requires finding many optimal paths between many many different states, and mapping out this space.

However, if we measure the robustness of a biped in the same manner that we measured r_{IDR} – that is, we measure the worst-case disturbance only – we only need to find the worst-case d_e value. That is, we only need to find the particular functional needed to evaluate d_e . Each time we measure d_e , we only need to solve one small part of the optimal control problem. This greatly reduces the required computational time.

Using this procedure, the same techniques used to derive optimal controllers numerically could be used to measure the robustness of a bipedal robot (or indeed any system with a limit cycle). Possibly similar to the way r_{IDR} was computed (see Appendix D.3), some sort of two-step evolutionary search algorithm could be an efficient way of searching a high-dimensional space.

In summary, the proposed method is thus:

1. Design some mechanical robots with limit cycles, and oscillation-sustaining controllers for these robots.
2. Measure these robots' worst-case disturbances in terms of d_e .
3. Repeat steps #1 and #2, varying the mechanical parameters until the Pareto front is found, and tradeoffs must be made between robustness and energetic efficiency.

4. Pick a robot on the Pareto front which has a gait that corresponds to the expected operating environment.
5. The resulting biped will have very close to optimal minimum energy use in this environment.
6. Use the same technique used to measure d_e to design the optimal controller.

BIBLIOGRAPHY

- [Ahmadi 1998] M. Ahmadi. "Stable Control of a One-Legged Robot Exploiting Passive Dynamics," *Ph.D Thesis, McGill University, Canada*, 1998.
- [Ahmadi, Buehler 2006] M. Ahmadi and M. Buehler. "Controlled Passive Dynamic Running Experiments with the ARL-Monopod II," *IEEE Transactions on Robotics*, vol.22, no.5, October 2006, pp.974-986.
- [Ahmadi, Buehler 1999] M. Ahmadi and M. Buehler. "The ARL Monopod II Running Robot: Control and Energetics," *Proceedings. 1999 IEEE International Conference on Robotics and Automation*, vol.3, 1999, pp.1689 - 1694.
- [Ahmadi, Buehler 1997] M. Ahmadi and M. Buehler. "Stable Control of a Simulated One-Legged Running Robot with Hip and Leg Compliance," *IEEE Transactions on Robotics and Automation*, vol.13, Feb 1997, pp.96-104.
- [Arimoto 1980] S. Arimoto and F. Miyazaki. "A control theoretic study on dynamical biped locomotion," *Trans. ASME, Journal of Dynamic Systems, Measurement, and Control*, 1980, pp.233-239.
- [Asano, Luo 2007] F. Asano and Z. Luo. "The Effect of Semicircular Feet on Energy Dissipation by Heel-Strike in Dynamic Biped Locomotion," *Proceedings of the 2007 IEEE/RSJ International Conference on Robotics and Automation*, 2007, pp.3976-3981.
- [Asano, Luo 2006] F. Asano and Z. Luo. "On Energy-Efficient and High-Speed Dynamic Biped Locomotion with Semicircular Feet," *Proceedings of the 2006 IEEE/RSJ International Conference on Intelligent Robots and Systems*, 2006, pp.5901-5906.
- [Asano, Luo, Hyon 2005] F. Asano, Z. Luo and S. Hyon. "Parametric Excitation Mechanisms for Dynamic Bipedal Walking," *Proceedings of the 2005 IEEE International Conference on Robotics and Automation*, 2005, pp.611-617.
- [Bicchi et al 2005] A. Bicchi, G. Tonietti, M. Bavaro and M. Piccigallo. "Variable Stiffness Actuators for Fast and Safe Motion Control," *Robotics Research, STAR 15*, 2005, pp.527-536.
- [Bicchi, Tonietti 2004] A. Bicchi and G. Tonietti. "Fast and "Soft-Arm" Tactics," *IEEE Robotics & Automation Magazine*, June 2004, pp.22-33.
- [Bicchi et al 2001] A. Bicchi, S. Rizzini and G. Tonietti. "Compliant design for intrinsic safety: General issues and preliminary design," *Proceedings of the 2001 IEEE/RSJ International Conference on Intelligent Robots and Systems*, vol.4, 2001, pp.1864-1869.
- [Boston Dynamics 2008] . Author Unknown. "Big Dog: The Most Advanced Quadruped on Earth," <http://www.bostondynamics.com/content/sec.php?section=BigDog>.
- [Brown, Zeglin] B. Brown and G. Zeglin. "The Bow Leg Hopping Robot," *Proceedings of the IEEE International Conference on Robotics and Automation*, May 1998.
- [Buchli et al 2006] J. Buchli, F. Iida and A. Ijspeert. "Finding Resonance: Adaptive Frequency Oscillators for Dynamic Legged Locomotion," *Proceedings of the 2006 IEEE/RSJ International Conference on Intelligent Robots and Systems*, October 2006, pp.3903-3909.
- [Byl, Tedrake 2006] K. Byl and R. Tedrake. "Stability of Passive Dynamic Walking on Uneven Terrain," *Proceedings of Dynamic Walking 2006*, May 2006.

- [Chevallereau et al 2004] C. Chevallereau, E. Westervelt and J. Grizzle. "Asymptotic Stabilization of a Five-link, Four-actuator, Planar Bipedal Runner," *43rd IEEE Conference on Decision and Control*, vol.1, Dec 2004, pp.303-310.
- [Collins et al 2005] S. Collins, A. Ruina, R. Tedrake and M. Wisse. "Efficient Bipedal Robots Based on Passive-Dynamic Walkers," *Science*, vol.307, 18 February 2005, pp.1082-1085.
- [Collins, Ruina 2005] S. Collins and A. Ruina. "A Bipedal Walking Robot with Efficient and Human-like Gait," *Proc. of ICRA*, 2005, pp.1983-1988.
- [Collins, et al 2001] S. Collins, M. Wisse and A. Ruina. "A Three-Dimensional Passive-Dynamic Walking Robot with Two Legs and Knees," *The International Journal of Robotics Research*, vol.20, no.7, 2001, pp.607-615.
- [Donelan 2002] J. Donelan, R. Kram and A. Kuo. "Mechanical work for step-to-step transitions is a major determinant of the metabolic cost of human walking," *The Journal of Experimental Biology*, vol.205, 2002, pp.3717-3727.
- [Endo, Paluska, Herr 2006] K. Endo, D. Paluska and H. Herr. "A quasi-passive model of human leg function in level-ground walking," *Proceedings of the 2006 IEEE/RSJ International Conference on Intelligent Robots and Systems*, 2006, pp.4935-4939.
- [Formalski 1978] A. Formalski. "The Movement of Anthropomorphic Mechanisms under Impulsive Control," *Selected Problems of Robot Mechanisms and Bio-Mechanics*, 1978, pp.17-34, (in Russian).
- [Fujita et al 2003] M. Fujita, K. Sabe, Y. Kuroki, T. Ishida and T. Doi. "SDR-4X II: A Small Humanoid as an Entertainer in Home Environment," *International Symposium of Robotics Research*, 2003, pp.960-967.
- [Garcia 1998] M. Garcia, A. Chatterjee, A. Ruina and M. Coleman. "The Simplest Walking Model: Stability, Complexity, and Scaling," *ASME Journal of Biomechanical Engineering*, Feb 1998.
- [Geng et al 2006] T. Geng, B. Porr and F. Worgotter. "Fast Biped Walking with A Sensor-driven Neuronal Controller and Real-time Online Learning," *The International Journal of Robotics Research*, vol.25, no.3, 2006, pp.243-259.
- [Geyer 2006] H. Geyer, A. Seyfarth and R. Blickhan. "An integrative view on legged locomotion obtained from the bipedal spring-mass dynamics," *Dynamic Walking Conference*, 2006.
- [Goswami et al 1996] A. Goswami, B. Thuilot and B. Espiau. "Compass-like biped robot. Part I: Stability and bifurcation of passive gaits," *INRIA Research Report*, 1996.
- [Grizzle 2001] J. Grizzle, G. Abba and F. Plestan. "Asymptotically Stable Walking for Biped Robots: Analysis via Systems with Impulse Effects," *Transactions on Automatic Control*, January 2001, pp.51-65.
- [Hobbeln 2007] D. Hobbeln and M. Wisse. "A Disturbance Rejection Measure for Limit Cycle Walkers: The Gait Sensitivity Norm," *IEEE Transactions on Robotics*, 2007.
- [Hurst 2004] J. Hurst, J. Chestnutt and A. Rizzi. "An Actuator with Physically Variable Stiffness for Highly Dynamic Legged Locomotion," *Proceedings of the 2004 IEEE International Conference on Robotics and Automation*, 2004, pp.4662-4667.
- [Hurst, Rizzi 2004] J. Hurst and A. Rizzi. "Physically Variable Compliance in Running," *CLAWAR*, SPRINGER-VERLAG, www.springer-online.com, September, 2004.

- [Ishiguro et al 2003] A. Ishiguro, K. Ishimaru, K. Hayakawa and T. Kawakatsu. "How Should Control and Body Dynamics be Coupled? A Robotic Case Study," *Proceedings of the 2003 IEEE/RSJ International Conference on Intelligent Robots and Systems*, 2003, pp.1727-1732.
- [Kajita et al 2002] S. Kajita, T. Nagasaki, K. Yokoi, K. Kaneko and K. Tanie. "Running Pattern Generation for a Humanoid Robot," *Proceedings of the 2002 IEEE/RSJ International Conference on Robotics and Automation*, 2002, pp.2755-2761.
- [Kaneko et al 2004] K. Kaneko, F. Kanehiro, S. Kajita, H. Hirukawa, T. Kawasaki, M. Hirata, K. Akachi and T. Isozumi. "Humanoid Robot HRP-2," *Proceedings of the 2004 IEEE International Conference on Robotics and Automation*, 2004, pp.1083-1090.
- [Kuo 2002] A. Kuo. "Energetics of Actively Powered Locomotion Using the Simplest Walking Model," *Journal of Biomechanical Engineering*, vol.124, 2002, pp.113-120.
- [Kuo 2001] A. Kuo. "A Simple Model of Bipedal Walking Predicts the Preferred Speed-Step Length Relationship," *Transactions of the ASME*, vol.123, June 2001, pp.264-269.
- [Marsaglia 1959] G. Marsaglia. "Choosing a Point from the Surface of a Sphere.,," *Ann. Math. Stat.*, vol.43, 1972, pp.645-646.
- [McGeer 1990a] T. McGeer. "Passive Dynamic Walking," *The International Journal of Robotics Research*, vol.9, no.2, 1990, pp.62-82.
- [McGeer, 1990b] T. McGeer. "Passive Dynamic Walking with Knees," *1990 IEEE Robotics & Automation Conference*, 1990, pp.1640-1645.
- [McGeer, 1988] T. McGeer. "Stability and Control of Two-Dimensional Biped Walking," *Simon Fraser University CSS-ISS TR 88-01, 1988*, 1988.
- [Meyer et al 2006] F. Meyer, A. Sprowitz and L. Berthouze. "Passive compliance for RC servo-controlled bouncing robot," *Advanced Robotics*, vol.20, no.8, 2006, pp.953-961.
- [Michalska 1996] H. Michalska, M. Ahmadi and M. Buehler. "Vertical Motion Control of a Hopping Robot," *Proceedings of the 1996 International Conference on Robotics and Automation*, 1996.
- [Migliore 2005] S. Migliore, E. Brown and S. DeWeerth. "Biologically Inspired Joint Stiffness Control," *Proceedings of the 2005 IEEE International Conference on Robotics and Automation*, pp.4508-4513.
- [Miyakoshi, Cheng 2004] S. Miyakoshi and G. Cheng. "Examining Human Walking Characteristics with a Telescopic Compass-like Biped Walker Model," *IEEE Intl. Conf. on Systems, Man and Cybernetics*, October 2004, pp.1538-1543.
- [Mombaur 2006] K. Mombaur and R. Longman. "Optimization of Stability and Efficiency of Dynamic Walking," *Dynamic Walking Conference, 2006*, 2006.
- [Nakanishi et al 2004] J. Nakanishi, J. Morimoto, G. Endo, G. Cheng, S. Schaal and M. Kawato. "An Empirical Exploration of Phase Resetting for Robust Biped Locomotion with Dynamical Movement Primitives," *2004 IEEE/RSJ International Conference on Intelligent Robots and Systems.*, vol.1, no.1, 2004, pp.919-924.
- [Olensek, Matajacic 2005] A. Olensek and Z. Matjacic. "Further Steps Toward More Human-like Passive Bipedal Walking Robots," *Proceedings of the 2005 IEEE International Conference on Robotics and Automation*, 2005, pp.7-11.
- [Owaki, Ishiguro 2006] D. Owaki and A. Ishiguro. "Enhancing Self-stability of a Passive Dynamic Runner by Exploiting Nonlinearity in the Leg Elasticity," *SICE-ICASE, 2006. International Joint Conference*, 2006, pp.4532-4537.

- [Pratt 2000] J. Pratt. "Exploiting Inherent Robustness and Natural Dynamics in the Control of Bipedal Walking Robots," *Ph.D Dissertation, MIT*, 2000.
- [Pratt et al 2001] J. Pratt, C. Chew, A. Torres, P. Dilworth and G. Pratt. "Virtual Model Control: An Intuitive Approach for Bipedal Locomotion," *The International Journal of Robotics Research*, vol.20, no.2, February 2001, pp.129-143.
- [Pratt, Krupp 2006] J. Pratt and B. Krupp. "Series Elastic Actuators for legged robots," *Unmanned Ground Vehicle Technology VI. Proceedings of the SPIE*, vol.5422, pp.135-144.
- [Pratt, Pratt 1998] J. Pratt and G. Pratt. "Intuitive Control of a Planar Bipedal Walking Robot," *Proceedings of the 1998 International Conference on Robotics and Automation*, 1998, pp.2014-2021.
- [Pratt, Williamson 1995] G. Pratt and M. Williamson. "Series Elastic Actuators," *Proceedings of the IEEE/RSJ International Conference on Intelligent Robots and Systems*, vol.1, 1995, pp.399-406.
- [Press et al 1988] W. Press, S. Teukolsky, W. Vetterling and B. Flannery. "Numerical Recipes in C: The Art of Scientific Computing, Second Edition," *Cambridge University Press, Cambridge NY*, 1988.
- [Rad et al 1993] H. Rad, P. Gregorio and M. Buehler. "Design, Modeling and Control of a Hopping Robot," *IROS 1993*, 1993, pp.1778-1785.
- [Raibert 1986] M. Raibert. "Legged Robots That Balance," *MIT Press, Cambridge MA*, 1986.
- [Ringrose 1997] R. Ringrose. "Self-Stabilizing Running," *Proc. of IEEE ICRA*, 1997, pp.487-493.
- [Robinson 2000] D. Robinson. "Design and Analysis of Series Elasticity in Closed-loop Actuator Force Control," *Ph.D Dissertation*, June 2000.
- [Ruina et al 2005] A. Ruina, J. Bertram and M. Srinivasan. "A collisional model of the energetic cost of support work qualitatively explains leg sequencing in walking and galloping, pseudo-elastic leg behavior in running and the walk-to-run transition," *Journal of Theoretical Biology*, vol.237, April 2005, pp.170-192.
- [Sakagami et al 2002] Y. Sakagami, R. Watanabe, C. Aoyama, S. Matsunaga, N. Higaki and K. Fujimura. "The Intelligent ASIMO: System overview and Integration," *Proceedings of the IEEE/RSJ International Conference on Intelligent Robots and Systems*, 2002, pp.2478-2483.
- [Satoh et al 2006] S. Satoh, K. Fujimoto and S. Hyon. "Gait Generation for Passive Running via Iterative Learning Control," *Proceedings of the 2006 IEEE/RSJ International Conference on Intelligent Robots and Systems*.
- [Schwab 2001] A. Schwab and M. Wisse. "Basin of Attraction of the Simplest Walking Model ,," *Proceedings of ASME Design Engineering Technical Conferences*, 2001.
- [Slotine 2004] J. Slotine. "Contraction Analysis of Synchronization in Networks of Nonlinearly Coupled Oscillators," *Sixteenth International Symposium on Mathematical Theory of Networks and Systems, Belgium*, 2004.
- [Spong 1999] M. Spong. "Passivity Based Control of The Compass Gait Biped," *IFAC World Congress, Beijing, China*, July, 1999.
- [Srinivasan 2006] M. Srinivasan. "Why Walk and Run: Energetic Costs and Energetic Optimality in Simple Mechanics-Based Models of a Bipedal Animal," *Ph.D Dissertation*, May 2006.
- [Srinivasan, Ruina 2005] M. Srinivasan and A. Ruina. "Computer optimization of a minimal biped model discovers walking and running," *Nature*, vol.439, Sept 2005, pp.27-75.

- [Su, Dingwell 2006] J. Su and J. Dingwell. "Orbital Stability of Passive Dynamic Walking on an Irregular Surface," *Dynamic Walking Conference 2006*.
- [Tedrake 2004] R. Tedrake and J. Dingwell. "Applied Optimal Control for Dynamically Stable Legged Locomotion," *Ph.D Dissertation, MIT*, 2004.
- [Thorson 2007] I. Thorson. "Design Considerations for a Variable Stiffness Actuator in a Robot that Walks and Runs," *Proceedings of ROBOMEC 2007, Akita, Japan.*, May 2007.
- [Uemura et al 2006] M. Uemura, K. Kanaoka and S. Kawamura. "Power Assist Systems based on Resonance of Passive Elements," *Proceedings of the 2006 IEEE/RSJ International Conference on Intelligent Robots and Systems*, 2006, pp.4316-4321.
- [Umedachi, Ishiguro 2006] T. Umedachi and A. Ishiguro. "A Development of a Fully Self-contained Real-time Tunable Spring," *Proceedings of the 2006 IEEE/RSJ International Conference on Intelligent Robots and Systems*, 2006, pp.1662-1667.
- [Van Ham et al 2005] R. Van Ham, B. Vanderborght, M. Van Damme, B. Verrelst and D. Lefeber. "MACCEPA: the Actuator with adaptable compliance for dynamic walking bipeds," *CLAWAR 2005: 8th International Conference on Climbing and Walking Robots and the Support Technologies for Mobile Machines*, pp.759-766.
- [Vanderborght et al 2006] B. Vanderborght, B. Verrelst, R. Van Ham, M. Van Damme, D. Lefeber, B. Duran and P. Beyl. "Exploiting Natural Dynamics to Reduce Energy Consumption by Controlling the Compliance of Soft Actuators," *The International Journal of Robotics Research.*, vol.25, no.4, April 2006, pp.343-358.
- [van der Linde 1998] R. van der Linde. "Active leg compliance for passive walking," *Proceedings of the 1998 IEEE International Conference on Robotics & Automation*, 1998, pp.2339-2344.
- [Williamson 1998] M. Williamson. "Exploiting Natural Dynamics in Robot Control," *Fourteenth European Meeting on Cybernetics and Systems Research (EMCSR '98)*, 1998.
- [Williamson 1999] M. Williamson. "Robot Arm Control Exploiting Natural Dynamics," *Ph.D Dissertation, MIT*, June 1999.
- [Wisse 2004] M. Wisse. "Essentials of dynamic walking: Analysis and design of two-legged robots," *Ph.D Dissertation, Technische Universiteit Delft*, 2004.
- [Zinn et al 2004] M. Zinn, O. Khatib, B. Roth and J. Salisbury. "Playing It Safe," *IEEE Robotics & Automation Magazine*, June 2004, pp.12-21.

Appendix A

MATHEMATICAL CONVENTIONS, ABBREVIATIONS, LIST OF SYMBOLS

Unless otherwise specified, all angles are measured counter-clockwise, starting from the vertical.

Subscripts:

- a Ankle. Denotes a quantity related to the ankle.
- f Free leg. Denotes a quantity related to the non-stance leg.
- H Hip. Denotes a quantity related to the hip.
- i Indicates element number. Ex: q_k is the k th element of vector q .
- s Stance leg, a quantity related to the stance leg.
- t Torso. Denotes a quantity related to the torso.
- LC Limit Cycle. Denotes any state on the limit cycle.
- NR Non-returning. Denotes any state which does not naturally return to the limit cycle.

Parameters, Variables, Vectors, Matrices:

- a Length of the lower part of a leg [m]
- b Length of the upper part of a leg [m]
- c_t Cost of transport.
- $c_e t$ Cost of transport, considering total metabolic or battery energy consumed.
- $c_m t$ Cost of transport, considering total mechanical work done.
- d Length of the torso [m]

d_e	The ‘Optimal Controller Energy Distance’; energy used by an optimal controller to return the robot to the limit cycle after a disturbance.
k	A spring stiffness coefficient
m	Mass of a point-mass. [kg]
p	Generalized (angular) momenta of a system.
q	Generalized coordinates. [rad]
\dot{q}	Generalized velocity.
r	Radius of arc foot.
r_{IDR}	Impulse Disturbance Rejection radius. The magnitude of the largest change in generalized momenta that the system can withstand and still return to the limit cycle.
r_{EDR}	Energy Disturbance Rejection radius. The change of energy of the largest change in generalized momenta that the system can withstand and still return to the limit cycle.
D	New geometric constraint matrix at the instant of collision, in the extended coordinate system.
$E(q, \dot{q})$	Total energy of the system. $E(q, \dot{q}) = T + V$. Alternatively, $E(q, \dot{q}) = \dot{q}^\alpha \frac{\partial L}{\partial \dot{q}^\alpha} - L$
F_r	Froude Number. A dimensionless number describing forward velocity.
G	Matrix containing the gravitational terms of a system.
M	Inertial matrix (tensor) of a mechanical system. For Lagrangian systems, this is also the metric tensor.
M_e	Inertial matrix of a mechanical system in the extended coordinate system, which includes extra degrees of freedom to express the collision instant constraint.
N	Matrix containing coriolis and other rotational terms.
$T(q, \dot{q})$	Kinetic energy. $T = \frac{1}{2}\dot{q}^T M \dot{q}$, where $M(q)$ is the inertial matrix of the system.
$V(q)$	Potential energy. Assumed to be conservative.

x_o, y_o	Coordinates of the origin of the robot's frame.
x_n, y_n	Coordinates of the origin of the robot's frame after a collision (i.e. in the next step)
x_r, y_r	Coordinates of the center of the stance leg's arc foot.
x_s, y_s	Coordinates of the center of the non-stance leg's arc foot.
α	Interleg angle. Usually equal to $(q_f - q_s)$
ϕ	The angle of the downhill slope the robot is walking down. [deg or rad]
θ	An angle defining the some particular angle of a rigid body, measured with respect to the vertical, in the counter-clockwise direction. [rad]
ξ	The angle that the torso leans away from the bisecting angle (For constrained torso biped only). In this thesis, it is generally set to 0.
ψ	The angle that the foot radius center makes relative to the lower leg. Measured clockwise from lower leg, so a positive value corresponds to a foot that is longer in front than behind.
Δp_{IDR}	The worst case disturbance which yields r_{IDR} .
Δp_{EDR}	The worst case disturbance which yields r_{EDR} .
\mathbb{Q}	The <i>configuration manifold</i> , the set of all configuration states q .
$\mathbf{T}\mathbb{Q}$	The <i>tangent manifold</i> , consisting of the states (q, \dot{q}) .
$\mathbf{T}_q\mathbb{Q}$	The <i>tangent bundle</i> , consisting of the states (\dot{q}) at a point q .
$\mathbf{T}^*\mathbb{Q}$	The <i>cotangent manifold</i> , consisting of the states (q, p) .
$\mathbf{T}_q^*\mathbb{Q}$	The <i>cotangent bundle</i> , consisting of the states (p) at a point q .

Appendix B

EQUATIONS OF MOTION, IMPACT EQUATIONS

B.1 Derivation of Equations of Motion

For convenience, the majority of the equations of motion for the systems in this thesis were derived with symbolic algebra systems such as Mathematica. The procedure used to derive the equations of motion is relatively straightforward, and we list it here.

1. Define the Cartesian positions of the important joints and masses of the system using the generalized coordinates. (The Cartesian velocities are derived automatically from these.)
2. Define the potential and kinetic energies of the system in Cartesian space. Use these to construct the Lagrangian.
3. Use mathematica script (below) to simplify the resulting lagrangian to use only generalized coordinates, and solve for the inertial, coriolis, and gravitational matrices.
4. Print all mathematical expressions using Mathematica's `FullForm` function. The `FullForm` expressions are essentially identical to LISP expressions, so with a small amount of regular expressions scripting, the two can be freely interchanged. The painful copying of large amounts of math from one program to another then becomes a simple matter of cut-and-paste.¹

We now include an example of the mathematica file used to derive the equations of motion for the compass biped.

B.1.1 Sample Derivation of Equations of Motion in Mathematica

```
(* DERIVATION OF COMPASS BIPED EQUATIONS OF MOTION *)
ClearAll[];
Off[General::spell1];
```

```
(*xo[t],yo[t] : Origin.*)
x0 = xo[t]; (*x0, y0 is the support leg tip *)
y0 = yo[t];
```

¹The author wishes he had heard of Maxima a little sooner; Maxima is written purely in Lisp and would likely not have even required a script to convert Maxima's internal representation of data into LISP code directly usable in the simulation.

```

x1 = x0 + -a * Sin[θs[t]]; (* support leg mass *)
y1 = y0 + a * Cos[θs[t]];
x2 = x0 + -(a + b) * Sin[θs[t]]; (* hip mass*)
y2 = y0 + (a + b) * Cos[θs[t]];
x3 = x2 + b * Sin[θf[t]]; (* free leg mass *)
y3 = y2 - b * Cos[θf[t]];
x4 = x2 + (a + b) * Sin[θf[t]]; (* free leg foot tip *)
y4 = y2 - (a + b) * Cos[θf[t]];
xn = x4; (*xn, yn = New origin after collision *)
yn = y4;

x1d = D[x1, t]; y1d = D[y1, t];
x2d = D[x2, t]; y2d = D[y2, t];
x3d = D[x3, t]; y3d = D[y3, t];
x4d = D[x4, t]; y4d = D[y4, t];

keng1 = (1/2) * m * (x1d^2 + y1d^2);
keng2 = (1/2) * mh * (x2d^2 + y2d^2);
keng3 = (1/2) * m * (x3d^2 + y3d^2);

peng1 = m * g * y1;
peng2 = mh * g * y2;
peng3 = m * g * y3;

T = FullSimplify[keng1 + keng2 + keng3]
V = FullSimplify[peng1 + peng2 + peng3]
Q = 0;


$$\begin{aligned} & \frac{1}{2} \left( m \left( (x_0'[t] - a \cos[\theta_s[t]] \theta_s'[t])^2 + (y_0'[t] - a \sin[\theta_s[t]] \theta_s'[t])^2 \right) + mh \right. \\ & \left( (x_0'[t] - (a+b) \cos[\theta_s[t]] \theta_s'[t])^2 + (y_0'[t] - (a+b) \sin[\theta_s[t]] \theta_s'[t])^2 \right) + \\ & m \left( (x_0'[t] + b \cos[\theta_f[t]] \theta_f'[t] - (a+b) \cos[\theta_s[t]] \theta_s'[t])^2 + \right. \\ & \left. (y_0'[t] + b \sin[\theta_f[t]] \theta_f'[t] - (a+b) \sin[\theta_s[t]] \theta_s'[t])^2 \right) \\ & g(-bm \cos[\theta_f[t]] + ((2a+b)m + (a+b)mh) \cos[\theta_s[t]] + (2m + mh)y_0[t]) \end{aligned}$$


(* EULER-LAGRANGE EQUATIONS AND INERTIAL MATRICIES *)
LagrangianEquations[T_, V_, Q_:0, genCoords_List]:=Module[{L = T - V}, (D[D[L, D[#, t]], t] - D[L, #] - Q)&/@genCoords];

BuildMassMatrix[Z_, genCoords_List]:=(D[Z, D[D[#, t], t]])&/@genCoords;

(*The impact model requires we use xo,
yo to express the collision constraint,

```

so we define the extended generalized coordinates,
and derive the extended inertial matrix using them.*)

```

SetAttributes[{a, b, m, mh, g}, Constant];
genCoords = {θf[t], θs[t]};
genCoordsExt = {θf[t], θs[t], xo[t], yo[t]};
exRule = {xo[t] → 0, yo[t] → 0, xo'[t] → 0, yo'[t] → 0};

ELeqnsExt = FullSimplify[LagrangianEquations[T, V, Q, genCoordsExt]];
ELeqnsBasic = FullSimplify[LagrangianEquations[T, V, Q, genCoords]]/.  

exRule;

M = BuildMassMatrix[ELeqnsBasic, genCoords];
Melt = MatrixForm[FullSimplify[
Transpose[Solve[{m11, m12}, {m21, m22}] == M, {m11, m12, m21, m22}]]]

Mext = BuildMassMatrix[ELeqnsExt, genCoordsExt];
Mextelt = MatrixForm[FullSimplify[
Transpose[
Solve[{m11, m12, m13, m14}, {m21, m22, m23, m24},
{m31, m32, m33, m34}, {m41, m42, m43, m44}] == Mext,
{m11, m12, m13, m14, m21, m22, m23, m24, m31, m32, m33, m34,
m41, m42, m43, m44}]]]


$$\left( \begin{array}{l} m11 \rightarrow b^2 m \\ m12 \rightarrow -b(a+b)m \cos[\theta f[t] - \theta s[t]] \\ m21 \rightarrow -b(a+b)m \cos[\theta f[t] - \theta s[t]] \\ m22 \rightarrow (2a^2 + 2ab + b^2) m + (a+b)^2 mh \\ \\ m11 \rightarrow b^2 m \\ m12 \rightarrow -b(a+b)m \cos[\theta f[t] - \theta s[t]] \\ m13 \rightarrow b m \cos[\theta f[t]] \\ m14 \rightarrow b m \sin[\theta f[t]] \\ m21 \rightarrow -b(a+b)m \cos[\theta f[t] - \theta s[t]] \\ m22 \rightarrow (2a^2 + 2ab + b^2) m + (a+b)^2 mh \\ m23 \rightarrow -(b(m+mh) + a(2m+mh)) \cos[\theta s[t]] \\ m24 \rightarrow -(b(m+mh) + a(2m+mh)) \sin[\theta s[t]] \\ m31 \rightarrow b m \cos[\theta f[t]] \\ m32 \rightarrow -(b(m+mh) + a(2m+mh)) \cos[\theta s[t]] \\ m33 \rightarrow 2m + mh \\ m34 \rightarrow 0 \\ m41 \rightarrow b m \sin[\theta f[t]] \\ m42 \rightarrow -(b(m+mh) + a(2m+mh)) \sin[\theta s[t]] \\ m43 \rightarrow 0 \\ m44 \rightarrow 2m + mh \end{array} \right)$$


```

(* CORIOLIS AND CENTRIPETAL TERMS *)

```
BuildCoriolisMatrix[Z_, genCoords_List]:=  
Transpose[((∫ D[Z, D[#, t]] dD[#, t])/D[#, t])&/@genCoords];
```

```
F = BuildCoriolisMatrix[ELeqnsBasic, genCoords];
```

```
Felts = MatrixForm[
```

```
Transpose[FullSimplify[Solve[{ {f11, f12}, {f21, f22} } == F,  
{f11, f12, f21, f22}]]]]
```

$$\begin{pmatrix} f11 \rightarrow 0 \\ f12 \rightarrow -b(a+b)m\sin[\theta f[t] - \theta s[t]]\theta s'[t] \\ f21 \rightarrow b(a+b)m\sin[\theta f[t] - \theta s[t]]\theta f'[t] \\ f22 \rightarrow 0 \end{pmatrix}$$

(* GRAVITATIONAL MATRIX *)

```
G =
```

```
FullSimplify[ELeqnsBasic - M.D[D[genCoords, t], t] - F.D[genCoords, t]]//.  
{x0''[t] → 0, y0''[t] → 0};  
Gelts = MatrixForm[FullSimplify[Transpose[Solve[{g1, g2} == G, {g1, g2}]]]]]
```

$$\begin{pmatrix} g1 \rightarrow bgm\sin[\theta f[t]] \\ g2 \rightarrow -g(b(m+mh) + a(2m+mh))\sin[\theta s[t]] \end{pmatrix}$$

(* COLLISION USING GENERALIZED INELASTIC IMPACT MODEL *)

```
<< LinearAlgebra`MatrixManipulation`
```

```
γ = {xn, yn}; (* New fixed point after collision *)
```

```
q = {θf[t], θs[t], xo[t], yo[t]};
```

```
Ee = D[γ, {q}]; MatrixForm[Ee]
```

$$\begin{pmatrix} (a+b)\cos[\theta f[t]] & (-a-b)\cos[\theta s[t]] & 1 & 0 \\ (a+b)\sin[\theta f[t]] & -(a+b)\sin[\theta s[t]] & 0 & 1 \end{pmatrix}$$

B.2 Derivation of Impact Model

Assuming a completely plastic collision between the foot and ground, momentum will be conserved about the collision point. Also, each rigid body will experience an internal impulse resulting from their connections with the rigid body connected to the foot. We now present two ways of computing the impact equations. One way to compute the impulse is to use the generalized Jacobian of the manipulator tip as a new geometric constraint. This method is similar to what was done in [Grizzle 2001]. The other method is based upon using the principle of conservation of momenta, and was used in [Goswami et al 1996]. Both methods were verified as being computationally identical when run in simulation, but the former was simpler to derive and was used more extensively in this thesis.

We now present a short description of each method, using the example of the compass

biped shown in figure 1.2.

B.2.1 Derivation via Generalized Jacobian

For this section, we use what this thesis will call the “extended” generalized coordinates, $q_e = (\theta_f, \theta_s, x_o, y_o)$, which for this section we will simply write q . The coordinates x_o, y_o are the origin, usually the center of the support foot. Although $\dot{x}_o, \dot{y}_o = 0$ are stationary during normal equations of motion, these coordinates are needed to model the impact impulse, which cannot be described in terms of just θ_f, θ_s .

We assume the equations of motion of the unconstrained system are of the form

$$M(q)\ddot{q} + C(q, \dot{q}) = \tau$$

We assume that the manipulator tip γ enters a non-slipping condition after impact. We can express this as a geometric constraint which applies a force λ . A geometric constraint does no work, so we let $D = \frac{\partial \gamma}{\partial q}$ and write $D\lambda = 0$. The new equations of motion for the constrained system are

$$M(q)\ddot{q} + C(q, \dot{q}) = \tau - D^T\lambda$$

If we integrate over a very small amount of time around the instant of impact, we can assume that q and τ do not change, and that only the generalized velocities change instantaneously due to impulse Λ . Thus C and τ vanish and we can write

$$\begin{aligned} M\Delta q &= -D^T\Lambda \\ M(\dot{q}^+ - \dot{q}^-) &= -D^T\Lambda \\ M\dot{q}^+ &= M\dot{q}^- - D^T\Lambda \\ \dot{q}^+ &= \dot{q}^- - M^{-1}D^T\Lambda \end{aligned}$$

The post-collision manipulator tip must also be motionless, so

$$D\dot{q}^+ = 0$$

We can now solve for the impact impulse Λ using the previous equation

$$\begin{aligned} D[\dot{q}^- - M^{-1}D^T\Lambda] &= 0 \\ DM^{-1}D^T\Lambda &= D\dot{q}^- \\ \Lambda &= (DM^{-1}D^T)^{-1}D\dot{q}^- \end{aligned}$$

Therefore, the post-collision velocities \dot{q}^+ can now be expressed using only the inertial matrix M , manipulator jacobian D , and pre-collision velocity \dot{q}^- :

$$\dot{q}^+ = \dot{q}^- - M^{-1}D^T(DM^{-1}D^T)^{-1}D\dot{q}^-$$

If desired, the expression for partially inelastic collisions can be derived in a similar manner as above, resulting in

$$\dot{q}^+ = \dot{q}^- - (1 + k)M^{-1}D^T(DM^{-1}D^T)^{-1}D\dot{q}^-$$

where

$$k = 0 \text{ (completely inelastic)}$$

$$k = 1 \text{ (completely elastic)}$$

B.2.2 Derivation via Conservation of Momenta

At the collision, angular momentum is conserved about the new contact point. Let $\dot{\theta}^-$ and $\dot{\theta}^+$ represent the velocities of the compass biped immediately before and after the collision, and let Q^- and Q^+ be two matrices that are selected so that angular momentum is conserved about the collision point through the collision.

Derivations for Q^-, Q^+ are not shown here, but can be found in [Goswami et al 1996].

$$Q^- \dot{\theta}^- = Q^+ \dot{\theta}^+$$

$$Q^- = \begin{pmatrix} q_{11}^- & q_{12}^- \\ q_{21}^- & q_{22}^- \end{pmatrix}$$

$$q_{11}^- = -abm$$

$$q_{12}^- = (a + b)(2am + (a + b)m_h) \cos(\theta_f - \theta_s) - abm$$

$$q_{21}^- = 0$$

$$q_{22}^- = -abm$$

$$Q^+ = \begin{pmatrix} q_{11}^+ & q_{12}^+ \\ q_{21}^+ & q_{22}^+ \end{pmatrix}$$

$$q_{11}^+ = -bm((a + b) \cos(\theta_f - \theta_s) - b)$$

$$q_{12}^+ = m_h(a + b)^2 - bm \cos(\theta_f - \theta_s)(a + b) \\ + (2a^2 + 2ba + b^2)m$$

$$q_{21}^+ = b^2m$$

$$q_{22}^+ = -b(a + b)m \cos(\theta_f - \theta_s)$$

$$\dot{\theta}^+ = Q^{+^{-1}} Q^- \dot{\theta}^-$$

B.3 Form of Equations of Motion for Easy Integration

For all of the bipeds presented in this thesis, the generalized coordinates are

$$q = \begin{bmatrix} \theta_f \\ \theta_s \end{bmatrix}$$

where θ_f is the non-stance or 'free' leg, and θ_s is the angle of the stance leg. Both angles are measured counter-clockwise from the vertical. We write the generalized velocities with primes or dots as is convenient:

$$\dot{q} = q' = \frac{dq}{dt}$$

Once a rigid body system's kinetic energy T and potential energy V has been derived, the Lagrangian $L = T - V$ can be defined. From this, the Euler-Lagrange equations

$$\frac{d}{dt} \frac{\partial \mathcal{L}}{\partial \dot{q}} - \frac{\partial \mathcal{L}}{\partial q} = 0$$

give us a set of differential equations. In order to numerically integrate the system, we need to have equations in the form $\dot{q} = f(q)$. Converting the the differential equations directly into the form $\ddot{q} = f(\dot{q}, q)$ is possible, but difficult. A simpler method is to regroup the set of equations as three matrixies

$$M(q)\ddot{q} + N(\dot{q}, q)\dot{q} + G(q) = Su$$

where $M(q)$ is the inertial matrix, $N(\dot{q}, q)$ is for coriolis and centripetal effects, $G(q)$ gravitational matrix, and Su represents control inputs.

Once the equations are in this form, it is then a rather simple matter to integrate using the equation

$$\ddot{q} = M^{-1}(q)[Su - N(\dot{q}, q)\dot{q} - G(q)]$$

using the numerical integrator of choice.

B.4 Controllers Can Mimic Springs

While it is straightforward to derive the equations of motion of the system with springs included, the equivilent effect can be achieved by deriving the equations of motion for the system without them, and then adding torques via a proportional controller. The effect is the same, mathematically and in simulation.

For example, the hip and ankle torques which simulate an interleg spring and an ankle spring can be achieved by using

$$S = \begin{bmatrix} 1 & 0 \\ -1 & -1 \end{bmatrix}$$

$$u = \begin{bmatrix} u_{hip} \\ u_{ankle} \end{bmatrix}$$

$$u_{\text{hip}} = k_{\text{hip}}(\theta_s - \theta_f)$$

$$u_{\text{ankle}} = k_{\text{ankle}}(\theta_s + \phi)$$

during the integration of the equations of motion shown in the previous section.

B.5 Heelstrike Conditions

The conditions which signaled heelstrike in all robots where $\psi = 0$ were the equations:

$$\begin{aligned} \theta_s - \phi &< 0 \\ \theta_f + \phi &> 0 \\ \frac{(\theta_s + \theta_f)^-}{2} &< \phi \\ \frac{(\theta_s + \theta_f)^+}{2} &> \phi \end{aligned}$$

where the superscripts $+, -$ indicate the post- and pre-heelstrike instants.

For the one robot studied in this paper which used the ψ parameter, the resulting equations used were

$$\begin{aligned} \theta_s - \phi &< 0 \\ \theta_f + \phi &> 0 \\ \arctan \left(\frac{(a+b)(\cos \theta_f - \cos \theta_s) + r \cos(\psi - \theta_s) - r \cos(\psi - \theta_f)}{(a+b)(\sin \theta_f - \sin \theta_s) - r \sin(\psi - \theta_s) + r \sin(\psi - \theta_f)} \right)^- &< \phi \\ \arctan \left(\frac{(a+b)(\cos \theta_f - \cos \theta_s) + r \cos(\psi - \theta_s) - r \cos(\psi - \theta_f)}{(a+b)(\sin \theta_f - \sin \theta_s) - r \sin(\psi - \theta_s) + r \sin(\psi - \theta_f)} \right)^+ &> \phi \end{aligned}$$

Both sets of equations can be derived from geometric constraints in straightforward manner.

B.6 Equations for Compass Biped

$$M = \begin{pmatrix} m_{11} = b^2 m \\ m_{12} = -b(a+b)m \cos(\theta_f - \theta_s) \\ m_{21} = -b(a+b)m \cos(\theta_f - \theta_s) \\ m_{22} = m_h(a+b)^2 + (2a^2 + 2ba + b^2)m \end{pmatrix}$$

$$N = \begin{pmatrix} n_{11} = 0 \\ n_{12} = -b(a+b)m \sin(\theta_f - \theta_s)\theta'_s \\ n_{21} = b(a+b)m \sin(\theta_f - \theta_s)\theta'_f \\ n_{22} = 0 \end{pmatrix}$$

$$G = \begin{pmatrix} g_1 = bgm \sin(\theta_f) \\ g_2 = -g(b(m + m_h) + a(2m + m_h)) \sin(\theta_s) \end{pmatrix}$$

$$E_e = \begin{pmatrix} (a+b) \cos(\theta_f) & (-a-b) \cos(\theta_s) & 1 & 0 \\ (a+b) \sin(\theta_f) & -(a+b) \sin(\theta_s) & 0 & 1 \end{pmatrix}$$

$$M_e = \left\{ \begin{array}{l} m_{11} = b^2 m \\ m_{12} = -b(a+b)m \cos(\theta_f - \theta_s) \\ m_{13} = bm \cos(\theta_f) \\ m_{14} = bm \sin(\theta_f) \\ m_{21} = -b(a+b)m \cos(\theta_f - \theta_s) \\ m_{22} = m_h(a+b)^2 + (2a^2 + 2ba + b^2)m \\ m_{23} = -(b(m+m_h) + a(2m+m_h)) \cos(\theta_s) \\ m_{24} = -(b(m+m_h) + a(2m+m_h)) \sin(\theta_s) \\ m_{31} = bm \cos(\theta_f) \\ m_{32} = -(b(m+m_h) + a(2m+m_h)) \cos(\theta_s) \\ m_{33} = 2m + m_h \\ m_{34} = 0 \\ m_{41} = bm \sin(\theta_f) \\ m_{42} = -(b(m+m_h) + a(2m+m_h)) \sin(\theta_s) \\ m_{43} = 0 \\ m_{44} = 2m + m_h \end{array} \right\}$$

$$\begin{aligned} T = & \frac{1}{2}(m((x'_o - a \cos(\theta_s)\theta s')^2 + (y'_o - a \sin(\theta_s)\theta s')^2) + \\ & m_h((x'_o - (a+b) \cos(\theta_s)\theta s')^2 + (y'_o - (a+b) \sin(\theta_s)\theta s')^2) + \\ & m((x'_o + b \cos(\theta_f)\theta f' - (a+b) \cos(\theta_s)\theta s')^2 + (y'_o + b \sin(\theta_f)\theta f' - (a+b) \sin(\theta_s)\theta s')^2)) \end{aligned}$$

$$V = g(-bm \cos(\theta_f) + ((2a+b)m + (a+b)m_h) \cos(\theta_s) + (2m+m_h)y_o)$$

B.7 Equations for Biped with Semicircular Feet

$$M = \left\{ \begin{array}{l} m_{11} = b^2 m \\ m_{12} = -bm(r \cos(\phi + \theta_f) + (a+b-r) \cos(\theta_f - \theta_s)) \\ m_{21} = -bm(r \cos(\phi + \theta_f) + (a+b-r) \cos(\theta_f - \theta_s)) \\ m_{22} = (2m+m_h)a^2 + 2b(m+m_h)a - 2(2m+m_h)ra + 2(2m+m_h)r^2 \\ + b^2(m+m_h) - 2b(m+m_h)r + 2r(b(m+m_h) + a(2m+m_h) - (2m+m_h)r) \\ \cos(\phi + \theta_s) \end{array} \right\}$$

$$N = \left\{ \begin{array}{l} n_{11} = 0 \\ n_{12} = -bm(a+b-r) \sin(\theta_f - \theta_s) \theta_s' \\ n_{21} = bm(r \sin(\phi + \theta_f) + (a+b-r) \sin(\theta_f - \theta_s)) \theta_f' \\ n_{22} = r(-b(m+m_h) - a(2m+m_h) + (2m+m_h)r) \sin(\phi + \theta_s) \theta_s' \end{array} \right\}$$

$$G = \begin{pmatrix} g_1 = bgm \sin(\theta_f) \\ g_2 = g((2m + m_h)r \sin(\phi) - (b(m + m_h) + a(2m + m_h) - (2m + m_h)r) \sin(\theta_s)) \end{pmatrix}$$

$$E_e = \begin{pmatrix} r \cos(\phi) + (a + b) \cos(\theta_f) - r \cos(\theta_f) & -r \cos(\phi) - (a + b) \cos(\theta_s) + r \cos(\theta_s) & 1 & 0 \\ -r \sin(\phi) + (a + b) \sin(\theta_f) - r \sin(\theta_f) & r \sin(\phi) - (a + b) \sin(\theta_s) + r \sin(\theta_s) & 0 & 1 \end{pmatrix}$$

$$M_e = \left(\begin{array}{l} m_{11} = b^2 m \\ m_{12} = -bm(r \cos(\phi + \theta_f) + (a + b - r) \cos(\theta_f - \theta_s)) \\ m_{13} = bm \cos(\theta_f) \\ m_{14} = bm \sin(\theta_f) \\ m_{21} = -bm(r \cos(\phi + \theta_f) + (a + b - r) \cos(\theta_f - \theta_s)) \\ m_{22} = (2m + m_h)a^2 + 2b(m + m_h)a - 2(2m + m_h)r a + 2(2m + m_h)r^2 + b^2(m + m_h) - 2b(m + m_h)r + 2r(b(m + m_h) + a(2m + m_h) - (2m + m_h)r) \cos(\phi + \theta_s) \\ m_{23} = -(2m + m_h)r \cos(\phi) - (b(m + m_h) + a(2m + m_h) - (2m + m_h)r) \cos(\theta_s) \\ m_{24} = (2m + m_h)r \sin(\phi) - (b(m + m_h) + a(2m + m_h) - (2m + m_h)r) \sin(\theta_s) \\ m_{31} = bm \cos(\theta_f) \\ m_{32} = -(2m + m_h)r \cos(\phi) - (b(m + m_h) + a(2m + m_h) - (2m + m_h)r) \cos(\theta_s) \\ m_{33} = 2m + m_h \\ m_{34} = 0 \\ m_{41} = bm \sin(\theta_f) \\ m_{42} = (2m + m_h)r \sin(\phi) - (b(m + m_h) + a(2m + m_h) - (2m + m_h)r) \sin(\theta_s) \\ m_{43} = 0 \\ m_{44} = 2m + m_h \end{array} \right)$$

$$\begin{aligned} T = & \frac{1}{2}(m_h((x'_o - (r \cos(\phi) + (a + b - r) \cos(\theta_s))\theta s')^2 + \\ & (y_o' + (r \sin(\phi) - (a + b - r) \sin(\theta_s))\theta s')^2) + m((x'_o + b \cos(\theta_f)\theta f' - (r \cos(\phi) + (a + b - r) \cos(\theta_s))\theta s')^2 + \\ & (y_o' + b \sin(\theta_f)\theta f' + (r \sin(\phi) - (a + b - r) \sin(\theta_s))\theta s')^2) + m((x'_o - (r \cos(\phi) + (a - r) \cos(\theta_s))\theta s')^2 + \\ & (y_o' + (r \sin(\phi) + (r - a) \sin(\theta_s))\theta s')^2)) \end{aligned}$$

$$\begin{aligned} V = & g((2m + m_h)r \cos(\phi) - bm \cos(\theta_f) + (b(m + m_h) + \\ & a(2m + m_h) - (2m + m_h)r) \cos(\theta_s) + (2m + m_h)(y_o + r \sin(\phi)\theta s)) \end{aligned}$$

B.8 Equations for Biped with Interleg Spring

Matrices M, M_e, N are the same as for the compass biped.

$$T = \frac{1}{2}(b^2 m \theta f'^2 - 2b(a+b)m \cos(\theta f - \theta s) \theta s' \theta f' + (m_h(a+b)^2 + (2a^2 + 2ba + b^2)m) \theta s'^2)$$

$$\begin{aligned} V &= \frac{1}{2} k_{hip} (\theta f - \theta s)^2 - bgm \cos(\theta_f) + g(b(m + m_h) + a(2m + m_h)) \cos(\theta_s) \\ &\quad \left(\begin{array}{l} g_1 = bgm \sin(\theta f) + k_{hip} \theta f - k_{hip} \theta_s \\ g_2 = -g((2a+b)m + (a+b)m_h) \sin(\theta s) - k_{hip} \theta f + k_{hip} \theta_s \end{array} \right) \end{aligned}$$

B.9 Equations for Biped with Forward-Pointing Feet

$$M = \begin{pmatrix} m_{11} = b^2 m \\ m_{12} = -bm(r \cos(\phi + \theta_f) + (a+b) \cos(\theta f - \theta_s) - r \cos(\psi + \theta f - \theta_s)) \\ m_{21} = -bm(r \cos(\phi + \theta_f) + (a+b) \cos(\theta f - \theta_s) - r \cos(\psi + \theta f - \theta_s)) \\ m_{22} = (2m + m_h)a^2 + 2b(m + m_h)a + 2(2m + m_h)r^2 + b^2(m + m_h) - \\ 2(b(m + m_h) + a(2m + m_h))r(\cos(\psi) - \cos(\phi + \theta_s)) - \\ 2(2m + m_h)r^2 \cos(\phi - \psi + \theta_s) \end{pmatrix}$$

$$N = \begin{pmatrix} n_{11} = 0 \\ n_{12} = bm(r \sin(\psi + \theta f - \theta s) - (a+b) \sin(\theta f - \theta_s))\theta'_s \\ n_{21} = bm(r \sin(\phi + \theta_f) + (a+b) \sin(\theta f - \theta_s) - r \sin(\psi + \theta f - \theta_s))\theta'_f \\ n_{22} = r((2m + m_h)r \sin(\phi - \psi + \theta_s) - (b(m + m_h) + a(2m + m_h)) \sin(\phi + \theta_s))\theta'_s \end{pmatrix}$$

$$G = \begin{pmatrix} g_1 = bgm \sin(\theta_f) \\ g_2 = g(2m + m_h)r(\sin(\phi) - \sin(\psi - \theta_s)) - g(b(m + m_h) + a(2m + m_h)) \sin(\theta_s) \end{pmatrix}$$

$$E_e = \begin{pmatrix} e_{11} = r \cos(\phi) - r \cos(\psi - \theta_f) + (a+b) \cos(\theta_f) \\ e_{12} = -r \cos(\phi) + r \cos(\psi - \theta_s) - (a+b) \cos(\theta_s) \\ e_{13} = 1 \\ e_{14} = 0 \\ e_{21} = -r \sin(\phi) + r \sin(\psi - \theta_f) + (a+b) \sin(\theta_f) \\ e_{22} = r \sin(\phi) - r \sin(\psi - \theta_s) - (a+b) \sin(\theta_s) \\ e_{23} = 0 \\ e_{24} = 1 \end{pmatrix}$$

$$M_e = \left(\begin{array}{l} m_{11} = b^2m \\ m_{12} = -bm(r \cos(\phi + \theta_f) + (a + b) \cos(\theta_f - \theta_s) - r \cos(\psi + \theta_f - \theta_s)) \\ m_{13} = bm \cos(\theta_f) \\ m_{14} = bm \sin(\theta_f) \\ m_{21} = -bm(r \cos(\phi + \theta_f) + (a + b) \cos(\theta_f - \theta_s) - r \cos(\psi + \theta_f - \theta_s)) \\ m_{22} = (2m + m_h)a^2 + 2b(m + m_h)a + 2(2m + m_h)r^2 + b^2(m + m_h) - \\ 2(b(m + m_h) + a(2m + m_h))r(\cos(\psi) - \cos(\phi + \theta_s)) - \\ 2(2m + m_h)r^2 \cos(\phi - \psi + \theta_s) \\ m_{23} = -(2m + m_h)r(\cos(\phi) - \cos(\psi - \theta_s)) - (b(m + m_h) + a(2m + m_h)) \cos(\theta_s) \\ m_{24} = (2m + m_h)r(\sin(\phi) - \sin(\psi - \theta_s)) - (b(m + m_h) + a(2m + m_h)) \sin(\theta_s) \\ m_{31} = bm \cos(\theta_f) \\ m_{32} = -(2m + m_h)r(\cos(\phi) - \cos(\psi - \theta_s)) - (b(m + m_h) + a(2m + m_h)) \cos(\theta_s) \\ m_{33} = 2m + m_h \\ m_{34} = 0 \\ m_{41} = bm \sin(\theta_f) \\ m_{42} = (2m + m_h)r(\sin(\phi) - \sin(\psi - \theta_s)) - (b(m + m_h) + a(2m + m_h)) \sin(\theta_s) \\ m_{43} = 0 \\ m_{44} = 2m + m_h \end{array} \right)$$

$$\begin{aligned} T = & \frac{1}{2}(m((x'_o - (r \cos(\phi) - r \cos(\psi - \theta_s) + a \cos(\theta_s))\theta s')^2 + \\ & (yo' + (r \sin(\phi) - r \sin(\psi - \theta_s) - a \sin(\theta_s))\theta s')^2) + \\ & m((x'_o + b \cos(\theta_f)\theta'_f - (r(\cos(\phi) - \cos(\psi - \theta_s)) + (a + b) \cos(\theta_s))\theta s')^2 + \\ & (yo' + b \sin(\theta_f)\theta'_f + (r(\sin(\phi) - \sin(\psi - \theta_s)) - (a + b) \sin(\theta_s))\theta s')^2) + \\ & m_h((x'_o - (r \cos(\phi) - r \cos(\psi - \theta_s) + (a + b) \cos(\theta_s))\theta s')^2 + \\ & (yo' + (r \sin(\phi) - r \sin(\psi - \theta_s) - (a + b) \sin(\theta_s))\theta s')^2)) \end{aligned}$$

$$V = g((2m + m_h)r \cos(\phi) - bm \cos(\theta_f) - (2m + m_h)r \cos(\psi - \theta_s) + (b(m + m_h) + a(2m + m_h)) \cos(\theta_s) + (2m + m_h)(y_o + r \sin(\phi)\theta s))$$

B.10 Equations for Biped with a Mechanically Constrained Torso

$$M = \left(\begin{array}{l} m_{11} = mb^2 + \frac{d^2 m_t}{4} \\ m_{12} = \frac{1}{4}(dm_t(d + 2(a + b) \cos(\frac{1}{2}(2\xi + \theta_f - \theta_s))) - 4b(a + b)m \cos(\theta_f - \theta_s)) \\ m_{21} = \frac{1}{4}(dm_t(d + 2(a + b) \cos(\frac{1}{2}(2\xi + \theta_f - \theta_s))) - 4b(a + b)m \cos(\theta_f - \theta_s)) \\ m_{22} = (2m + m_h + m_t)a^2 + 2b(m + m_h + m_t)a + \frac{d^2 m_t}{4} \\ + b^2(m + m_h + m_t) + (a + b)dm_t \cos(\frac{1}{2}(2\xi + \theta_f - \theta_s)) \end{array} \right)$$

$$\begin{aligned}
N &= \begin{pmatrix} n_{11} = 0 \\ n_{12} = \frac{1}{2}(a+b)(dm_t \sin(\frac{1}{2}(2\xi + \theta_f - \theta_s)) - 2bm \sin(\theta_f - \theta_s)\theta_s') \\ n_{21} = -\frac{1}{4}(a+b)((dm_t \sin(\frac{1}{2}(2\xi + \theta_f - \theta_s)) - 4bm \sin(\theta_f - \theta_s)\theta_f' + \\ &\quad 2dm_t \sin(\frac{1}{2}(2\xi + \theta_f - \theta_s))\theta_s') \\ n_{22} = -\frac{1}{4}(a+b)dm_t \sin(\frac{1}{2}(2\xi + \theta_f - \theta_s))(2\theta_f' - \theta_s') \end{pmatrix} \\
G &= \begin{pmatrix} g_1 = bgm \sin(\theta_f) - \frac{1}{2}dgm_t \sin(\frac{1}{2}(2\xi + \theta_f + \theta_s)) \\ g_2 = \frac{1}{2}(-2g(b(m+m_h+m_t) + a(2m+m_h+m_t)) \sin(\theta_s) - \\ &\quad dgm_t \sin(\frac{1}{2}(2\xi + \theta_f + \theta_s)) + (a+b)dm_t \sin(\frac{1}{2}(2\xi + \theta_f - \theta_s))\theta_f'\theta_s') \end{pmatrix} \\
E_e &= \begin{pmatrix} (a+b) \cos(\theta_f) & -(a+b) \cos(\theta_s) & 1 & 0 \\ (a+b) \sin(\theta_f) & -(a+b) \sin(\theta_s) & 0 & 1 \end{pmatrix} \\
M_e &= \begin{pmatrix} m_{11} = mb^2 + \frac{d^2m_t}{4} \\ m_{12} = \frac{1}{4}(dm_t(d+2(a+b)\cos(\frac{1}{2}(2\xi + \theta_f - \theta_s))) - 4b(a+b)m \cos(\theta_f - \theta_s)) \\ m_{13} = bm \cos(\theta_f) - \frac{1}{2}dm_t \cos(\xi + \frac{1}{2}(\theta_f + \theta_s)) \\ m_{14} = bm \sin(\theta_f) - \frac{1}{2}dm_t \sin(\xi + \frac{1}{2}(\theta_f + \theta_s)) \\ m_{21} = \frac{1}{4}(dm_t(d+2(a+b)\cos(\frac{1}{2}(2\xi + \theta_f - \theta_s))) - 4b(a+b)m \cos(\theta_f - \theta_s)) \\ m_{22} = (2m+m_h+m_t)a^2 + 2b(m+m_h+m_t)a + \frac{d^2m_t}{4} + b^2(m+m_h+m_t) + \\ &\quad (a+b)dm_t \cos(\frac{1}{2}(2\xi + \theta_f - \theta_s)) \\ m_{23} = -(b(m+m_h+m_t) + a(2m+m_h+m_t)) \cos(\theta_s) - \frac{1}{2}dm_t \cos(\xi + \frac{1}{2}(\theta_f + \theta_s)) \\ m_{24} = -(b(m+m_h+m_t) + a(2m+m_h+m_t)) \sin(\theta_s) - \frac{1}{2}dm_t \sin(\xi + \frac{1}{2}(\theta_f + \theta_s)) \\ m_{31} = bm \cos(\theta_f) - \frac{1}{2}dm_t \cos(\xi + \frac{1}{2}(\theta_f + \theta_s)) \\ m_{32} = -(b(m+m_h+m_t) + a(2m+m_h+m_t)) \cos(\theta_s) - \frac{1}{2}dm_t \cos(\xi + \frac{1}{2}(\theta_f + \theta_s)) \\ m_{33} = 2m+m_h+m_t \\ m_{34} = 0 \\ m_{41} = bm \sin(\theta_f) - \frac{1}{2}dm_t \sin(\xi + \frac{1}{2}(\theta_f + \theta_s)) \\ m_{42} = -(b(m+m_h+m_t) + a(2m+m_h+m_t)) \sin(\theta_s) - \frac{1}{2}dm_t \sin(\xi + \frac{1}{2}(\theta_f + \theta_s)) \\ m_{43} = 0 \\ m_{44} = 2m+m_h+m_t \end{pmatrix} \\
T &= \frac{1}{2}(m((x'_o - a \cos(\theta_s)\theta_s')^2 + (y'_o - a \sin(\theta_s)\theta_s')^2) + \\
&\quad m_h((x'_o - (a+b) \cos(\theta_s)\theta_s')^2 + (y'_o - (a+b) \sin(\theta_s)\theta_s')^2) + \\
&\quad m((x'_o + b \cos(\theta_f)\theta'_f - (a+b) \cos(\theta_s)\theta_s')^2 + (y'_o + b \sin(\theta_f)\theta'_f - (a+b) \sin(\theta_s)\theta_s')^2) + \\
&\quad m_t((x'_o - (a+b) \cos(\theta_s)\theta_s' - \frac{1}{2}d \cos(\xi + \frac{1}{2}(\theta_f + \theta_s))(\theta_f' + \theta_s'))^2 + \\
&\quad (y'_o - (a+b) \sin(\theta_s)\theta_s' - \frac{1}{2}d \sin(\xi + \frac{1}{2}(\theta_f + \theta_s))(\theta_f' + \theta_s'))^2))
\end{aligned}$$

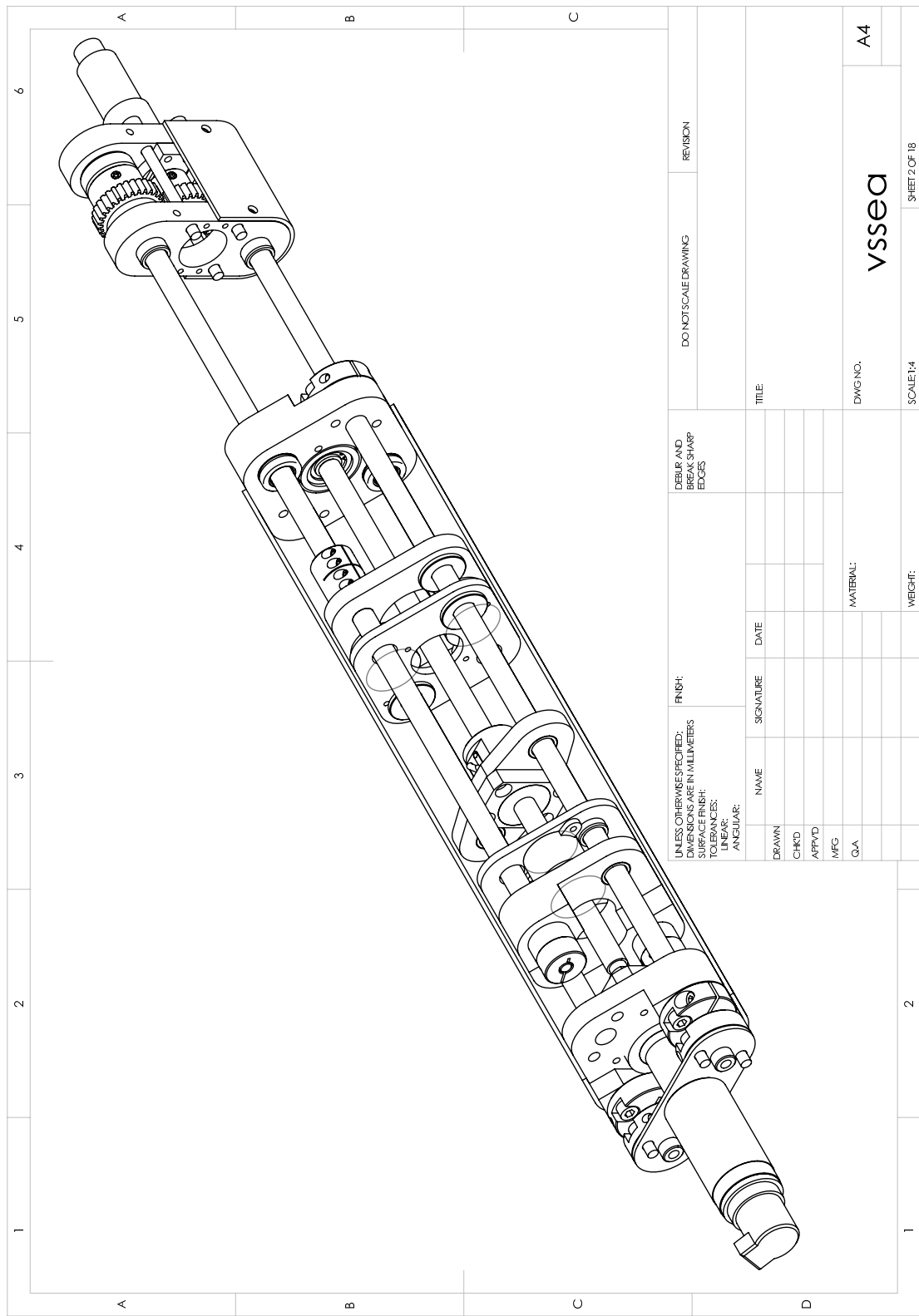
$$\begin{aligned} V = & g(-bm \cos(\theta_f) + (b(m + m_h + m_t) + a(2m + m_h + m_t)) \cos(\theta_s) + \\ & dm_t \cos(\xi + \frac{1}{2}(\theta_f + \theta_s)) + (2m + m_h + m_t)y_o) \end{aligned}$$

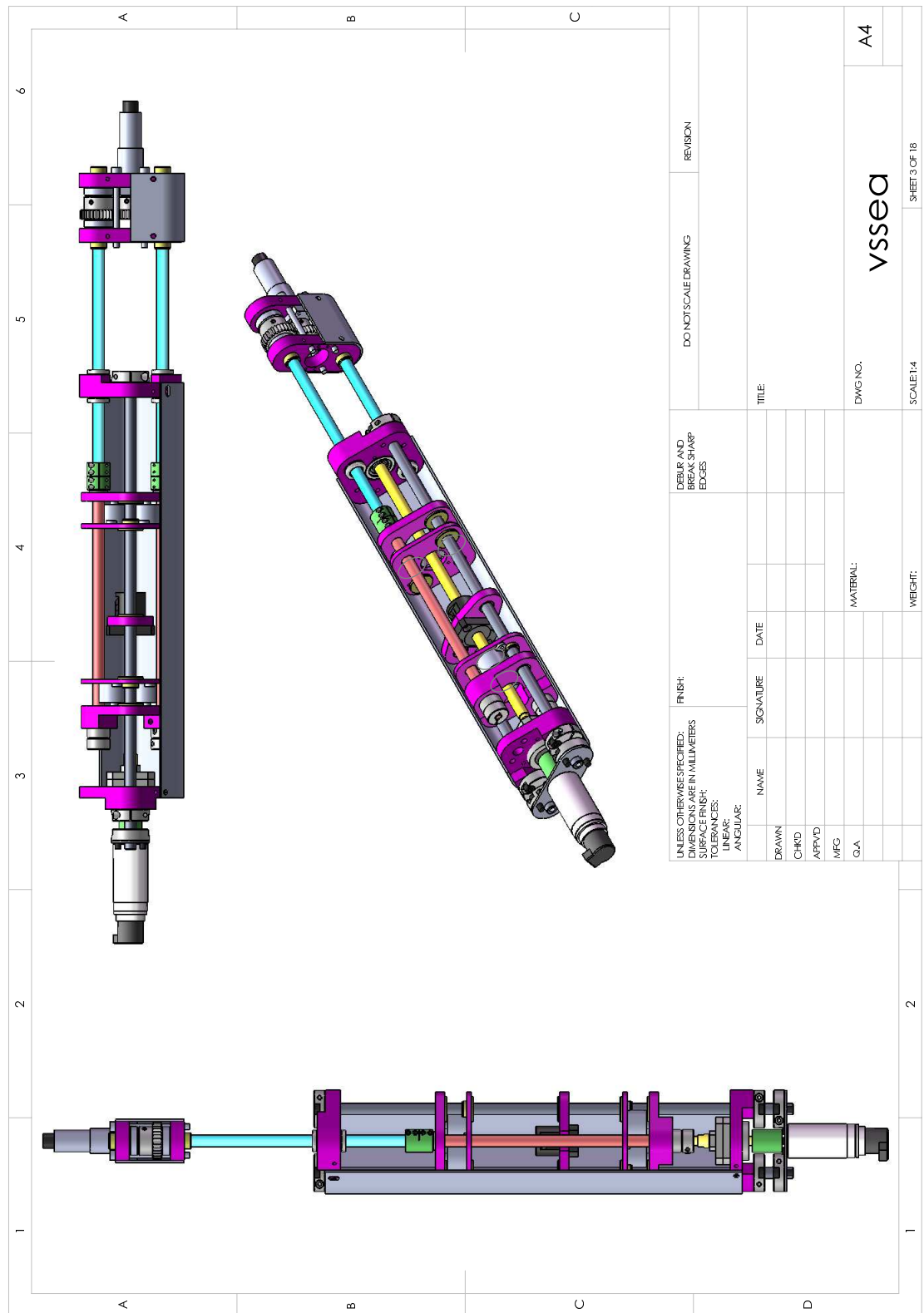
Appendix C

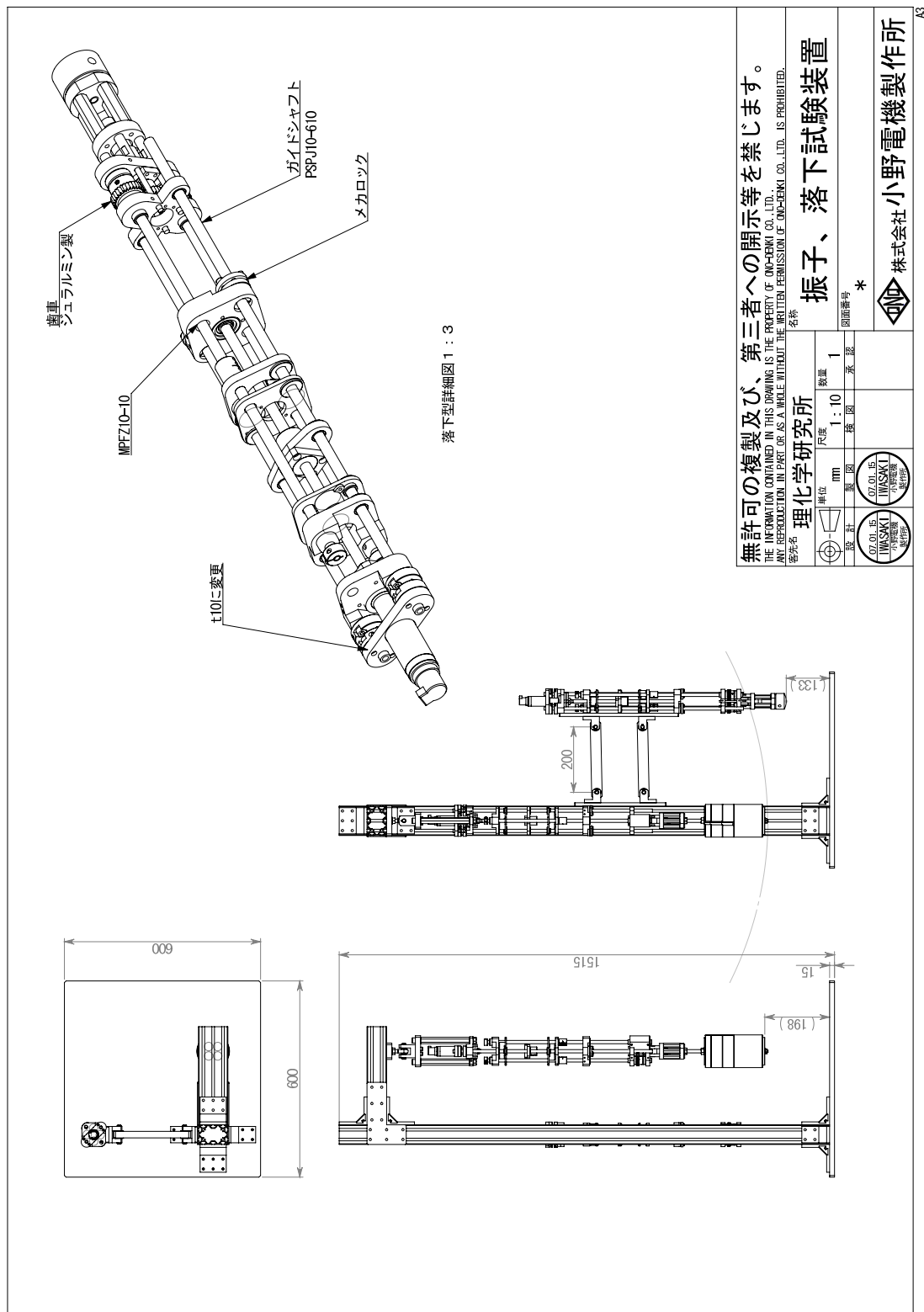
VSSEA MECHANICAL DESIGN

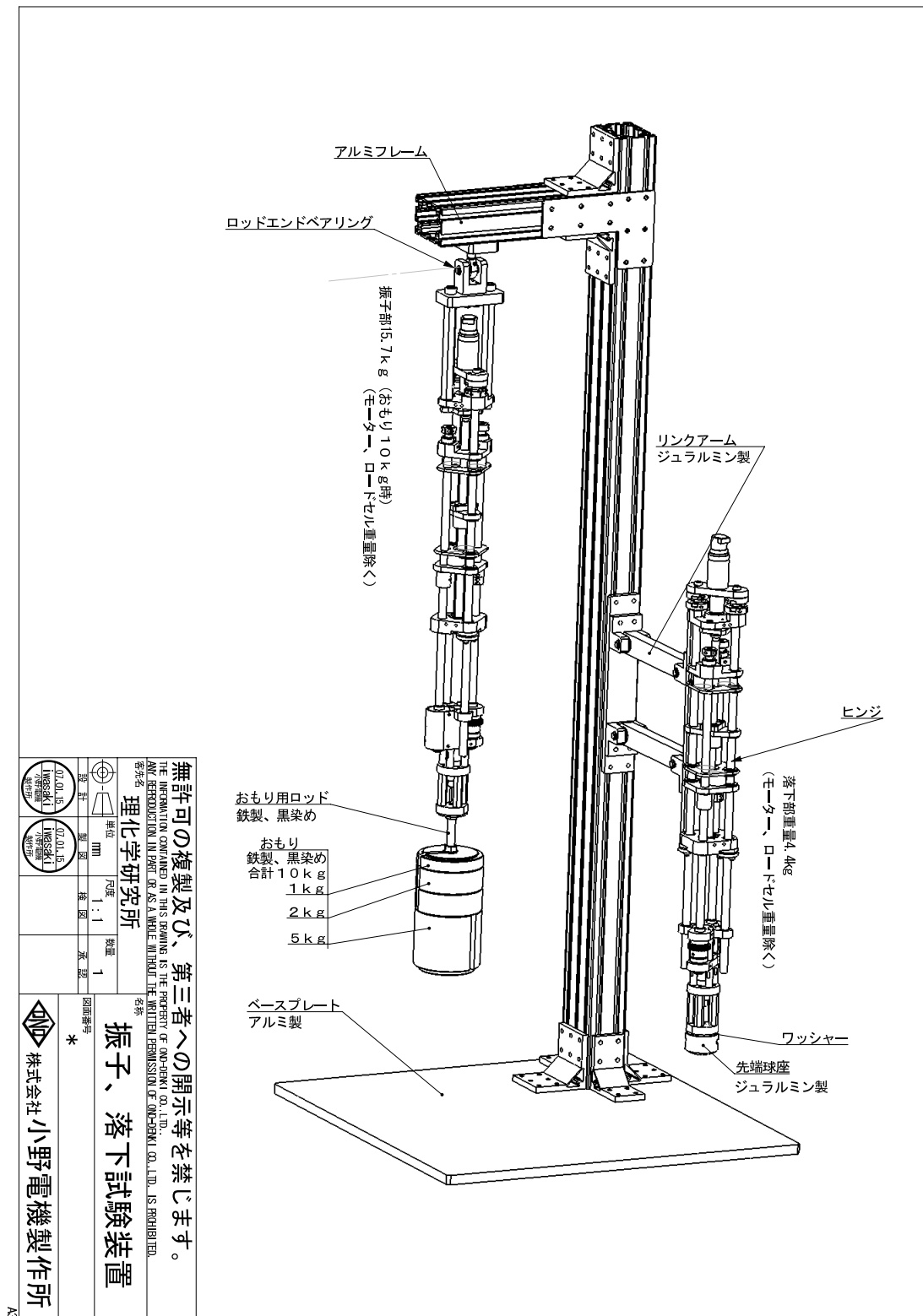
Four pages of the mechanical schematics for the VSSEA are included here. The first two show the actuator by itself. The second two show the actuator connected to a test stand, with two configurations for vertical swinging and impact/jump tests.

It is important to note that there is a slight design difference between the first two CAD schematics and the second two. A design revision was made rather late, and the two grayish guide tubes were extended to match the two sky blue colored guide tubes. This reduced buckling friction effects somewhat, and is a relatively minor change. The visual simplicity of the first two schematics warrant their inclusion here.









Appendix D

DETAILS ON THE CUSTOM SIMULATOR

In this thesis, a custom rigid body simulator was used extensively to measure the gait robustness of several different robot models. The simulator was developed by the author and is written in Common Lisp. The simulator runs in Linux, and uses GNU software such as gnuplot for minor tasks. It uses the Matlisp interface to LAPACK to perform linear algebra, and the CL-OPENGL interface to OpenGL for visualization purposes. On a single-core 2.4Ghz desktop computer and typical video card several thousand frames per second is typically achieved when running a single, simple model. If OpenGL output is disabled, which can be done via the GUI interface, simulation proceeds even faster.

A screenshot of the simulator is shown in figure D.1.

Multiple simulations and parameter searches can be run simultaneously and independently, as is shown in figure D.1. A fixed step size Runge-Kutta 4/5th order numerical integrator is used to numerically integrate the equations of motion. Heelstrike collision instants, transitions between hybrid states of motion, and the inverses of nonlinear functions were evaluated using numerical zero-finding algorithms (Bisection, Newton-Raphson, Secant methods) to machine precision (32 bit), and total system energy variation error per step at the limit cycle is $< 10^{-13} \text{ J}$.

Realtime visualization and on-the-fly editing of each object's parameters is possible. Other features include automatic limit cycle discovery, automatic sweeping and testing of an object parameter, a flexible graphing system, PNG graphical output of models for illustration purposes, automatic mapping of the momenta plane $\mathbf{T}_q^* \mathbb{Q}$ for models with 2DOF, computing r_{IDR} and r_{EDR} , and a flexible system for saving and loading models.

Future programming work for the simulator could include improving the efficiency and intelligence of the evolutionary search, simulating objects on separate threads and improving parallelism, further simplifying the process of adding new robot models, and increasing the speed of plotting via gnuplot.

D.1 Data Parameter Details

The data presented in this thesis used the mechanical simulation parameters shown in table D.1. A timestep of $dt = 0.01$ resulted in essentially identical r_{IDR} results as $dt = 0.001$, provided that the exact timing of heelstrike was evaluated to machine precision.

D.2 Numerical Integration and Root Finding

This simulation uses a Runge-Kutta 4th/5th order integrator. The technique is simple, reasonably accurate, and relatively stable method of numerical integration. Details can be found in any standard text on numerical programming techniques, such as [Press et al 1988].

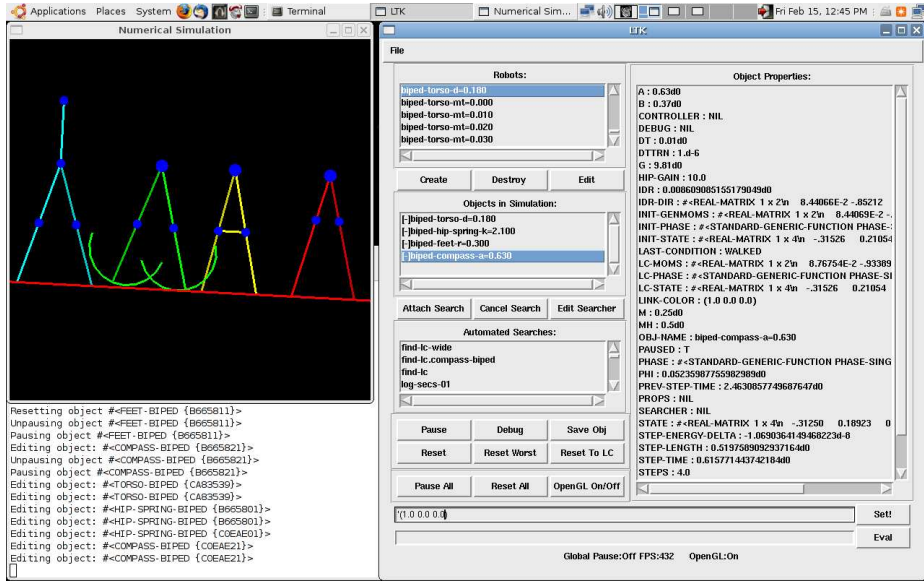


Figure D.1: **Screenshot of the simulation developed for this thesis.** Multiple models can be simulated simultaneously and viewed in OpenGL, as can be seen on the left side of the screen. The right side shows a TCL/TK based GUI which allows editing of any object quantity, in real time. Arbitrary LISP code may be run through a REPL interface at the bottom of the GUI. Terminal output useful for debugging is shown in the lower left.

Table D.1: Simulation Parameters

Parameter	Value	Units
Default integration timestep	0.01	s
Collision instant timestep	2^{-30}	s
Considered to be at limit cycle after this many steps	100	steps
Estimated accuracy of r_{IDR} is at least	0.0001	kg m/s
Considered to be stable against a disturbance if walked for	20	s
r_{IDR} Global random hypersphere search shrinks after this many failures to find smaller r_{IDR}	40	trials
r_{IDR} Local random hypersphere search shrinks after this many failures to find a smaller r_{IDR}	20	trials
Shrink coefficient	0.5	

Root finding is another problem that commonly occurs in numerical simulations. In this thesis, root finding methods were used to accurately compute the instant of collision. Doing so improved the numerical accuracy of the rigid body simulation even when larger integration timesteps were used during the continuous phase of the motion. Root finding methods used include bisection, Newton-Raphson, and secant methods. Bifurcation was used initially as a general method which worked even for pathological functions, and the current implementation predominantly uses secant methods. Newton methods would have been preferable, but computing the gradient of a many multivariate functions was more trouble than it was worth. Again, details can be found in any standard text on numerical programming techniques, such as [Press et al 1988].

D.3 r_{IDR} Search Algorithm

D.3.1 Discussion of Search Algorithm

This simulation uses a two-stage heuristic search algorithm to calculate r_{IDR} and r_{EDR} . It is probably best thought of as a very primitive evolutionary optimization system. The emphasis on the mechanical simulation was accuracy; the emphasis on the evolutionary optimization system was on computation time. Experimentally, the evolutionary optimization seems to get stuck on local minima about 2% of the time, depending on the model being studied.

When many data points are being taken, these local minima are very obvious when plotted. To fix the problem, such prematurely converged r_{IDR} were recomputed several times, and the smallest r_{IDR} was selected as the point that is most likely the real global minima. This solution is slightly inelegant, but reliable and reduced computation time dramatically.

Convergence to local minima could be avoided by spending more time doing global evolutionary search to ensure that the global minima is found, but computing time rises several fold during this case. The author found it ended up being more efficient to use a human brain to detect the local minima, and just recalculate r_{IDR} when it is obvious the search algorithm got stuck on a local minima.

Although using a better gradient descent method would have been preferred, the great difficulty of evaluating the gradient of the stability function of the limit cycle made this option prohibitively difficult. A hand-rolled solution was used instead. Although the author would have preferred to have spent more time studying optimization techniques for problems such as this, the simple method of simulated annealing worked sufficiently well that more complex methods were not needed.

Typical values chosen for a 2D search space were to search until there were 40 sequential searches without a superior point having been found. The search radius was then shrunk by 50% radius. This is expressed in table form in Table D.1. The search converged to what appears to be the global minimum about 98% of the time, depending on the model. It is computationally reasonably fast. When convergence failed or the system converged to a local minima, trying new starting values randomly or by hand resulted in successful convergence. Work could be done to improve the program's response to non-convergence.

D.3.2 Detailed Description of Search Algorithm

The optimization method used to find r_{IDR} has two steps. It can be described fairly simply.

In words, the algorithm is: Began searching random points in the volume of the hypersphere of radius r centered at the limit cycle. As better points are found (ie, points for which the robot falls but are closer to the limit cycle than the current guess), r is decreased to match the radius of this 'better point'. When a better point has not been found in a certain number of trials (say, 40), shrink the radius of the hypersphere by some amount α . Once r is sufficiently small that the global search is no longer significantly improving results, switch to a local search mode, which means the center of the hypersphere is shifted to the current 'best point'. About this new point, continue to shrink r until it is smaller than the stopping criterion radius r_s .

A more precise explanation using some pseudocode follows. Let r be the current radius of the hypersphere whose interior is being searched, O be the center of the search hypersphere, x be the current point being tested for stability, x^* be the current best guess of the smallest disturbance which knocks the robot down, α, n_g, n_l, r_s be a various coefficients which control the speed of the search space contraction, p_{LC} be the momenta at the limit cycle, $d_{LC}(x)$ be the Euclidean distance between a point x and p_{LC} , $s(r, O)$ be a function which returns a random point in the interior of the hypersphere of radius r centered at O , and $f(x)$ be a function that returns true if an only if the robot successfully walks and its state while walking returns to the limit cycle. Below, $:=$ means assignment.

1. Let $O = p_{LC}$, and $x = r = 10^3$ or any sufficiently large number.
2. **while** $r > d_{LC}(x)$
 - (a) $x := s(r, O)$
 - (b) **if** $f(x)$ { $n := n - 1$ } **else** { $n := n_g$; $r := d(x, O)$ }
 - (c) **if** $n == 0$ { $n := n_g$; $r := \alpha * r$ }
3. **while** $r > r_s$
 - (a) $O := x^*$
 - (b) $x := s(r, O)$
 - (c) **if** $f(x)$ { $n := n - 1$ } **else** { $n := n_l$; $r := d(x, O)$ }
 - (d) **if** $n == 0$ { $n := n_l$; $r := \alpha * r$ }
4. **return** $r_{IDR} = r^*$

In this thesis, values of $\alpha = 0.5$, $r_s = 0.0001$, $n_g = 40$, $n_l = 20$ were used.

D.3.3 Picking Evenly Distributed Random Points on a Hypersphere Surface

The equations for defining points on the surface of sphere in polar coordinates, and the method for converting into euclidean coordinates are well known to any high school graduate.

$$\begin{aligned}x &= r \sin \phi \cos \theta \\y &= r \sin \phi \sin \theta \\z &= r \cos \phi\end{aligned}$$

Higher dimensional spaces have a regular pattern of sines and cosines that allow programmatic calculation of points on a sphere with relative simplicity.

However, it is not as obvious how to select uniformly distributed points on the surface of the sphere. If we choose ϕ, θ via uniform distributions between $[0, \pi]$ and $[0, 2\pi]$, the resulting distribution is clustered near the poles. The problem gets worse as the dimensionality increases.

To solve this problem, we use a method introduced by [Marsaglia 1959]. This method allows easy generalization to higher dimensional spaces.

Written simply, a point on the hypersphere of radius r can be found by generating n Gaussian random variables x_1, x_2, \dots, x_n . Then the distribution of

$$\frac{r}{\sqrt{x_1^2 + x_2^2 + \dots + x_n^2}} \begin{bmatrix} x_1 \\ x_2 \\ \vdots \\ x_n \end{bmatrix}$$

is uniform over the n dimensional hypersphere's surface.

D.4 Simulation Verification

Great care was taken to make simulation results as accurate as possible given the time available for research. Collision mechanics were derived in two different ways and tested to ensure identical results. Similarly, equations of motion for complex models were checked to verify that the models reduced to simpler models when certain parameters were set to zero. Simulation rounding, numerical errors, and the conservation of energy for passive systems were also checked.

The author jokes to himself that even if the quantities r_{IDR} and r_{EDR} turn out to be completely unimportant, at least they were measured precisely!

VITA

Ivar Thorson graduated from the University of Washington with a B.S. of Electrical Engineering in 2004. After working a short time at a friend's start-up company, he traveled to Japan on the MEXT (Japanese Ministry of Education, Culture, Sports, Science and Technology) scholarship and studied at Nagoya University and the RIKEN Bio-mimetic Control Research Center until his graduation in April 2008 with a M.S. in Mechatronics.

His hobbies include travel, swimming, martial arts, guitar, piano, sailing, studying Japanese, programming, video games, and taking himself too seriously. In the future he hopes to work as a comedian, mixed-martial arts instructor, and entrepreneur; three jobs which are intimately related.